Generalised Differential Golden Code Modulation: Error Performance Analysis and Bandwidth Efficiency

Gevira Omondi Otieno

A thesis submitted in fulfilment of the requirement for the degree of

Doctor of Philosophy in Electronic Engineering

School of Engineering
University of KwaZulu-Natal,
South Africa

Mar, 2022

As the candidate's supervisor, I, **Hongjun Xu**, approve the submission of this thesis.

Signed.....Date.....

Declaration 1 - Plagiarism

I, **Gevira Omondi Otieno**, declare that;

1. The research reported in this thesis, except where otherwise indicated, is my original research.
2. This thesis has not been submitted for any degree or examination at any other university.
3. This thesis does not contain other persons' data, pictures, graphs or other information, unless specifically acknowledged as being sourced from other persons.
4. This thesis does not contain other persons' writing, unless specifically acknowledged as being sourced from other researchers. Where other written sources have been quoted, then:
   (a) Their words have been re-written but the general information attributed to them has been referenced,
   (b) Where their exact words have been used, then their writing has been placed in italics and inside quotation marks, and referenced.
5. This thesis does not contain text, graphics or tables copied and pasted from the Internet, unless specifically acknowledged, and the source being detailed in the thesis and in the references sections.

Signed.....Date.....March 25, 2022.....

Declaration 2 - Publication

DETAILS OF CONTRIBUTION TO PUBLICATIONS that form part and/or include research presented in this thesis, including publications in preparation, submitted, *in press* and published, to which the candidate is the primary author, are listed as follows:

1. Generalised differential Golden code. *Submitted for publication to the Institution of Electronics and Telecommunications Engineers (IETE) Technical Review*.
2. Multiple input symbol generalised differential Golden code modulation. *Published in the International Journal of Communication Systems*.
3. Enhanced bandwidth efficiency of the generalised differential Golden code modulation. *Submitted for publication to the International Journal of Communication Systems*.
4. Enhanced bandwidth efficiency of the Golden code. *Published in proceedings of the Institute of Electrical and Electronic Engineers (IEEE) AFRICON 2021*.

Signed:.....

Dedication

To my beloved parents...for your lessons on resilience!

"Dost thou know the balancings of the clouds, the wondrous works of Him which is perfect in knowledge?" ∼ Job 37:16

Acknowledgements

I wish to express my sincere gratefulness to the University of Nairobi for supporting my academic endeavours. I am also forever indebted to my supervisors, Prof. Xu and Dr Akuon, without whom I would not have completed this research.

To the "men of honour", thank you for always showing interest in my progress. I cannot forget my great friend Andrew and his family for creating many moments of adventure. Those moments gave me a much-needed break.

Finally, to my caring and supportive wife Damaris and our daughter Zahra, I am deeply grateful. Your reassurances during tough times kept me motivated. I was relieved by your willingness to take charge of our household affairs while I spent long hours in research.

Abstract

The receiver of a conventional differential modulation scheme performs detection without knowledge of the channel state information (CSI). This results in a 3dB performance loss compared to coherent modulation. In order to enhance this error performance, generalised differential modulation is utilised.

This thesis firstly presents a generalised differential modulation scheme for the Golden code (GDM-GC) based on quadrature amplitude modulation (QAM). The average bit error probability (ABEP) for the GDM-GC scheme is derived and simulations on bit error rates (BER) are carried out in order to verify the derived theoretical framework, where it is shown that BER results lie well within the derived bounds. In addition, compared to coherent GC with maximum likelihood (ML) detection both 16QAM and 64QAM GDM-GC result in approximately 0.4 dB performance loss for a frame length of $L = 400$. However, the computational complexity of the GDM-GC scheme is reduced significantly in comparison to the coherent ML detector.

Secondly, this thesis extends the generalised differential modulation scheme to multiple input symbol Golden code and proposes a multiple input symbol generalised differential Golden code (MIS-GD-GC) scheme. This scheme not only boosts error performance in comparison to conventional differential multiple input symbol Golden code (MIS-GC), but it also produces multiple diversity order compared to the conventional Golden code. The simulations on BER for the MIS-GD-GC scheme not only compare very well to the derived theoretical bounds but also show that the BER draws closer to that of coherent MIS-GC when the frame length is increased. For instance, at a frame length of $L = 400$, the error performance gap between MIS-GD-GC and its coherent counterpart is only 0.4 dB.

Finally, driven by the need to develop a scheme that can allow for transmission of more data to help meet the demands of modern wireless communication systems, this thesis seeks to improve the bandwidth efficiency of the GDM-GC scheme. An enhanced bandwidth efficient generalised differential Golden code (EBE-GD-GC) scheme based on QAM is proposed and its ABEP derived. The simulated BER results for the EBE-GD-GC scheme are shown to lie well within the derived

ABEP and achieve almost the same error performance as GDM-GC at high signal-to-noise ratio (SNR) regions but with extra bit(s) of information sent in each transmitted space-time block code (STBC) compared to the typical GDM-GC scheme. In addition, compared to the conventional generalised differential Golden code, both 16QAM and 64QAM EBE-GD-GC result in $<$ 1dB performance loss from a BER of 1×10^{-5}.

Contents

List of Figures

List of Figures

List of Tables

List of Tables

List of Acronyms

5G	Fifth Generation Communication Systems
6G	Sixth Generation Communication Systems
ABEP	Average Bit Error Probability
AWGN	Additive White Gaussian Noise
BER	Bit Error Rate
CI-GC-MQAM	Component Interleaved Golden Codeword-based M-ary Quadrature Amplitude Modulation
CSI	Channel State Information
EBE-GD-GC	Enhanced Bandwidth Efficiency of the Generalised Differential Golden Code
ED	Euclidean Distance
EGC	Equal Gain Combining
GC	Golden Code
GC-MQAM	Golden Codeword-based M-ary Quadrature Amplitude Modulation
GD-GC	Generalised Differential Golden Code
GDM-GC	Generalised Differential Modulation of the Golden Code
IBI	Inter-Beam Interference
IC	Interference Cancellation
IEEE	Institute of Electrical and Electronic Engineering
MIMO	Multiple-Input Multiple-Output
MIS-GC	Multiple-Input Symbol Golden Code

MIS-GD-GC Multiple-Input Symbol Generalised Differential Golden Code

ML Maximum Likelihood

MMSE Minimum Mean-Square Error

MPSK M-ary Phase Shift Keying

MRC Maximal Ratio Combining

MQAM M-ary Quadrature Amplitude Modulation

ODP Orthogonally Dual Polarised

OFDM Orthogonal Frequency Division Multiplexing

PIC Parallel Interference Cancellation

QAM Quadrature Amplitude Modulation

Q-STBC Quasi-orthogonal Space Time Block Code

RVs Random variables

SC Selection Combining

SD Sphere Decoding

SD-DS Sphere Decoding with Detection Subset

SDS Sorted Detection Subset

SD-SDS Sphere Decoding with Sorted Detection Subset

SIC Successive Interference Cancellation

SIMO Single-Input Multiple-Output

SNR Signal-to-Noise Ratio

STC Space-Time Coding

STLC Space-Time Line Code

STLD Space-Time Labeling Diversity

STTC Space-Time Trellis Code

STBC Space-Time Block Code

USTLD Uncoded Space-Time Labeling Diversity

WiMAX	Worldwide Interoperability for Microwave Access
2IS-GC	Two-Input Symbol Golden Code
2IS-GD-GC	Two-Input Symbol Generalised Differential Golden Code

Preface

The research discussed in this thesis is carried out in the College of Agriculture, Engineering and Science of the University of Kwa-Zulu Natal, Durban, from January 2018 until Nov 2021 by Gevira Omondi Otieno under the supervision of Prof. Hongjun Xu and co-supervised by Dr Peter Akuon.

As the candidate's supervisor, I, Hongjun Xu, agree to the submission of this thesis.

Signed:..... Date:.....

As the candidate's co-supervisor, I, Peter Akuon, agree to the submission of this thesis.

Signed:..... Date:25/03/2022

I, Gevira Omondi Otieno, hereby declare that all the material incorporated in this thesis are my own original work, except where acknowledgement is made by name or in the form of a reference. The work contained in herein has not been submitted in any form for any degree or diploma to any other institution.

Signed:..... Date:March 25, 2022

University of KwaZulu-Natal, March 25, 2022

Part I

Introduction

1 Fundamentals of Wireless Communication Systems

Wireless communication is the most dynamic and fastest-growing technological advancement in the communication sector. Its rapid growth has, inevitably, resulted in increased need for higher data rates as well as improved reliability, particularly with modern wireless communication systems such as the current fifth generation $(5G)$ technology [1, 2]. The deployment of $5G$ networks is accelerating globally due to its ability to provide wider channels (speeds), lower latency (responsiveness) and more bandwidth [3]. Driven by the ever-growing scientific and technological innovation, there is already ongoing research on "Beyond $5G$" [3]. Moreover, the global industry is already promoting the development of $6G$ technology for future digital transformation [4].

Extensive research in wireless communication systems has revealed that communication systems' overall throughput and reliability is significantly improved using multiple-input multiple-output (MIMO) technology. MIMO communication makes use of the physical channel by transmitting the same data on multiple streams simultaneously using multiple antennas, as illustrated in **Figure 1**, thereby providing several gains over the classic single-input single-output (SISO) communication. For instance, multiple spatial paths lead to spatial diversity, which in turn helps to reduce fading sensitivity. In addition, MIMO systems have the ability to dramatically increase spectral efficiency [5–7]. Spectral efficiency, here, refers to the total number of transmitted information bits per second per Hertz [5].

An effective way to achieve the full potential of a MIMO system is to utilise space-time coding (STC). STC is a coding technique comprising multiple transmit antennas designed to improve data transmission reliability in wireless communication systems. STCs transmit signals across spatial and temporal domains to achieve transmit diversity without sacrificing the bandwidth [8]. Space-time codes may be categorised into (i) space-time trellis codes (STTCs) [9], where a trellis code is distributed over multiple antennas and multiple time-slots, resulting in both coding gain and diversity gain at the price of a pretty high detection complexity. (ii) Space-time block codes (STBCs) [10, 11], where the stream of data is encoded in blocks before transmission to provide diversity gain. However, no coding gain is achieved. (iii) The more recently proposed space-time line codes (STLCs) [12] which is an asymmetric scheme for transmitting STBCs. STLCs provide diversity gain even in the absence of channel state information (CSI). The research presented in this thesis only focuses on space-time block codes.

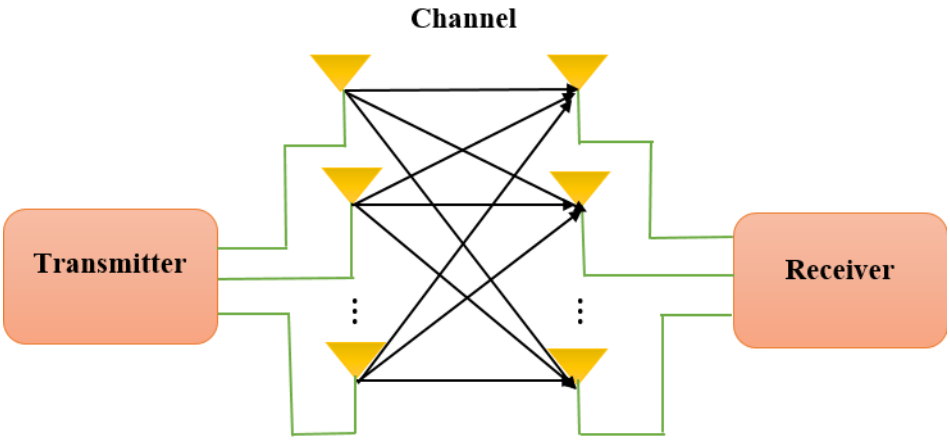

Figure 1: Multiple input multiple output (MIMO) system [5]

1.1 Space-Time Block Codes

Space-time block coding is an approach used in wireless communication systems. Several copies of information stream are transmitted across many antennas, thereby utilising the different variants of the received information to enhance the reliability of data transfer [9, 13]. Inevitably, some of copies of the received information stream will be distorted since the transmitted signal traverses a potentially challenging environment characterised by scattering, reflection, refraction and ultimately corrupted by the thermal noise in the receiver. The redundancy in the data provides a higher chance of using any one of the received copies to decode the received signal correctly. In fact, all the received signals are combined optimally to extract as much information as possible from each copy in space-time coding. Before transmission of STBCs, the stream of data is encoded in blocks. These data blocks are subsequently assigned to multiple antennas (spaced out to allow the decorrelation of transmission paths) across time [13]. Typically, an STBC is represented by a matrix whose rows represent the time-slots while the columns represent the transmit antennas, as illustrated in **Figure 2**.

$$\overset{\text{Transmit antennas}}{\longrightarrow} \qquad \text{Time slots} \downarrow \begin{pmatrix} s_{11} & s_{12} & \cdots & s_{1N_t} \\ s_{21} & s_{22} & \cdots & s_{2N_t} \\ \vdots & \vdots & \ddots & \vdots \\ s_{m1} & s_{m2} & \cdots & s_{mN_t} \end{pmatrix}$$

Figure 2: A typical STBC codeword matrix

s_{ik} is the symbol transmitted in time slot i by antenna k. There are a total of m time slots as well as N_t transmit antennas and N_r receive antennas. A particularly simple yet elegant MIMO STBC is the Alamouti scheme.

1.1.1 The Alamouti code

The Alamouti code is a novel transmit diversity scheme with two transmit antennas [10]. This code requires no knowledge of the transmit channel since it assumes perfect CSI at the receiver. In the MIMO Alamouti scheme, the encoder constructs an orthogonal codeword matrix that easily decodes the two transmitted symbols. Mathematically, the Alamouti scheme's codeword matrix may be represented as:

$$\boldsymbol{X} = \begin{bmatrix} x_1 & x_2 \\ -x_2^* & x_1^* \end{bmatrix}, \tag{1}$$

where x_1 and x_2 can be drawn from either M-ary quadrature amplitude modulation (MQAM) or M-ary phase-shift keying (MPSK) constellations. It has been shown that the Alamouti STBC achieves full diversity gain [9] without sacrificing the data rate. However, Alamouti coding does not achieve multiplexing gain [10]. Another STBC that is important to the research presented in this thesis is the Golden code.

1.1.2 The Golden code

The Golden code is a perfect space-time block code that utilises the Golden number $(1 + \sqrt{5})/2$ [14, 15]. The conventional Golden code (GC) comprises two pairs of Golden codewords, with each pair containing two input symbols as shown in **Figure 3**. Each Golden codeword pair is transmitted in different time slots. The codeword matrix for the Golden code may be written as:

$$\boldsymbol{S} = \begin{bmatrix} s_1 & s_3 \\ s_2 & s_4 \end{bmatrix}, \tag{2}$$

where $s_1 = \frac{1}{\sqrt{5}}\alpha(x_1 + x_2\tau)$, $s_2 = \frac{1}{\sqrt{5}}\alpha(x_3 + x_4\tau)$, $s_3 = \frac{1}{\sqrt{5}}j\hat{\alpha}(x_3 + x_4\mu)$, and $s_4 = \frac{1}{\sqrt{5}}\hat{\alpha}(x_1 + x_2\mu)$ with $\tau = \frac{1+\sqrt{5}}{2}$, $\mu = 1-\tau$, $\alpha = 1+j\mu$, $\hat{\alpha} = 1+j\tau$ and $j = \sqrt{-1}$. The input symbols $x_i, i \in [1:4]$ are drawn from either MQAM or MPSK constellations. Since each input transmitted symbol undergoes two diverse fadings in two time-slots, the Golden code attains a diversity order of $2N_r$, where N_r is the number of receive antennas. In contrast with the Alamouti STBC, the Golden code STBC achieves full-multiplexing gain as well as full diversity [15].

1.1.3 Higher-order space-time block codes

Tarokh et al. [11, 16] proposed a set of STBCs with three or more transmit antennas and quickly discovered that these STBCs could not achieve full rate. Therefore STBCs with more than two transmit antennas must sacrifice rate to achieve orthogonality. Other codes which exhibit partial orthogonality

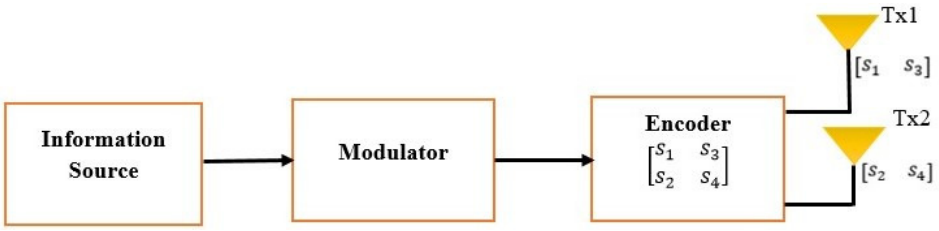

Figure 3: A block diagram of the Golden code encoder

have also been proposed in literature [17]. These codes, referred to as quasi-orthogonal STBCs (Q-STBCs), only achieve partial diversity gain compared to conventional STBCs.

1.1.4 Differential space-time block codes

Differential space-time block codes [18, 19], are based on conventional STBCs but decode the received signal without knowledge of the channel impairments at the receiver. Each block code in a set is only transmitted when a change in the input signal occurs. The receiver extracts data from each block with good reliability by exploiting the differences that exist among the blocks.

1.2 Channel Impairments

Wireless communication systems are carefully designed to ensure link reliability between the transmitter and the receiver. However, there exist certain impairments in the wireless channel that affect the robustness of the network system. Key among these impairments are (1) noise, (2) path loss, (3) shadowing and (4) fading [20, 21].

1.2.1 Noise

Noise occurs as a result of several natural phenomena such as thermal agitation of electrons in electrical circuits (thermal noise) and noise due to black body radiation [21]. Any unwanted signal at the receiver is also regarded as noise [22]. Typically, the noise components are modelled as additive white Gaussian noise (AWGN) because its random variables (RVs) are presumed to have a Gaussian distribution and the noise effects are not frequency selective [20, 21].

1.2.2 Path loss

As radio signals travel through space, they are attenuated due to such factors as refraction, reflection, diffraction, absorption and free space loss. Other factors that may affect path loss include terrain, propagation medium, environment and the gap between the transmitter and receiver. Generally, the signal power at the receiver is always less than the transmitted signal power due path loss [23].

1.2.3 Shadowing

Shadowing occurs when objects block the propagation path between the transmitter and the receiver, causing the received signal power to fluctuate [24]. In wireless propagation, shadowing effects can either be included in path loss modelling or separately calculated.

1.2.4 Fading

Fading occurs when changes in transmission paths result in the received signal power varying in time. The level of fading depends upon the transmission path obstacles, which vary with respect to time. The complex effects of scattering, refraction and reflection arising from the transmission are accounted for by multipath fading [20, 21]. Fading distorts both the amplitude and phase of the transmitted signal. The most common statistical model employed to analyse the effects of fading in wireless networks is the Rayleigh fading model [20, 21, 25]. Ideally, the Rayleigh fading model is best suited for environments with large numbers of signal paths and reflectors. A typical environment would be cellular telecommunications in dense urban areas. Rayleigh fading is also used to model tropospheric and ionospheric radio propagation [22, 26]. It assumes that there is no direct line of sight between the transmitter and the receiver. The real and imaginary fading components are modelled as independent and identically distributed (iid) Gaussian random variables [25]. For more severe conditions that Rayleigh distribution cannot model, the Nakagami-q (or Hoyt) fading channel is used [27, 28]. The Nakagami-q model is also shown to be most suitable in modelling satellite links that undergo strong ionospheric scintillation [28]. Other prominent models in literature include the Nakagami-m [29], which was designed to model fast fading that occurs in long-distance wireless channels, and Nakagami-n (Rice) [30] fading channels, which is suitable in cases where a line-of-sight is dominant [26]. Research work contained in this thesis focuses only on the Rayleigh fading model as it is analytically tractable and models worst-case scenarios.

In general, fading may be classified into two main categories: small-scale fading and large-scale fading. Small-scale fading is characterised by sudden fluctuations in amplitude and deep fades of just a few wavelengths [26]. This type of fading occurs mainly due to signal fades, caused by multiple paths and reflections resulting from mobile movement [26]. Conversely, large-scale fading results from shadowing effects caused by variation in the terrain profile as well as the nature of surroundings. Microscopic diversity techniques prevent small-signal fades, while large-signal fades are counteracted by macroscopic diversity techniques [31].

1.3 Diversity Techniques

Diversity techniques are exploited primarily to combat fading and enhance the reliability of wireless communication systems. In such systems, the receiver uses multiple copies of the same transmitted signal for detection. The availability of redundant information at the receiver ultimately improves performance over the fading radio channel. Practical diversity techniques comprises the following: (1) frequency diversity, (2) time diversity, (3) polarisation diversity, (4) angle diversity and (5) space diversity.

1.3.1 Frequency diversity

Frequency diversity is obtained when the same information signal is transmitted over several carrier frequencies. The frequency separation between each carrier and the other carriers is at least the coherence bandwidth [32]. This ensures that diverse copies of the signal experience independent fading. The receiver optimally combines the independently faded signals using a maximum ratio combiner, discussed in subsection 4.5. Frequency diversity can also be used to mitigate against frequency selective fading.

1.3.2 Time diversity

Time diversity is brought about by repeated transmission of the same information signal at different time intervals [20]. The gap between the same information signal transmissions must be at least the coherence time to ensure that the different signal copies fade independently [26]. In addition, the time interval is inversely proportional to the rate of fading. Time diversity also does not require any increase in transmission power.

1.3.3 Polarisation diversity

In polarisation diversity, the electromagnetic fields of the information-carrying signal are modified, and then used to transmit the same data stream. Polarisation diversity requires orthogonally dual-polarised (ODP) antennas [33–35]. The first utilises a horizontal and vertical pair of polarisation antenna, while the second utilises a left and right-hand circular pair of polarisation antennas. The polarisation of each single antenna constitutes a different transmission or reception stream due to the orthogonality of the polarisations. A key factor of consideration in systems utilising polarisation diversity is the inter-beam interference (IBI) effects [36] caused by manufacturing defects that could lead to the dual-polarised antennas being imperfectly orthogonal. Polarisation diversity allows for small-size designs, thereby reducing its overall cost since even a single dual-polarised antenna can

achieve polarisation diversity.

1.3.4 Angle diversity

Angle diversity is realised by creating separate copies of the transmitted signal in a multipath environment using directional antennas [33]. The received signals would arrive from different incident angles due to any one of the propagation losses such as reflection, diffraction or scattered signals. By using selective angle antennas, the independent faded signals can be received. This type of diversity is suitable for the mobile terminal end, where limited directions of signals at a base station are linked [22].

1.3.5 Space diversity

Space diversity involves placing different antennas at distinct locations in space in order to receive multiple copies of the same signal. The separation between the antennas is such that the different received signal copies undergo independent fading [26, 32]. Space diversity can help prevent shadowing and also decrease large-scale fading. It offers different transmission paths without an increase in bandwidth or transmit power. However, the applications of space diversity may be limited by physical constraints. For example, mobile handsets require only a small form factor to guarantee mobility. In addition, smaller multi-antenna satellites usually have a two-antenna limit [36]. Nevertheless, space diversity can be employed to withstand both frequency selective and time selective fading.

This research work only focuses on time diversity, where several variants of the same signal are transmitted at different time slots [20], and space diversity, where the signal is transmitted using multiple transmit antennas and multiple receive antennas [20]. A recently developed diversity technique worth mentioning in this research thesis is the space-time labeling diversity (STLD), investigated in coded as well as uncoded systems [37]- [38]. In STLD systems, the same information stream is encoded using different mappers before being transmitted. The design of the mappers is such that for each mapper, there exist different neighbours for every symbol corresponding to a given label [37]. An essential requirement for STLD systems is that all the constellation symbols remain the same despite their corresponding labels [37]. The uncoded space-time labeling diversity (USTLD) scheme is particularly attractive since it achieves a significant SNR gain compared to the STBC scheme.

Diversity techniques can be combined using different methods, namely: selection combining (SC), equal gain combining (EGC) and maximal ratio combining (MRC). Selection combining involves

choosing only the branch with the most superior received signal. In equal gain combining, all the diversity branches are coherently added with the same weighting factor. This scheme also co-phases all the diversity branches and finally adds them up. Finally, in maximal ratio combining, all the branches are used concurrently. Each branch is weighted using a gain factor that is proportional to its SNR. Among the different combining techniques, MRC has the best error performance [39]. This is why MRC has been adopted in this research work to process the redundant signals at the receiver.

1.4 Digital Modulation Techniques

A crucial component that determines the error performance as well as detection complexity of MIMO communication systems is the detection scheme employed. Digital modulation techniques are classified into two main categories, coherent and non-coherent modulation. Coherent modulation techniques employ coherent detection, while non-coherent modulation techniques employ non-coherent detection. Since the receiver of a coherent detector requires full knowledge of the channel state information (CSI) for optimum performance, its detection complexity is high, thereby making it very expensive to implement on hardware [26, 32]. Non-coherent detection, therefore, provides an attractive alternative to coherent detection. Non-coherent detection does not need CSI, resulting in reduced complexity, and since coherent receive signals need not be generated, the non-coherent receiver is easier to implement on hardware [40].

Differential modulation is one avenue that allows reliable estimation of data at the receiver without full knowledge of the CSI [26]. Consequently, differential modulation is widely discussed in literature and find many applications in practice. Recent research has applied differential transmission to STBC systems to ensure no CSI at the receiver [41]. A differential modulation method using STBCs is presented in [42] based on [43]. This method is characterised by a low bit error rate (BER) and its detection complexity is linear. Other authors [44, 45] generalised the works of Ganessan et al. to include constellations with multiple amplitudes. However, differential detection experiences a 3dB error performance loss in comparison to coherent detection [26]. This is due to the additional signal-to-noise ratio (SNR) required at a given BER. Moreover, the conventional differential transmission scheme is based on MPSK and cannot be directly applied to MQAM constellation signals due to issues of phase ambiguity in the conventional MQAM signal demodulation [25].

A new differential transmission technique referred to as generalised differential transmission scheme is proposed in [41] to improve the error performance of STBCs using differential transmission. The proposed scheme differentially transmits each block of encoded STBC where the frame structure consists of a reference block as well as normal blocks, all of which are responsible for conveying

information. The error performance of this scheme is improved by apportioning more transmit power to the reference block in comparison to the normal blocks. This allocation ensures that the combined channel matrix at the receiver is estimated more accurately. In other research work, the generalised differential transmission scheme is applied to amplify-and-forward relay networks [46, 47] as well as on spatial modulation [48].

1.5 Detection Techniques and their Complexity

A key challenge in the implementation of MIMO technology is the decoding scheme at the receiver. This is due to the trade-off that exists between the MIMO scheme's error performance and the computational complexity of its receiver [49, 50]. Increased detection complexity at the receiver results in high power consumption, higher latencies and increased hardware requirements. Therefore, several studies on low-complexity detection techniques for MIMO systems have been carried out [49]- [51]. Computational complexity can be evaluated either in terms of search latencies [51] or by determining the number of floating-point operations that the receiver performs [52] while decoding.

The detection techniques for MIMO systems are categorised into three main classes: (i) linear detectors, (ii) interference cancellation-based detectors and (iii) tree search-based detectors. The performance of all these detectors is benchmarked with the optimal maximum likelihood (ML) detector [53]. ML detection involves a comprehensive search of all possible transmitted symbols to give the best result. However, its computational complexity is proportional to the number of transmit antennas making the ML decoding too complex to implement in the hardware of many communication systems. Nevertheless, ML detection is still used in some instances to decode subsets of possible solutions. [15, 52].

While linear detectors such as zero-forcing (ZF) [54] and minimum mean-square error (MMSE) [55] may exhibit a reduced computational complexity compared to the ML detector, they cannot adequately handle the receive diversity of MIMO systems; hence their error performance is severely degraded [55, 56]. Interference cancellation (IC) detectors such as the successive interference cancellation (SIC) [57] and parallel interference cancellation (PIC) [57] are based on the principle of cancelling signal interference to achieve better performance compared to the linear detectors. However, IC detectors are prone to error propagation [57].

Currently, tree search-based algorithms are very popular in research because they interpret the detection problem as a search for the best path in a tree. In order to efficiently do this, they use QR decomposition to iteratively compute the objective function, traditionally called the Euclidean

distance (ED) [57]. Sphere decoding (SD) [58, 59], is the most popular depth-first tree search algorithm. The sphere decoder limits the detection search space to a hyper-sphere of radius, d, around the received signal. The search radius determines the compromise between the average computational complexity of the SD algorithm and its decoding efficiency [60].

If properly implemented, the error performance of SD closely matches that of the optimal ML detector [59, 61]. The average detection complexity of the SD algorithm can be reduced further by sorting all the symbols in the constellation set from those that are most likely to be transmitted to those that are least likely to be transmitted. The most likely transmitted symbols then form a subset that is used to perform sphere detection [52, 62]. Since the goal is to employ a decoder that achieves the error performance of the optimal ML detector with as low complexity as possible, the research in this thesis adopts sphere decoding.

1.6 Bandwidth and Data Rate

Bandwidth efficiency is a critical measure of evaluating the performance of digital transmission systems, particularly in wireless communication. Moreover, the usable frequency spectrum is a limited resource that must be utilised efficiently to ensure end-users get the best quality of experience [3]. However, efficient use of available bandwidth poses a significant challenge to both policymakers and network operators regarding the most suitable wireless technology to deploy [63] and the configuration to deploy it in.

In MIMO systems, there exists a trade-off between bandwidth efficiency and reliability. Nevertheless, there exist techniques that can be exploited to enhance spectral efficiency. One way in which the bandwidth efficiency can be improved is by using higher modulation orders of the encoding scheme [21, 64]. Typically for higher-order modulation schemes, more information bits can be encoded before being transmitted [20, 21]. However, this degrades the error performance of the system due to the reduced gap between symbols in a constellation set. In addition, research studies have shown that the modulation technique adopted plays a crucial role in improving bandwidth efficiency. For instance, MQAM signals are more spectrally efficient than the MPSK counterpart [20, 22].

Another method of improving bandwidth efficiency is through spatial multiplexing of data. For example, MIMO systems such as the vertical-bell laboratories layered space-time (V-BLAST) [65] adopts spatial multiplexing by transmitting multiple streams of data simultaneously in a single frequency band. This allows for higher data rates by increasing the number of transmit antennas. However, as mentioned earlier, the complexity of its optimal ML detector increases exponentially with the number of transmit antennas [53, 65]. This prohibitive complexity poses significant

challenges in the hardware implementation of the system [51]. Modulation techniques such as spatial modulation also help to enhance the spectral efficiency of MIMO systems. In spatial modulation [66, 67], only one transmit antenna remains active during transmission, while all the other transmit antennas remain idle. However, spatial modulation achieves lower data rates compared to the V-BLAST architecture.

2 Research Motivation

As mentioned previously, differential modulation allows the receiver to make credible data estimates without the exact knowledge of the channel state information [26]. This provides a less complex alternative to coherent detection [40]. In addition, a generalised differential transmission scheme is proposed in [41] to enhance the error performance of the conventional differential modulation. However, due to the proposed structure of its frame, this scheme cannot be applied to the more spectrally efficient M-ary quadrature amplitude modulation (MQAM) constellation because of phase ambiguity issues.

Therefore, the research carried out in this thesis primarily seeks to enhance the error performance of the conventional differential Golden code STBC and also accommodate the MQAM constellation. Drawing inspiration from the scheme in [41], each frame of the Golden code STBC will be partitioned into a reference block part that remains constant during transmission and data blocks that convey information. This is to allow for the more spectrally efficient MQAM signals to be transmitted. In addition, the reference block is assigned more transmit power than the data blocks to enhance the error performance of the scheme. Motivated by the works of Xu et al. [62], this research work also aims to extend the generalised differential modulation technique to multiple input symbols in the GC codeword matrix. The error performance of the resultant scheme will be investigated. In addition, this study endeavours to investigate an enhanced bandwidth-efficient scheme for the differential Golden code to help cater for the rising demands of next-generation wireless communication systems.

Finally, this research will also use the union bound method to derive the theoretical average bit error probabilities of the investigated schemes to validate simulation results. As detailed in section (6), the detection complexity at the receiver is a crucial factor in designing MIMO schemes that are implementable on hardware. As a result, the low complexity sphere decoder will be deployed to recover the transmitted symbols throughout this research work. A sorted detection subset will be incorporated in the SD to reduce its average detection complexity further. Accordingly, the main contributions of this thesis are covered in papers A, B and C as outlined in Section 3.

2.1 Research Objectives

In summary, this research work aims to achieve the following objectives:

1. To enhance the error performance of the conventional differential Golden code STBC while accommodating the MQAM constellation.
2. Extend the generalised differential modulation technique to multiple input symbols in the GC codeword matrix. In addition, investigate the error performance of the resultant scheme and compare the results with its coherent counterpart.
3. Investigate an enhanced bandwidth-efficient scheme for the differential Golden code to help meet the rising demands of modern wireless communication systems.
4. Derive theoretical average bit error probabilities for all the schemes under investigation to compare with the simulated results for validation.

3 Research Contributions

Article 1

Title	Generalised Differential Golden Code
Authors	Gevira Omondi, Hongjun Xu, Peter Akuon and Narushan Pillay
Type	Journal Article
Status	Submitted for Publication to the *Institution of Electronics and Telecommunication Engineers (IETE) Technical Review*
Summary	This journal article presents a generalised differential modulation scheme of the Golden code (GDM-GC) based on quadrature amplitude modulation. The scheme uses a reference block as well as data blocks in each transmission frame. Simulations on bit error rates are carried out to verify the derived theoretical framework, where it is shown that the BER results lie well within the derived bounds. In addition, compared to coherent GC with maximum likelihood detection, both 16QAM and 64QAM GDM-GC result in approximately 0.4 dB performance loss for a frame length of $L = 400$. However, the computational complexity of the GDM-GC scheme is reduced significantly when compared to the coherent ML detector.

Article 2

Title	Multiple Input Symbol Generalised Differential Golden Code Modulation
Authors	Gevira Omondi, Hongjun Xu, Peter Akuon and Narushan Pillay
Type	Journal Article
Status	Published in the *International Journal of Communication Systems*
Summary	This journal paper extends the generalised differential modulation scheme to multiple input symbol Golden code and proposes a multiple-input symbol generalised differential Golden code (MIS-GD-GC) scheme. This scheme improves the error performance compared to the conventional differential multiple input symbol Golden code (MIS-GC) and achieves multiple diversity order compared to the conventional Golden code. The average bit error probability for the MIS-GD-GC scheme is also derived. The simulations on bit error rate compare very well to the derived theoretical bounds and show that the BER of MIS-GD-GC draws closer to that of coherent MIS-GC as the frame length increases. For instance, at a frame length of $B = 400$, the error performance gap between MIS-GD-GC and its coherent counterpart is only 0.4 dB.

Article 3

Title	Enhanced Bandwidth Efficiency of the Generalised Differential Golden Code Modulation
Authors	Gevira Omondi, Hongjun Xu, Peter Akuon and Narushan Pillay
Type	Journal Article
Status	Submitted for publication to the *International Journal of Communication Systems*
Summary	In MIMO STBC systems, there exists a trade-off between bandwidth efficiency and reliability. Nevertheless, there exist techniques that can be exploited to enhance bandwidth efficiency to help meet the demands of modern wireless communication systems. This paper proposes an enhanced bandwidth-efficient generalised differential Golden code (EBE-GD-GC) scheme based on QAM. The average bit error probability for the EBE-GD-GC scheme is also derived. Simulations on bit error rate are carried out to verify the derived theoretical framework, where it is shown that the BER results lie well within the derived bounds. In addition, compared to the conventional generalised differential Golden code, both 16QAM and 64QAM EBE-GD-GC result in $<$ 1dB performance loss from a BER of 1×10^{-5}.

Article 4

Title	Enhanced Bandwidth Efficiency of the Golden Code
Authors	Gevira Omondi, Hongjun Xu, Peter Akuon and Narushan Pillay
Type	Conference Paper
Status	Published in *Proceedings of the IEEE AFRICON 2021*
Summary	The conventional Golden code consists of two pairs of Golden codewords, each being a combination of two input symbols. This paper proposes an enhanced bandwidth-efficient scheme for the Golden code (EBE-GC) based on quadrature amplitude modulation. The average bit error probability for the EBE-GC scheme is also derived. Simulations on bit error rates are carried out to verify the derived theoretical framework, where it is shown that the BER results lie well within the derived bounds. In addition, compared to the conventional Golden code with sphere detection, both 16QAM and 64QAM EBE-GC result in $< 1dB$ performance loss from a BER of 1×10^{-4}.

References

[1] V. Yadav, L. Kumar, and P. Kumar, "Evolution and Development of Wireless Communication System," in *Proc. IEEE International Conference on Computing, Power and Communication Technologies (GUCON)*, (New Delhi, India), pp. 53–57, Sep. 2019.

[2] F. Boccardi, R. Heath, A. Lozano, T. Marzetta, and P. Popovski, "Five Disruptive Technology Directions for 5G," *IEEE Commun. Mag.*, vol. 52, no. 2, pp. 74–80, Feb. 2014.

[3] Huawei, "5G-Advanced Techhnology Evolution from a Network Perspective - Towards an Era of Intelligent Connect X," tech. rep., Huawei Technologies, Aug. 2021.

[4] M. Katz, M. Matinmikko-Blue, and M. Latva-Aho, "6Genesis Flagship Program: Building the Bridges Towards 6G-Enabled Wireless Smart Society and Ecosystem," in *Proc. IEEE 10th Latin-American Conference on Communications (LATINCOM)*, (Guadalajara, Mexico), pp. 1–9, Nov. 2018.

[5] W. Daniel, W. Keith, and M. Amanda, "MIMO Wireless Communication," *Lincoln Laboratory Journal*, vol. 15, no. 1, pp. 97–126, 2005.

[6] S. Diggavi, N. Al-Dhahir, A. Stamoulis, and A. Calderbank, "Great Expectations: The Value of Spatial Diversity in Wireless Networks," in *Proc. IEEE*, pp. 219–270, Feb. 2004.

[7] D. Gesbert, M. Shafi, D. Shiu, and A. Naigub, "From Theory to Practice: An Overview of MIMO Space-Time Coded Wireless Systems," *IEEE Journ. on Select. Areas in Commun.*, vol. 21, no. 3, pp. 281–302, Apr. 2003.

[8] B. Vucetic and J. Yuan, *Space-Time Coding*. John Wiley, Apr. 2003.

[9] V. Tarokh, N. Seshadari, and A. Calderbank, "Space-Time Codes for High Data Rate Wireless Communication: Performance Analysis and Code Construction," *IEEE Trans. on Inf. Theory*, vol. 44, no. 2, pp. 744–765, Mar. 1998.

[10] S. Alamouti, "A Simple Transmit Diversity Technique for Wireless Communications," *IEEE Journ. on Select. Areas in Commun.*, vol. 16, no. 8, pp. 1451–1458, Oct. 1998.

[11] V. Tarokh, H. Jafarkhani, and A. Calderbank, "Space-Time Block Codes from Orthogonal Designs," *IEEE Trans. on Inf. Theory*, vol. 45, no. 5, pp. 1456–1467, Jul. 1999.

[12] J. Joung, "Space-Time Line Code," *IEEE Access*, vol. 6, pp. 1023–1041, Nov. 2017.

[13] E. Larsson and P. Stoica, *Space-Time Block Coding for Wireless Communications*. Cambridge University Press, 2003.

[14] J. Belfiore, G. Rekaya, and E. Viterbo, "The Golden Code: A 2x2 Full-rate Space-Time Code with Nonvanishing Determinants," *IEEE Trans. on Inform. Theory*, vol. 51, no. 4, pp. 1432–1436, 2005.

[15] M. Sinnokrot and J. Barry, "Fast Maximum-likelihood Decoding of the Golden Code," *IEEE Trans. on Wireless Commun.*, vol. 9, no. 1, pp. 26–31, 2010.

[16] V. Tarokh, H. Jafarkhani, and A. Calderbank, "Space-Time Block Coding for Wireless Communications: Performance Results," *IEEE Journ. on Select. Areas in Commun.*, vol. 17, no. 3, pp. 451–460, Mar. 1999.

[17] H. Jafarkhani, "A Quasi-orthogonal Space- Time Block Code," *IEEE Transact. on Commun.*, vol. 49, no. 1, pp. 1–4, Jan. 2001.

[18] V. Tarokh and H. Jafarkhani, "A Differential Detection Scheme for Transmit Diversity," *IEEE Journ. on Select. Areas in Commun.*, vol. 18, no. 7, pp. 1169–1174, Jul. 2000.

[19] H. Jafarkhani and V. Tarokh, "Multiple Transmit Antenna Differential Detection from Generalized Orthogonal Designs," *IEEE Transact. on Inf. Theory*, vol. 47, no. 6, pp. 2626–2631, Sep. 2001.

[20] A. Goldsmith, *Wireless Communications*. Cambridge University Press, 2005.

[21] S. Haykin and M. Moher, *Communication Systems*. John Wiley, 2010.

[22] S. Haykin, *An Introduction to Analog and Digital Communication*. John Wiley, 1994.

[23] J. Karedal, N. Czink, A. Paier, F. Tufvesson, and A. Molisch, "Path Loss Modeling for Vehicular-to-Vehicular Communications," *IEEE Trans. on Vehic. Technology*, vol. 60, no. 1, pp. 323–328, Nov. 2010.

[24] R. Parasuraman, K. Kershaw, and M. Ferre, "Experimental Investigation of Radio Signal Propagation in Scientific Fcalilities for Telerobotic Applications," *International Journal of Advanced Robotic Systems*, vol. 10, no. 10, pp. 364–369, Oct. 2013.

[25] M. Simon and M.-S. Alouini, *Digital Communication over Fading Channels: A Unified Approach to Performance Analysis*. New York, USA: John Wiley, 2000.

[26] J. Proakis and M. Salehi, *Digital Communications, 5th Edition*. New york: Mc-Graw Hill, 2007.

[27] J. Romero-Jerez and F. Lopez-Martinez, "A New Framework for the Performance Analysis of Wireless Communications under Hoyt (Nakagami-q) Fading," *IEEE Trans. on Inf. Theory*, vol. 63, no. 3, pp. 1693–1702, 2017.

[28] R. Amol and K. Kaur, "Performance Analysis of Hoyt Fading Channel for M-ary and Monte Carlo Simulation," *Int. Journ. of Adv. Computronics and Management Studies*, vol. 1, no. 3, pp. 13–19, 2016.

[29] M. Nakagami, "The m-distribution - A General Formula of Intensity Distribution of Rapid Fading," in *Statistical Methods in Radio Wave Propagation*, (Oxford, UK), pp. 3–36, 1960.

[30] G. Karagiannidis, N. Sagias, and T. Mathiopoulos, "The N* Nakagami Fading Channel Model," in *IEEE 2nd International Symposium on Wireless Communication Systems*, pp. 185–189, Sep. 2005.

[31] S. Mukherjee and D. Avidor, "Effect of Microdiversity and Correlated Macrodiversity on Outages in a Cellular System," *IEEE Transactions on Wireless Communications*, vol. 2, no. 1, pp. 50–58, Feb. 2003.

[32] B. Sklar and F. Harris, *Digital Communications: Fundamentals and Applications, 3rd Edition*. Pearson, 2020.

[33] J. Carruther and J. Kahn, "Angle Diversity for Nondirected Wireless Infrared Communication," *IEEE Transactions on Communications*, vol. 48, no. 6, pp. 960–969, Jun. 2000.

[34] R. Vaughan, "Polarization Diversity in Mobile Communications," *IEEE Trans. Vehicular Tech.*, vol. 39, no. 3, pp. 177–186, 1990.

[35] K. Raoof, B. Zid, N. Prayongpun, and A. Bouallegue, "Advanced MIMO Techniques: Polarization Diversity and Antenna Selection," tech. rep., MIMO Sytems, Theory and Applications, Apr. 2011.

[36] P.-D. Arapoglou, P. Burzigotti, M. Bertinelli, A. Bolea, and R. Gaudenzi, "To MIMO or Not to MIMO in Mobile Satellite Broadcasting Systems," *IEEE Trans. on Wireless Commun.*, vol. 10, no. 9, pp. 2807–2811, 2011.

[37] H. Xu, K. Govindasamy, and N. Pillay, "Uncoded Space-Time Labeling Diversity," *IEEE Commun. Letters*, vol. 20, no. 8, pp. 1511–1514, 2016.

[38] D. Ayanda, H. Xu, and N. Pillay, "Uncoded M-ary Quadrature Amplitude Modulation Space-Time Labeling Diversity with Three Transmit Antennas," *International Journ. of Commun. Sytems*, vol. 31, no. 18, pp. 1–14, Dec. 2018.

[39] D. Brennan, "Linear Diversity Combining Techniques," in *Proceedings of the IRE*, pp. 1075–1102, Jun. 1959.

[40] S. Hussain and S. Barton, "Comparison of Coherent and Non-coherent Modulation Schemes for Low-data Rate Hand-held Satellite Terminals Subject to High Phase Noise," in *Proc. 10th International Conference on Digital Satellite Communications (ICDSC-10)*, pp. 339–342, 1995.

[41] L. Li, Z. Fang, Y. Zhu, and Z. Wang, "Generalized Differential Transmission for STBC Systems," in *Proc. IEEE GLOBECOM Telecommuncations Conference*, (New Orleans, USA), pp. 1–5, Dec. 2008.

[42] G. Ganessan and P. Stoica, "Differential Modulation using Space-Time Block Codes," *IEEE Signal Processing Letters*, vol. 9, no. 2, pp. 57–60, 2002.

[43] G. Ganessan and P. Stoica, "Space-Time Block Codes: A Maximum SNR Approach," *IEEE Trans. on Inform. Theory*, vol. 47, no. 4, pp. 1650–1656, 2001.

[44] Z. Chen, G. Zhu, D. Qu, and Y. Liu, "General Differential Space Time Modulation," in *Proc. IEEE Global Telecommunications Conference*, (San Francisco, CA, USA), pp. 282–286, Dec. 2003.

[45] M. Tao and R. Chen, "Differential Space Time Block Codes," in *Proc. IEEE Global Telecommunications Conference*, (San Antonio, USA), pp. 1098–1102, Nov. 2001.

[46] S. Kahraman and M. Celebi, "Dimensionality Reduction for the Golden Code with Worst-case Decoding Complexity of $O(m^{1.5})$," in *Proc. IEEE Wireless Communications and Networking Conference*, (Paris, France), pp. 246–250, Apr. 2012.

[47] Z. Fang, L. Li, X. Bao, and Z. Wang, "Generalized Differential Modulation for Amplify-and-forward Wireless Relay Networks," *IEEE Trans. Vehicular Technology*, vol. 58, no. 6, pp. 3058–3062, 2008.

[48] K. Kadathlal, H. Xu, and N. Pillay, "Generalized Differential Scheme for Spatial Modulation Systems," *IET Commun.*, vol. 11, no. 13, pp. 2020–2026, 2017.

[49] C. Mirsad, *Efficient MIMO Detection Methods*. PhD thesis, Linkoping University, Sweden, 2014.

[50] E. Larsson, "MIMO Detection Methods: How they Work [Lecture Notes]," *IEEE Signal Processing Magazine*, vol. 26, no. 3, pp. 91–95, May.2009.

[51] P. Radosavljevic, K. Kim, H. Shen, and J. Cavallaro, "Parallel Searching-Based Sphere Detector for MIMO Downlink OFDM Systems," *IEEE Trans. Signal Process*, vol. 60, no. 6, pp. 3240–3252, 2012.

[52] H. Xu and N. Pillay, "Reduced Complexity Detection Schemes for Golden Code Systems," *IEEE Access*, vol. 7, no. 1, pp. 139140–139149, Dec. 2019.

[53] U. Fincke and M. Pohst, "Improved Methods for Calculating Vectors of Short Length in a Lattice Including a Complexity Analysis," *Mathematics of Computations*, vol. 44, no. 170, pp. 463–471, 1985.

[54] R. Xu and F. Lau, "Performance Analysis for MIMO Systems using Zero Forcing Detector over Fading Channels," *IEEE Proc. Commun.*, vol. 153, no. 1, pp. 74–80, 2006.

[55] Y. Jiang, M. Varanasi, and J. Li, "Performance Analysis of ZF and MMSE Equalizers for MIMO Systems: An in-depth Study of the High SNR Regime," *IEEE Trans. Inf. Theory*, vol. 57, no. 4, pp. 2008–2026, 2011.

[56] M. Neinavaie and M. Derakhtian, "ML Performance Achieving Algorithm with Zero-Forcing Complexity at High SNR Regime," *IEEE Trans. Wireless Commun.*, vol. 15, no. 7, pp. 4651–4659, 2016.

[57] T. Bastien, N. Amor, and L. Yves, "A Review to Massive MIMO Detection Algorithms: Theory and Implementation," *Advanced Radio Frequency Antennas for Modern Communication and Medical Systems*, pp. 1–19, Jul. 2020.

[58] J. Jalden and B. Ottersen, "On the Complexity of Sphere Decoding in Digital Communications," *IEEE Trans. Siganl Proc.*, vol. 53, no. 4, pp. 1474–1484, Apr. 2005.

[59] H. Vikalo and B. Hassibi, "On the Sphere-Decoding Algorithm II. Generalizations, Second-Order Statistics, and Applications to Communications," *IEEE Trans. Signal Process*, vol. 53, no. 8, pp. 2819–2834, 2005.

[60] B. Hochwald and S. Brink, "A chieving Near-Capacity on a Multiple Antenna Channel," *IEEE Trans. on Commun.*, vol. 51, no. 3, pp. 389–399, Mar. 2003.

[61] B. Hassibi and H. Vikalo, "On Sphere Decoding Algorithm Part 1: The Expected Complexity," *IEEE Trans. Signal Proc.*, vol. 54, no. 5, pp. 2806–2818, 2005.

[62] H. Xu and N. Pillay, "Multiple Complex Symbol Golden Code," *IEEE Access*, vol. 8, no. 1, pp. 103576–103584, 2020.

[63] P. Rysavy, "Challenges and Considerations in Defining Spectrum Efficiency," in *Proceedings of the IEEE*, pp. 386–392, Mar. 2014.

[64] G. Stuber, *Principles of Mobile Communication*. Kluwer Academic Publishers, 2nd Edition.

[65] P. Wolniansky, G. Foschini, G. Golden, and R. Valenzuela, "V-BLAST: An Architecture for Realizing Very High Data Rates over the Rich-Scattering Wireless Channel," in *Proc. URSI International Symposium on Signals, Systems and Electronics*, (Pisa, Italy), pp. 295–300, oct. 1998.

[66] K. Govindasamy, H. Xu, and N. Pillay, "Space-Time Block Coded Spatial Modulation with Labeling Diversity," *Int. Journ. of Commun. Systems*, vol. 31, no. 8, pp. 1–15, 2017.

[67] R. Mesleh, H. Haas, S. Sinanovic, C. Ahn, and S. Yun, "Spatial Modulation," *IEEE Trans. Vehicular Tech.*, vol. 57, no. 4, pp. 2228–2241, 2008.

[68] R. Saeed, "Cognitive Radio and Advanced Spectrum Management," in *Proc. Mosharaka International Conference on Communications, Computers and Applications*, (Amman, Jordan), pp. xii–xii, 2008.

[69] H. Xu and N. Pillay, "Golden Codeword Based Modulation Schemes for Single-Input Multiple-Output Systems," *International Journ. of Commun. Systems*, vol. 32, no. 10, pp. 1–12, Jul. 2019.

[70] L. Zheng and T. DNC, "Diversity and Multiplexing: A Fundamental Tradeoff in Multiple-Antenna Channels," *IEEE Trans. Inform. Theory*, vol. 49, no. 5, pp. 1073–1096, 2003.

[71] S. Han and C. Tellambura, "A Complexity-Efficient Sphere Decoder for MIMO Systems," in *Proc. IEEE international Conference on Communications (ICC)*, (Kyoto, Japan), pp. 1–5, Jun. 2011.

[72] N. Pillay and H. Xu, "Uncoded Space-Time Labeling Diversity: Applications of Media-based Modulation with RF Mirrors," *IEEE Commun. Letters*, vol. 22, no. 2, pp. 272–275, 2017.

[73] S. Ejaz, F. Yang, and H. Xu, "Labeling Diversity for 2x2 WLAN Coded-Cooperative Networks," *Radioengineering*, vol. 24, no. 2, pp. 470–480, 2015.

[74] B. Dlodlo and H. Xu, "Trellis Code-aided High-rate M-QAM Space-Time Labeling Diversity using a Unitary Expansion," *International Journ. of Commun. Systems*, vol. 31, no. 11, pp. 1–14, 2018.

Part II

Paper A

Paper A

Generalised Differential Golden Code

1 Abstract

Differential modulation systems are known to execute signal detection at the receiver without the knowledge of the channel state information (CSI). This paper presents a generalised differential Golden code (GDM-GC) system based on quadrature-amplitude modulation (QAM). We then derive the average bit error probability for the GDM-GC scheme. Simulations on bit error rates (BER) are carried out to verify the derived theoretical framework, where it is shown that the BER results lie well within the derived bounds. In addition, compared to coherent GC with maximum-likelihood (ML) detection both 16QAM and 64QAM GDM-GC result in approximately 0.4 dB performance loss for a frame length of $L = 400$. However, the computational complexity of the GDM-GC scheme is reduced significantly when compared to the coherent ML detector.

2 Introduction

Emerging trends in wireless communications have led to an increase in demand for high data transmission rates, as well as the need to improve communication reliability. This demand is achieved by deploying multiple-input multiple-output (MIMO) transmission schemes that are spectrally efficient [1]. A key component in determining the error performance and complexity of a MIMO communication system is the signal detection scheme employed. The ideal coherent detection demands full knowledge of the channel state information (CSI) at the receiver. However, this inevitably increases its detection complexity [2] hence the need to employ a non-coherent detector at the receiving end. Non-coherent detection does not require CSI, resulting in reduced complexity, and since coherent receive signals need not be generated, the non-coherent receiver is easier to implement on hardware.

Differential modulation is one approach that enables the receiver to make reliable data estimates without explicit knowledge of the CSI [3]. Recent research has applied differential transmission to space-time block code (STBC) systems to ensure there is no need for CSI at the receiver [4]. Based on the works of [5], a differential modulation method using STBCs is presented in [6] which exhibits a low bit error rate (BER) and a linear decoding complexity. Other authors [7, 8] generalised it to constellations with multiple amplitudes. However, compared to coherent detection, differential transmission suffers a 3 dB performance loss [3]. In addition, the conventional differential transmission scheme is based on M-ary phase shift keying (MPSK). It cannot be applied to M-ary quadrature amplitude modulation (MQAM) constellation signals directly due to the common issues of phase ambiguity in the conventional MQAM signal demodulation [9, 10].

A new differential transmission technique referred to as generalised differential transmission scheme, is put forward in [4] to enhance the error performance of the conventional differential transmission. This scheme differentially transmits each block of the encoded STBC, whose frame structure is partitioned to form a reference block portion and normal blocks portion. Both these portions are responsible for conveying information. The error performance of this scheme is enhanced by assigning the reference block a higher transmission power than the normal blocks. This, in turn, yields a more accurate approximation of the joint channel matrix at the receiver side [10]. In this scheme, both the reference block and the normal blocks are encoded differentially based upon their respective previous blocks.

Motivated by the limitations of [4] we propose a new differential technique that also employs a reference block and normal blocks in each transmitted frame. However, unlike the case of [4], the

reference block remains constant during transmission, thereby allowing symbols carrying information in the normal blocks to accommodate the more spectrally efficient MQAM signals. The proposed technique is applied to Golden code symbols. It exploits the benefits of optimal allocation of transmit power and the less complex sphere decoding (SD) technique to achieve a better error performance than the conventional differential transmission. The resultant scheme is referred to here as generalised differential modulation for the Golden code (GDM-GC). The Golden code is a perfect space-time block code with an unprecedented error performance based on the golden number $(1 + \sqrt{5})/2$ [11]. It is a full-rate, full-diversity space-time block code for two transmit antennas and N_r receive antennas. The IEEE 802.16 standard incorporates this code as it attains the best possible trade-off between rate and reliability [12]. Other useful applications of the Golden code exist in space-time block-coded, and trellis-coded modulation [13, 14].

The three main contributions of this paper are as follows: a) a differential Golden code system that differs from [4] is presented. Instead of differentially encoding both the normal blocks and the reference blocks of the Golden code STBC, we hold the reference block constant for the entire duration of transmission and only encode the normal blocks to allow for use of the more spectrally efficient MQAM signals. Also, since [15] adopts the Alamouti scheme in the transmission of its symbols, the proposed GDM-GC scheme uses the GC codeword matrix; b) Since no theoretical framework is provided in [4] we also derive the expression for the average bit error probability for the GDM-GC scheme and compare it to the simulated results; c) In order to improve the detection complexity of the proposed system, a low complexity detection scheme that combines the sphere detection algorithm and symbol detection subset is formulated.

The remaining part of this paper is organized as follows: the Golden code system and the proposed GDM-GC scheme are presented in section 2. Section 3 provides the error performance analysis of GDM-GC. We then give the formulae for the detection schemes in Section 4. Simulation of the detection complexities for the scheme is provided in section 5. Numerical results obtained from Monte Carlo simulations are presented in section 6. Section 7 provides the conclusion of the paper.

Notation: Bold lowercase denotes vectors while bold uppercase denotes matrices. The transpose, Hermitian and Frobenius norm operations are denoted by $(\cdot)^T$, $(\cdot)^H$ and $\| \cdot \|_F$ respectively. $E[\cdot]$ is the expected value of an argument and $\boldsymbol{I}_N$ represents an $N \times N$ identity matrix.

3 System Model

This section briefly presents the conventional Golden code.Thereafter, a detailed discussion of the proposed GDM-GC scheme is provided.

3.1 The Golden Code

Consider an $N_t \times N_r$ space-time block code (STBC), where $N_t = 2$ and $N_r \geq N_t$ are the numbers of the transmit and receive antennas, respectively. Four bit streams, $\boldsymbol{b}_i = [b_{i1} b_{i2} \dots b_{ik}], i \in [1:4], k = \log_2 M$ are fed into the STBC encoder, where M is the modulation order. Let $\boldsymbol{\Omega}_M$ be the signal set of MQAM signals. Every bit stream $\boldsymbol{b}_i$ is subsequently projected onto a constellation point x_i of MQAM, $x_i \in \boldsymbol{\Omega}_M$ and $E\left[|x_i|^2\right] = 1, i \in [1:4]$.

The Golden code codeword matrix is as shown in (A.1) [11]

$$\boldsymbol{X} = \begin{bmatrix} s_1 & s_3 \\ s_2 & s_4 \end{bmatrix}, \tag{A.1}$$

where $s_1 = \frac{1}{\sqrt{5}}\alpha(x_1 + x_2\tau), s_2 = \frac{1}{\sqrt{5}}\alpha(x_3 + x_4\tau), s_3 = \frac{1}{\sqrt{5}}j\hat{\alpha}(x_3 + x_4\mu)$ and $s_4 = \frac{1}{\sqrt{5}}\hat{\alpha}(x_1 + x_2\mu)$ with $\tau = \frac{1+\sqrt{5}}{2}, \mu = \frac{1-\sqrt{5}}{2} = -\frac{1}{\tau}, \alpha = 1 + j\mu, \hat{\alpha} = 1 + j\tau$ and $j = \sqrt{-1}$.

The received signal is given by

$$\boldsymbol{Y} = \boldsymbol{H}\boldsymbol{X} + \boldsymbol{N}, \tag{A.2}$$

where $\boldsymbol{Y} \in \mathbb{C}^{(N_r \times 1)}$ denotes the signal vector at the receiver. The fading channel matrix is denoted by $\boldsymbol{H} \in \mathbb{C}^{(N_r \times N_t)}$, where $\boldsymbol{H} = \begin{bmatrix} \boldsymbol{h}_1 & \boldsymbol{h}_2 \end{bmatrix}$. $\boldsymbol{N} \in \mathbb{C}^{(N_r \times 1)}$ is the additive white Gaussian noise (AWGN) vector. In addition, the entries $\boldsymbol{h}_i, i \in [1:2]$ and $\boldsymbol{N}$ are complex Gaussian random variables (RVs) which are independent and identically distributed (iid) as $CN(0,1)$ and $CN(0, 2/\rho)$ respectively, with the average SNR at each receive antenna being $\rho/2$.

3.2 The GDM-GC System Model

Consider the $N_t = 2$ and $N_r \geq N_t$ Golden code STBC whose codeword is described in (A.1) above. In each codeword, a pair of modulated symbols are transmitted through the two transmit antennas. In GDM-GC, information is transmitted in frames consisting of L space-time blocks. $K = (L-1)$ blocks are referred to as normal blocks and are responsible for conveying information. The reference block is the first block to be transmitted in a frame since it serves as a reference point to all the succeeding K blocks within that frame. Each of the two transmit antennas sends a reference signal to the receiver with an estimation of the channel between each transmit antenna and the corresponding

receive antenna. Therefore, the reference block helps to retrieve information from all the subsequent normal blocks. In addition, the reference block is allocated more transmit power than the normal blocks [16].

The reference block transmitted in a single frame is given by:

$$\boldsymbol{Y}_0 = \boldsymbol{H}_0\boldsymbol{X}_0 + \boldsymbol{N}_0, \tag{A.3}$$

where $\boldsymbol{X}_0 = \boldsymbol{I}_{N_t}$ is the differential matrix in the reference block. $\boldsymbol{H}_0 \in \mathbb{C}^{(N_r \times N_t)}$ is the fading channel matrix, where $\boldsymbol{H}_0 = \begin{bmatrix}\boldsymbol{h}_1 & \boldsymbol{h}_2\end{bmatrix}$. $\boldsymbol{N}_0 \in \mathbb{C}^{(N_r \times N_t)}$ is the noise vector in the reference block. The entries of $\boldsymbol{h}_i, i \in [1:2]$ and $\boldsymbol{N}_0$ are i.i.d. complex RVs having Gaussian distributions $CN(0,1)$ and $CN(0,\sigma_0^2)$ respectively, where $\sigma_0^2 = \frac{2}{\rho_0}$. ρ_0 is the signal-to-noise ratio of the reference block and is discussed further in section 3.3. The reference matrix at the receiver is given by $\boldsymbol{Y}_0 \in \mathbb{C}^{(N_r \times N_t)}$. The entries of $\boldsymbol{h}_i$ and those of $\boldsymbol{N}_0$ are i.i.d. complex Gaussian random variables. Consequently, the entries of $\boldsymbol{Y}_0$ are also i.i.d. random variables with the distribution $CN(0, 1+\sigma_0^2)$.

The Golden codeword matrix given by $\boldsymbol{X}^{(t)} = \begin{bmatrix} s_1 & s_3 \\ s_2 & s_4 \end{bmatrix}$ is differentially encoded using $\boldsymbol{X}_0$ as

$$\boldsymbol{X}_n^{(t)} = \boldsymbol{X}_0\boldsymbol{X}^{(t)}, \quad t \in [1:K] \tag{A.4}$$

It is quite obvious, from (A.4), that $\boldsymbol{X}_n^{(t)} = \boldsymbol{X}^{(t)}$ since $\boldsymbol{X}_0$ is an identity matrix. In the GDM-GC scheme,the channel fading matrix is assumed to remain constant for the duration of transmission of each frame of L blocks (quasi-static fading) and only assume independent values in the course of transmitting subsequent L blocks. The received signal in the $t^{th}, t \in [1:K]$ normal block is then expressed as:

$$\boldsymbol{Y}_n^{(t)} = \boldsymbol{H}_n^{(t)}\boldsymbol{X}_n^{(t)} + \boldsymbol{N}_n^{(t)}, \quad t \in [1:K] \tag{A.5}$$

where $\boldsymbol{Y}_n^{(t)} \in \mathbb{C}^{(N_r \times N_t)}$ is the information signal matrix at the receiver. $\boldsymbol{H}_n^{(t)} = \begin{bmatrix}\boldsymbol{h}_1 & \boldsymbol{h}_2\end{bmatrix}$ is the channel fading matrix and $\boldsymbol{N}_n^{(t)} \in \mathbb{C}^{(N_r \times N_t)}$ is the AWGN matrix. The entries of $\boldsymbol{N}_n^{(t)}$ are i.i.d complex RVs with Gaussian distribution $CN(0,\sigma_n^2)$ where $\sigma_n^2 = \frac{2}{\rho_n}$. ρ_n is the SNR of the normal blocks and is discussed further in section 3.3.

3.3 Power Allocation in GDM-GC

A fraction of power, denoted as δ, is removed from each normal block. This power is then re-allocated to the reference block as given by [16]. Mathematically, we represent this as $\rho_0 = (1+K\delta)\rho$ and $\rho_n = (1-\delta)\rho$ where ρ is the system's average SNR, ρ_0 is the average SNR of the reference block and ρ_n is the average SNR of the normal blocks.

Since $\boldsymbol{Y}_0$ is regarded as the estimation of the channel in (A.5), the received signal contains two noise elements, each with a distinct noise variance. Therefore, an effective SNR is obtained by summing the two distinct variances. Consequently, the effective SNR, ρ_e is expressed as [16]

$$\rho_e = \left[\frac{2(1-\delta)(1+K\delta)}{2+(K-1)\delta}\right]\rho, \tag{A.6}$$

with the optimal value for δ obtained by minimizing the noise variance in (A.6) to give

$$\delta_{optimum} = \frac{\sqrt{K}-1}{\sqrt{K}+K}, \tag{A.7}$$

It is noted that the power allocation scheme can find applications in all differential modulation techniques since no information is required on the statistics of the system.

4 Error Performance Analysis of GDM-GC

In order to evaluate the error performance of the GDM-GC scheme, we derive a closed form expression for its theoretical ABEP. In this scheme, the channel $\boldsymbol{H}_n^{(t)} = \begin{bmatrix}\boldsymbol{h}_1 & \boldsymbol{h}_2\end{bmatrix}$ in the received signal (A.5) is unknown at the receiver. However, this channel can be estimated using the received signal at the reference block in (A.3). Consequently, the received signal matrix in (A.5) can be converted into an equivalent received signal matrix containing $\boldsymbol{Y}_0$. Substituting (A.4) in (A.5) and noting that $\boldsymbol{H}_n^{(t)} = \boldsymbol{H}_0$, we re-write (A.5) as:

$$\boldsymbol{Y}_n^{(t)} = \boldsymbol{Y}_0\boldsymbol{X}^{(t)} - \boldsymbol{N}_0\boldsymbol{X}^{(t)} + \boldsymbol{N}_n^{(t)}, \tag{A.8}$$

The entries of the channel estimation $\boldsymbol{Y}_0$ and noise $\boldsymbol{N}_e$, where $\boldsymbol{N}_e = \boldsymbol{N}_n^{(t)} - \boldsymbol{N}_0\boldsymbol{X}^{(t)}$, are complex Gaussian RVs which are independent and identically distributed as $CN(0, 1+\sigma_0^2)$ and $CN(0,\sigma_e^2)$ respectively, where $\sigma_e^2 = \sigma_n^2 + \sigma_0^2$. As a result, the channel estimation $\boldsymbol{Y}_0$ and the noise term $\boldsymbol{N}_e$ have their variances given by $\left(1+\frac{2}{\rho_0}\right)$ and $\left(\frac{2}{\rho_n}+\frac{2}{\rho_0}\right)$. Therefore, the error performance analysis of GDM-GC is based on the equivalent received signal (A.8). Since $\boldsymbol{Y}_0$ in (A.8) is known at the receiver, the ABEP of GDM-GC is derived from the classical expression of the symbol error probability for MQAM in Eq. (8.10) of [9] together with the Gaussian Q-function which is tightly approximated by the trapezoidal rule of numerical intergration. The ABEP of the GDM-GC scheme is therefore derived as:

$$\begin{aligned} P_e \geq \frac{c}{n\log_2 M}\Bigg[&\frac{1}{2}\prod_{i=1}^{2}\left(\frac{2}{2+\omega_i d\hat{\gamma}}\right)^{N_r} - \left(\frac{c}{2}\right)\times\prod_{i=1}^{2}\left(\frac{1}{1+\omega_i d\hat{\gamma}}\right)^{N_r} \\ &+(1-c)\sum_{k=1}^{n-1}\prod_{i=1}^{2}\left(\frac{u_k}{u_k+\omega_i d\hat{\gamma}}\right)^{N_r} + \sum_{k=n}^{2n-1}\prod_{i=1}^{2}\left(\frac{u_k}{u_k+\omega_i d\hat{\gamma}}\right)^{N_r}\Bigg], \end{aligned} \tag{A.9}$$

with $n \geq 10$ being the total amount of summations required to achieve convergence, $\hat{\gamma} = \frac{1}{2}\left(1+\sigma_0^2\right)\left(\frac{1}{\rho_0}+\frac{1}{\rho_n}\right)^{-1}$, $c = 1-\frac{1}{\sqrt{M}}, d = \frac{3}{M-1}, \omega_1 = \left|\frac{1}{\sqrt{5}}\alpha\tau\right|^2, \omega_2 = \left|\frac{1}{\sqrt{5}}\hat{\alpha}\mu\right|^2$, and $u_k = 2\sin^2\left(\frac{k\pi}{4n}\right)$.

5 Detection Schemes

The optimal detection technique for GDM-GC is by using ML decoding. However,the computational complexity of ML decoding is extremely high for the Golden code (proportional to $\mathcal{O}(M^4)$) as a result of the four complex-valued symbols contained in its matrix. In order to reduce this complexity without compromising the performance, we employ sphere decoding.

5.1 ML Detection of GDM-GC

Since the channel estimation $\boldsymbol{Y}_0$ in (A.8) is known at the receiving end, we can apply coherent detection directly to (A.8). The expression for maximum likelihood (ML) detection of (A.8) is given by:

$$\hat{x}_i, i \in [1:4] = \underset{x_i \in \boldsymbol{\Omega}_M, i \in [1:4]}{\operatorname{argmin}} \left\| \boldsymbol{Y}_n^{(t)} - \boldsymbol{Y}_0 \boldsymbol{X}^{(t)} \right\|_F^2, \tag{A.10}$$

where $\hat{x}_i, i \in [1:4]$ are the estimated symbols at the receiver. From (A.10), it is clear that $\boldsymbol{Y}_0$ is regarded as the estimation of the channel.

5.2 Low Complexity Detection of GDM-GC

In (A.10), the maximum likelihood detector utilizes channel state information to carry out a full search over the signal set to achieve optimal error performance. The main drawback, however, is that ML detection has a computational complexity proportional to $\mathcal{O}(M^4)$, which is exceptionally high. In [12], a comparison of the determinants of two covariant matrices results in a simple but fast detection algorithm for Golden code. In [17], a low complexity scheme is proposed for the Golden codeword–based MQAM (GC-MQAM) as well as component–interleaved MQAM (CI-GC-MQAM) for single-input multiple-output (SIMO) systems, assuming a perfect CSI at the receiver. However, in this paper, the sphere decoder (SD) has been employed as an alternative, providing ML performance with reduced complexity [18].

The main objective of sphere decoding is to confine the detection search space to a hyper-sphere of radius, d around the received signal. [18] The SD algorithm seeks to find all points $x_i \in \boldsymbol{\Omega}_M, i \in [1:4]$ that satisfy $\left\| \boldsymbol{Y}_n^{(t)} - \boldsymbol{Y}_0 \boldsymbol{X}^{(t)} \right\|^2 \leq d^2$ without having to examine the distance to all elements in $\boldsymbol{\Omega}_M$. An efficient way to check this criterion is to make use of QR factorisation of $\boldsymbol{H} \in \mathbb{C}^{(N_r \times N_t)}$ such that $\boldsymbol{H} = \boldsymbol{QR}$, where $\boldsymbol{R} \in \mathbb{C}^{(N_r \times N_t)}$ and $\boldsymbol{Q} \in \mathbb{C}^{(N_r \times N_r)}$ represent an upper triangular matrix and orthogonal matrix respectively. From (A.10), we may write:

$$\left\| \boldsymbol{Y}_n^{(t)} - \boldsymbol{Y}_0 \boldsymbol{X}^{(t)} \right\|^2 = \left\| \boldsymbol{Q}^H \boldsymbol{Y}_n^{(t)} - \boldsymbol{Q}^H \boldsymbol{Q} \boldsymbol{R} \boldsymbol{X}^{(t)} \right\|^2 = \left\| \hat{\boldsymbol{Y}}_n^{(t)} - \boldsymbol{R} \boldsymbol{X}^{(t)} \right\|^2, \tag{A.11}$$

where $\hat{\boldsymbol{Y}}_n^{(t)} = \boldsymbol{Q}^H \boldsymbol{Y}_n^{(t)}$. Note that $\boldsymbol{Y}_0$ is used to estimate the channel $\boldsymbol{H}$ in this paper. The sphere decoder then solves the problem:

$$\hat{x}_i, i \in [1:4] = \underset{x_i \in \boldsymbol{\Omega}_M, i \in [1:4]}{\operatorname{argmin}} \left\| \boldsymbol{Q}^H \boldsymbol{Y}_n^{(t)} - \boldsymbol{R}\boldsymbol{X}^{(t)} \right\|_F^2, \tag{A.12}$$

where $\hat{x}_i, i \in [1:4]$ are the estimated symbols at the receiver, $\boldsymbol{\Omega}_M$ is the set of all points which satisfy $\left\| \hat{\boldsymbol{Y}}_n^{(t)} - \boldsymbol{R}\boldsymbol{X}^{(t)} \right\|^2 \leq d^2$ and d is the radius of the hyper-sphere. It is worth noting that the search radius must be chosen carefully. Choosing a very small value of d provides only a few points inside the hyper-sphere while choosing a large d increases the complexity of the decoder since it searches through many candidates before finding the best. A typical criteria in choosing d is described in [19]. The detection complexity of (A.12) remains high for $M \geq 64$. In order to significantly reduce this complexity, it is important that the entire signal set of (A.12) be replaced with a detection subset defined as [20]:

Definition 1: The i^{th} symbol detection subset of a given i^{th} symbol, x_i, is expressed as $\boldsymbol{\Omega}(x_i, \epsilon) = \{x_k, |x_k - x_i|^2 \leq \epsilon, k \in [1:M]\}$.

Therefore, the following steps summarise the proposed sphere detection of GDM-GC with detection subset.

Initialisation: Establish a symbol detection subset for every symbol $x_i, i \in [1:M]$

Step 1: Perform QR factorisation of $\boldsymbol{H}$.

Step 2: Estimate the Golden symbols s_1, s_2, s_3 and s_4 using $\hat{\boldsymbol{Y}}_n^{(t)} = \boldsymbol{R}\boldsymbol{X}^{(t)} + \hat{\boldsymbol{N}}_n^{(t)}$ where $\hat{\boldsymbol{Y}}_n^{(t)} = \boldsymbol{Q}^H \boldsymbol{Y}_n^{(t)}$ and $\hat{\boldsymbol{N}}_n^{(t)} = \boldsymbol{Q}^H \boldsymbol{N}_n^{(t)}$

Step 3: Estimate $x_i, i \in [1:4]$ of MQAM symbols using the estimated Golden symbols as follows:

$$x_1 = \frac{\sqrt{5}}{\beta}\left(\frac{\tau s_4}{\hat{\alpha}} - \frac{\mu s_1}{\alpha}\right) \tag{A13.1}$$

$$x_2 = \frac{\sqrt{5}}{\beta}\left(\frac{s_1}{\alpha} - \frac{s_4}{\hat{\alpha}}\right) \tag{A13.2}$$

$$x_3 = \frac{\sqrt{5}}{\beta}\left(\frac{\tau s_3}{j\hat{\alpha}} - \frac{\mu s_2}{\alpha}\right) \tag{A13.3}$$

$$x_4 = \frac{\sqrt{5}}{\beta}\left(\frac{s_2}{\alpha} - \frac{s_3}{j\hat{\alpha}}\right) \tag{A13.4}$$

where $\beta = \tau - \mu$

Step 4: Obtain the detection subset for the estimated symbols in step 3.

Step 5: Carry out sphere detection based on (A.12).

6 Detection Complexity Analysis

In this section, we analyse the computational complexity of the GDM-GC scheme. For the coherent receiver, the optimal ML detection complexity can be viewed as a measure of the maximum number of symbols that require mutual detection in minimising the ML decoding metric [21]. Typically, the Golden code exhibits a high ML detection complexity of $\mathcal{O}(M^4)$, where M is the modulation order [12]. This is due to the four symbols contained in its matrix. On the other hand, the complexity of SD is proportional to the number of nodes visited within the hyper-sphere in order to obtain a solution.

For GDM-GC with SD, we first examine the pre-detection and initialisation stages of the algorithm. This consists of calculating the upper triangular matrix $\boldsymbol{R}$ from the matrix $\boldsymbol{H}$ using QR decomposition. The orthogonal matrix $\boldsymbol{Q}$ is then used to establish the minimum and maximum bounds for each closest lattice point. For the $2 \times N_r$ STBC the complexity of QR decomposition via the Householder algorithm [22] for each iteration step k is $4(2-k)(N_r-k)$. Iterating over all transmit antennas yields

$$C_{QR} = \sum_{k=1}^{2} 4(2-k)(N_r-k) = 8N_r - \frac{16}{3} \tag{A.14}$$

However, for large dimensional lattices, the computational complexity of the pre-detection stage is minimal compared to the searching stage and therefore does not have any significant influence on the total complexity of the algorithm [23]. Unlike the initialisation stage of the detection, it is not practical to build a closed-form expression for the number of real-valued multiplications in the search stage since the number of loops in the search algorithm is completely random. Since the iterative search of the optimal point in the lattice of an SD algorithm is entirely random, the complexity of GDM-GC with SD is best estimated by Monte Carlo simulations. Consequently, we simulate the complexity of the proposed schemes using SD with the depth-first search.

The simulations are carried out to obtain the average number of nodes visited, yielding results that are represented here only as 'complexity'. It should be noted, however, that the complexity of GDM-GC with ML detection is based on numerical values and is only used in **Figure A.1** for comparison purposes. In addition, we only consider the 16QAM signal constellation with $N_r = 2$ and $N_r = 4$. Other constellation sizes can be analysed similarly and are only omitted here for conciseness.

Figure A.1 clearly illustrates the following:

(i) The complexity of SD decreases with increasing SNR. In other words, at low SNR, the SD algorithm searches through most nodes in the tree hence the resulting complexity becomes

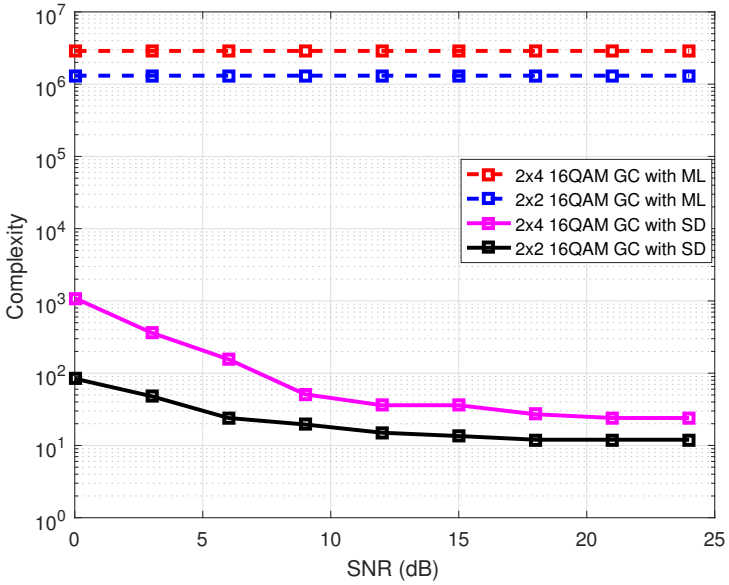

Figure A.1: Detection complexity of GDM-GC for 16QAM with $N_r = 2$ and $N_r = 4$

exponential.

(ii) The complexity of GDM-GC with SD for $N_r = 4$ is higher that the complexity of GDM-GC with SD for $N_r = 2$.

(iii) Maximum likelihood detection exhibits a high complexity compared to sphere decoding.

7 Simulation Results

In this section, we present the Monte Carlo simulation results for the proposed GDM-GC scheme with the following assumptions and parameters:

(a) for all configurations, the number of transmit antennas is assumed to be $N_t = 2$

(b) we also assume a quasi-static Rayleigh frequency flat fading channel with AWGN

(c) the simulations are carried out for:

(i) $M = 16$ and $M = 64$

(ii) $N_r = 2$ and $N_r = 4$

(iii) $L = 100$ and $L = 400$

(d) The length of the transmitted message bits used in the simulations is $2k$, where $k = \log_2 M$

By carrying out simulations, a plot of the bit error rate versus the average SNR in decibels (dB) is

provided for different schemes of the Golden code STBC. The simulated curves are then compared with the corresponding theoretical lower bound obtained from (A.9).

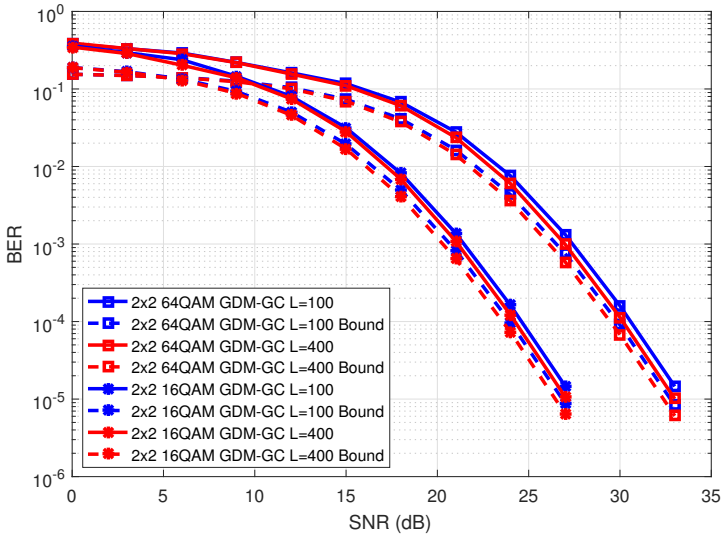

Figure A.2: BER Performance for 16QAM and 64QAM GDM-GC with $N_r = 2$

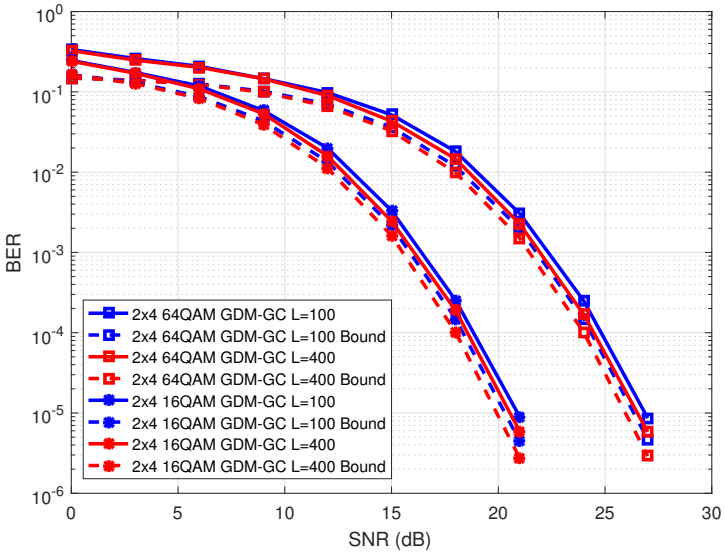

Figure A.3: BER Performance for 16QAM and 64QAM GDM-GC with $N_r = 4$

From **Figure A.2** and **Figure A.3**, we observe that the simulated results lie well within the theoretical bit error bounds, especially at higher values of SNR. This is true for both the 16QAM and 64QAM configurations. In addition, it is evident from **Figure A.4** and **Figure A.3** that when the frame length is $L = 100$, the proposed GDM-GC scheme suffers a performance penalty of approximately 0.8 dB compared to the coherent detection of GC. However, when the frame length is increased to $L = 400$, the scheme achieves an additional gain of 0.4 dB at a BER of 10^{-4}. This is a small price to pay,

considering that no channel state information is available for GDM-GC.

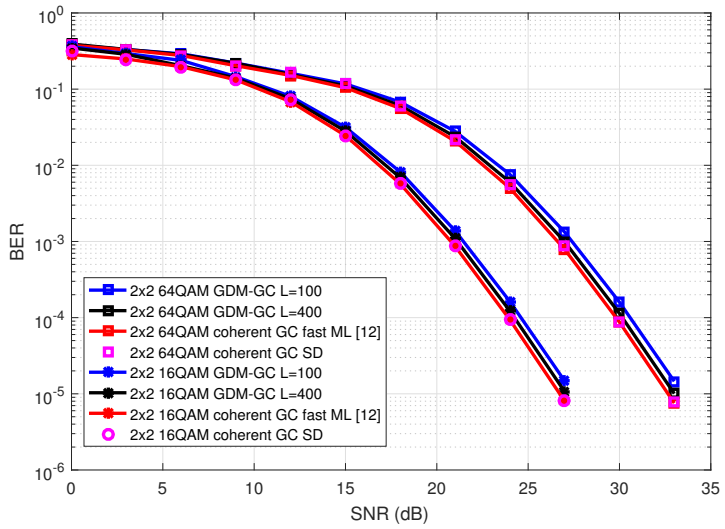

Figure A.4: BER Performance Comparison Between GDM-GC and Coherent Detection with $N_r = 2$

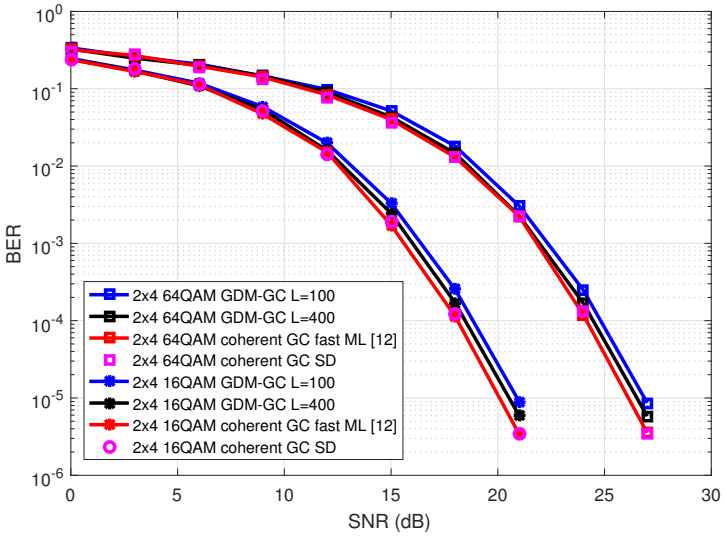

Figure A.5: BER Performance Comparison Between GDM-GC and Coherent Detection with $N_r = 4$

A closer examination of the theoretical results and the simulations reveal that as the frame length L is increased, the error performance of GDM-GC also improves. This is attributed to the fact that the channel matrix at the receiver end is more accurately estimated due to increased transmit power assigned to the reference block. This inevitably reduces the errors that may be sustained while performing detection of information carried by the normal blocks. Consequently, the value of L can be adjusted to a point in which the system's error performance closely matches that of coherent detection. Nevertheless, the value of L must be selected very carefully as it inherently affects the maximum power necessary in the reference block [4].

8 Conclusion

This paper proposed a GDM-GC scheme that uses a novel power allocation technique to enhance error performance. Through simulations and theoretical analysis, it is verified that an increase in the frame length L inevitably helps to improve the error performance of the GDM-GC scheme. This performance, coupled with a substantial reduction in its computational complexity, provides a trade-off between the complexity of the coherent optimal ML detector and the probability of error in non-coherent systems. It is worth noting that although there is a tremendous reduction in the complexity of the proposed schemes with sphere decoding, higher-order constellations $M \geq 64$ still exhibit very high complexity at low SNR regions. Further research investigations should be carried out in this area.

References

[1] L. Zheng and T. DNC, "Diversity and Multiplexing: A fundamental tradeoff in multiple-antenna channels," *IEEE Trans Inform Theory*, vol. 49, no. 5, pp. 1073–1096, 2003.

[2] B. Sklar, *Digital Communications:Fundamentals and Applications, 2nd Edition*. New Jersey: Prentice Hall, 2013.

[3] J. Proakis and M. Salehi, *Digital Communications, 5th Edition*. New York: McGraw Hill, 2007.

[4] L. Li, Z. Fang, Y. Zhu, and Z. Wang, "Generalised differential transmission for STBC systems," ser. IEEE GLOBECOM Telecommunications Conference, New Orleans, USA, December 1–5, 2008.

[5] G. Ganessan and P. Stoica, "Space time block codes: A maximum SNR approach," *IEEE Trans Inform Theory*, vol. 47, no. 4, pp. 1650–1656, 2001.

[6] G. Girish and P. Stoica, "Differential modulation using space time block codes," *IEEE Signal Process Lett*, vol. 9, no. 2, pp. 57–60, 2002.

[7] Z. Chen, G. Zhu, D. Qu, and Y. Liu, "General differential space time modulation," ser. IEEE Global Telecommunications Conference, San Francisco, CA, USA, December 1–5, 2003.

[8] M. Tao and R. Cheng, "Differential space time block codes," ser. IEEE Global Telecommunications Conference, San Antonio, USA, November 25–29, 2001.

[9] M. Simon and M.-S. Alouini, *Digital Communication over Fading Channels: A Unified Approach to Performance Analysis*. A Wiley Interscience Publication, 2000.

[10] K. Kadathlal, H. Xu, and N. Pillay, "Generalized differential scheme for spatial modulation systems," *IET Communications*, vol. 11, no. 13, pp. 2020–2026, 2017.

[11] J. Belfiore, G. Rekaya, and E. Viterbo, "The Golden code: A 2x2 full-rate space-time code with non-vanishing determinants," *IEEE Trans Inform Theory*, vol. 51, no. 4, pp. 1432–1436, 2005.

[12] S. Sirinaunpiboon, A. Calderbank, and S. Howard, "Fast essentially maximum likelihood decoding of the Golden code," *IEEE Trans Inform Theory*, vol. 57, no. 6, pp. 3537–3541, 2011.

[13] L. Luzzi, G. Othman, J. Belfiore, and E. Viterbo, "Golden space-time block coded modulation," *IEEE Trans Inform Theory*, vol. 55, no. 2, pp. 584–597, 2009.

[14] E. Viterbo and Y. Hong, "On the performance of Golden space-time trellis coded modulation over MIMO block fading channels," *IEEE Trans Commun*, vol. 8, no. 6, pp. 2337–2741, 2009.

[15] H. Xu, N. Pillay, and X. Jin, "Golden Codeword based Generalized Differential Alamouti Modulation," *IEEE Access*, vol. 8, no. 1, pp. 65 649–65 657, 2020.

[16] K. Dwarika and H. Xu, "Power allocation and low complexity detector for differential full diversity spatial modulation using two transmit antennas," *Radioengineering*, vol. 26, no. 2, pp. 461–469, 2017.

[17] H. Xu and N. Pillay, "Golden codeword-based modulation schemes for single-input multiple-output systems," *Int Journal Commun Syst*, vol. 32, no. 10, pp. 1–12, July 2019.

[18] S. Han and C. Tellambura, "A complexity-efficient sphere decoder for MIMO systems," ser. 8th Annual IEEE Communications Society, Salt Lake City, UT, USA, September, 2011.

[19] B. Hochwald and S. Brink, "Achieving near-capacity on a multiple-antenna channel," *IEEE Transactions on Communications*, vol. 51, no. 3, 2003.

[20] H. Xu and N. Pillay, "Reduced complexity detection schemes for Golden code systems," *IEEE Access*, vol. 1, no. 1, pp. 139 140–139 149, Dec 2019.

[21] K. Srinath and B. Rajan, "Low-ML decoding complexity, large coding gain, full-rate full-diversity STBC for 2x2 and 4x2 MIMO systems," *IEEE Journal of Selected Topics in Signal Process*, vol. 3, no. 6, 2009.

[22] G. Golub and C. Loan, *Matrix Computations, 4th Edition*. Baltimore: The John Hopkins University Press, 1988.

[23] G. Rekaya and J.-C. Belfiore, "Complexity of ML lattice decoders for the decoding of linear full rate space-time codes," ser. ENST Proceedings, Paris, France, August, 2003.

[24] S. Das, N. Al-Dhahir, and R. Calderbank, "Novel full-diversity high rate STBC for 2 and 4 transmt antennas," *IEEE Communication Letters*, vol. 10, no. 3, pp. 171–173, 2006.

[25] H. Xu, K. Govindasamy, and N. Pillay, "Uncoded space-time labelling diversity," *IEEE Communication Letters*, vol. 20, no. 8, pp. 111–114, 2016.

[26] R. Pillay, N. Pillay, and H. Xu, "Space-time labelling diversity with enhanced spectral efficiency," ser. South Africa Telecommunication Networks and Applications Conference (SATNAC), Western Cape, South Africa, September 2–5, 2018.

[27] B. Hassibi and H. Vikalo, "On the sphere-decoding algorithm I expected complexity," *IEEE Trans Signal Process*, vol. 53, no. 8, pp. 2806–2818, 2005.

[28] J. Jalden and B. Ottersten, "On the complexity of sphere decoding on digital communications," *IEEE Trans Signal Process*, vol. 53, no. 4, 2005.

[29] K. Dwarika and H. Xu, "Differential full-diversity spatial modulation using amplitude phase shift keying," *Radioengineering*, vol. 27, no. 1, pp. 151–159, 2018.

Part III

Paper B

Paper B

Multiple Input Symbol Generalised Differential Golden Code Modulation

1 Abstract

The receiver of a conventional differential modulation scheme performs detection without knowledge of the channel state information (CSI). This results in a 3 dB performance loss compared to coherent modulation. In order to enhance this error performance, generalised differential modulation is utilised. This paper extends the generalised differential modulation scheme to multiple-input symbol Golden code and proposes a multiple-input symbol generalised differential Golden code (MIS-GD-GC) scheme. This scheme improves the error performance when compared to conventional differential multiple-input symbol Golden code (MIS-GC) and achieves a diversity order of $2^l N_r$ compared to the conventional Golden code, where $l \geq 1$ is an integer, N_r is the number of receive antennas and 2^l represents the number of multiple input symbols in the MIS-GC system. We also derive the average bit error probability for the MIS-GD-GC scheme. The simulations of bit error rate (BER) compare very well to the derived theoretical bounds and show that the BER of MIS-GD-GC draws closer to that of coherent MIS-GC as the frame length increases. For instance, at a frame length of $B = 400$, the error performance gap between MIS-GD-GC and its coherent counterpart is only 0.4 dB.

2 Introduction

Over the years, next-generation wireless communication systems have been characterised by an increase in demand for higher data rates and a clamour for highly reliable communication systems. Consequently, multiple-input multiple-output (MIMO) systems have been widely exploited to increase the rate of data transmission and/or ensure improved communication reliability. However, the theoretical analysis of MIMO systems reveals a trade-off between data transmission rate and the reliability of communication regarding diversity order and/or multiplexing gain [1]. In MIMO systems, the diversity order and/or multiplexing gain attained is dependent upon the encoding scheme implemented in that system.

An example of a MIMO system that utilises two transmit antennas is the Alamouti space-time block code (STBC) [2]. In this scheme, the encoder constructs an orthogonal codeword matrix that easily allows for decoupling of the two transmitted symbols. This, in turn, enables a straightforward maximum likelihood (ML) detection in quasi-static frequency-flat Rayleigh fading channels. Consequently, the detection complexity of the Alamouti STBC is very low. It has been shown that the Alamouti STBC achieves full diversity. However, it does not achieve any multiplexing gain [2]. Another example of a MIMO system with two transmit antennas is the Golden code STBC [3, 4]. The conventional Golden code (GC) consists of two pairs of Golden codewords, with each pair comprising of two input symbols. Each pair of the Golden codewords is transmitted in different time slots. Since each input symbol that is transmitted undergoes two different fadings in two time slots, the diversity order of the conventional GC is $2N_r$, where N_r is the number of receive antennas. In contrast with the Alamouti STBC, the Golden code STBC achieves full-multiplexing gain as well as full diversity [5].

A new type of Golden code STBC, referred to as multiple complex symbol Golden code (MCS-Golden code) [6], is proposed. In this scheme, each transmit antenna in the MCS-Golden code system transmits 2^l MCS-Golden codewords in 2^l time slots, where $l \geq 1$ is an integer. This scheme also achieves full-rate, and since every input symbol in MCS-Golden encoding experiences 2^l different fadings in 2^l time slots, the scheme achieves a diversity order of $2^l N_r$ [6]. Clearly, this diversity order is a multiple of the conventional GC diversity order and is therefore referred to as multiple diversity order [6]. This, in turn, significantly improves its error performance compared to the conventional Golden code. The Golden code finds its application in the IEEE 802.16e WiMAX standard [4]. However, the biggest drawback of the Golden code STBC is the exceptionally high detection complexity of the ML detector at the receiver. This high complexity of order $\mathcal{O}(M^4)$ where

M is the modulation order is due to the four complex symbols in the Golden codeword. This high complexity inevitably limits the applications of the Golden code due to increased challenges in hardware implementation. As a result, several research undertakings have been undertaken to reduce the Golden code's detection complexity.

A fast-ML detection scheme that achieves a worst-case complexity of order $\mathcal{O}(M^{2.5})$ was proposed in [4]. Another efficient technique based on reducing the dimensions of the search tree in sphere decoding was also proposed in [7]. However, a 1dB signal-to-noise ratio (SNR) loss is incurred in its error performance compared to the optimal detector. A sphere decoding technique that utilises a detection subset (SD-DS) [8] was recently proposed for the conventional Golden code. However, more recently, a modified version of SD-DS whose detection subset is sorted from the most probable to the least probable was proposed to further reduce the detection complexity [6]. The assumption made in the works of [4] and [6, 8] is that the receiver has perfect knowledge of the channel state information (CSI). Even so, the estimation of the CSI inevitably contributes to the complexity of the receiver. In order to carry out detection of transmitted symbols at the receiver without knowledge of the CSI, differential modulation is utilized. However, the main drawback of the differential modulation scheme is its 3 dB error performance loss when compared to coherent modulation [9].

A generalised differential transmission scheme [9] was proposed to enhance the error performance of the conventional differential modulation. In this scheme, each transmission frame consists of a reference block that estimates the CSI as well as normal blocks that are responsible for conveying information. The error performance of the system is improved by allocating more transmission power to the reference block. Consequently, the error performance of this scheme is shown to outperform the conventional differential transmission and approach that of coherent detection. However, due to the proposed structure of its frame, this scheme cannot be applied to the more spectrally efficient M-ary quadrature amplitude modulation (MQAM) constellation because of phase ambiguity issues. In addition, no attempt is made to derive the theoretical error performance of the scheme. While other differential schemes are also proposed in [10] and [11], they are only applicable in arbitrarily correlated channel conditions and use the more complex ML decoder at the receiver. In other research work, the generalised differential transmission scheme was also applied to amplify-and-forward relay networks [7, 12] and on spatial modulation [13].

Motivated by the works of [6], [9], [10], and [11] we extend the generalised differential modulation technique to multiple-input symbol Golden code (MIS-GC), hereinafter referred to as the multiple-input symbol generalised differential Golden code (MIS-GD-GC). The proposed scheme significantly enhances the error performance compared to conventional differential MIS-GC. Making use of the

union bound method, we then derive the theoretical average bit error probability (ABEP) based on the equivalent transmission model of MIS-GD-GC. We also incorporate the low complexity sphere decoding with sorted detection subset to decode the system. In summary, this paper provides the following contributions:

1. A new differential modulation scheme, MIS-GD-GC modulation, is presented.
2. The average bit-error probability of MIS-GD-GC modulation is also derived.

The remaining part of this paper is organised as follows: The system model for the two-input symbol and the multiple-input symbol Golden code is presented in section 2. Section 3 introduces the generalised differential Golden code. We then provide the equivalent detection model of the proposed MIS-GD-GC and incorporate sphere decoding with sorted detection subset in section 4. The error performance analysis of MIS-GD-GC is discussed in section 5, while its computational complexity is analysed in section 6. Section 7 presents the Monte Carlo simulation results. Section 8 concludes the paper.

Notation: Bold letters are used to denote vectors and matrices. The transpose, Hermitian and Frobenius norm operations are denoted by $(\cdot)^T$, $(\cdot)^H$ and $\| \cdot \|_F$, respectively. The expected value of an argument is denoted by $E[\cdot]$. $\mathfrak{D}(\cdot)$ represents the demodulator function for the signal constellation. The inverse function is denoted by $(\cdot)^{-1}$, and j denotes a complex number.

3 System Model

The conventional Golden code is the basis upon which the proposed MIS-GD-GC is formulated. This section briefly presents the two-input symbol Golden code (2IS-GC) and the multiple-input symbol Golden code (MIS-GC).

3.1 Two-Input Symbol Golden Code (2IS-GC)

Consider an $N_t \times N_r$ Golden code STBC with two transmit antennas $(N_t = 2)$ and two or more receive antennas $(N_r \geq N_t)$ [3]. The input of the encoder is fed with a bitstream of information denoted by $\boldsymbol{b}_t^k = [b_{t,1}^k b_{t,2}^k \cdots b_{t,r}^k], r = \log_2 M, k \in [1 : N_t], t \in [1 : 2]$, where M denotes the modulation order. The bitstream $\boldsymbol{b}_t^k$ is subsequently passed through a mapper which maps the r input bits onto constellation points from the signal set $\boldsymbol{\Omega}_M$ in the Argand plane, yielding the symbol $s_{0,t}^k, t \in [1 : 2]$ and $k \in [1 : N_t]$. In addition, let $s_{0,t}^k \in \boldsymbol{\Omega}_M$, where $\boldsymbol{\Omega}_M$ represents the signal set of either MQAM or M-ary phase-shift keying (MPSK) signals. The encoder of the Golden code STBC uses the four input symbols $s_{0,t}^k$ to generate four Golden codewords:

$s^1_{1,1} = \frac{\alpha}{\sqrt{5}}(s^1_{0,1}+s^1_{0,2}\tau)$, $s^2_{1,2} = \frac{\hat{\alpha}}{\sqrt{5}}(s^1_{0,1}+s^1_{0,2}\mu)$, $s^2_{1,1} = \frac{\alpha}{\sqrt{5}}(s^2_{0,1}+s^2_{0,2}\tau)$ and $s^1_{1,2} = j\frac{\hat{\alpha}}{\sqrt{5}}(s^2_{0,1}+s^2_{0,2}\mu)$ where $\tau = \frac{1+\sqrt{5}}{2}, \mu = 1-\tau, \alpha = 1+j\mu, \hat{\alpha} = 1+j\tau$ and $j = \sqrt{-1}$.

Let $s^1_{1,1} \in \mathbf{\Omega}_G$ where $\mathbf{\Omega}_G$ is the signal set of $s^1_{1,1}$. Consequently, $s^1_{1,2} \in \mathbf{\Omega}_G$, $s^2_{1,1} \in \mathbf{\Omega}_G$ and $s^2_{1,2} \in \mathbf{\Omega}_G$ as shown in Appendix A of [8]. The four Golden codewords are grouped into two pairs as follows:

$\left\{\frac{\alpha}{\sqrt{5}}(s^1_{0,1}+s^1_{0,2}\tau), \frac{\hat{\alpha}}{\sqrt{5}}(s^1_{0,1}+s^1_{0,2}\mu)\right\}$ and $\left\{\frac{\alpha}{\sqrt{5}}(s^2_{0,1}+s^2_{0,2}\tau), j\frac{\hat{\alpha}}{\sqrt{5}}(s^2_{0,1}+s^2_{0,2}\mu)\right\}$

It should be noted that each of these two pairs is just a combination of two input symbols; thus, they convey the same information. The four Golden codewords form the Golden codeword matrix given by (B.1) [3]:

$$\boldsymbol{S} = \begin{bmatrix} s^1_{1,1} & s^1_{1,2} \\ s^2_{1,1} & s^2_{1,2} \end{bmatrix}, \tag{B.1}$$

This conventional Golden code is also referred to in this paper as the two-input symbol Golden code (2IS-GC). The two input symbols in each pair of the Golden codewords can be extended into multiple input symbols in each vector of Golden codewords and is hereafter referred to as multiple-input-symbol Golden code (MIS-GC).

3.2 Multiple-Input Symbol Golden Code (MIS-GC)

Consider an MIS-GC system whose antenna configuration is similar to the one described in section 3.1. In this case, however, the input of the encoder is fed with a bitstream of information denoted by $\boldsymbol{b}^k_t = [b^k_{t,1}b^k_{t,2}\cdots b^k_{t,r}], r = \log_2 M, k \in [1:N_t], t \in [1:2^l]$ where l is a positive integer, $l \geq 1$. The bitstream $\boldsymbol{b}^k_t$ is subsequently passed through a mapper which takes the r input bits and maps them onto constellation points from the signal set $\mathbf{\Omega}_M$ in the Argand plane. This yields symbol $s^k_{0,t}, s^k_{0,t} \in \mathbf{\Omega}_M$. We also assume that $E\left[|s^k_{0,t}|^2\right] = 1$. The encoding of the MIS-GC is based on that of the conventional Golden code [6].

For the $m^{th}, m \in [1:l]$ encoding, the outputs are expressed as [6]:

$$s^k_{m,2n-1} = \frac{\alpha}{\sqrt{5}}\left(s^k_{m-1,n} + s^k_{m-1,n+2^{l-1}}\tau\right), \tag{B2.1}$$

$$s^k_{m,2n} = \frac{\hat{\alpha}}{\sqrt{5}}\left(s^k_{m-1,n} + s^k_{m-1,n+2^{l-1}}\mu\right), \tag{B2.2}$$

where $n \in [1:2^{l-1}]$ with l being the number of decoding iterations. It should be noted at this point that, for conciseness, only the pair of the Golden codewords $\left\{\frac{\alpha}{\sqrt{5}}(s^1_{0,1}+s^1_{0,2}\tau), \frac{\hat{\alpha}}{\sqrt{5}}(s^1_{0,1}+s^1_{0,2}\mu)\right\}$ has been used in the construction of the MIS-GC. Since $E\left[|s^k_{0,t}|^2\right] = 1$, we also have $E\left[|s^k_{m,t}|^2\right] = 1$ where $m \in [1:l]$ and $t \in [1:2^l]$.

Table B.1: Encoding for the four-input symbol Golden code (4IS-GC)

$\mathbf{s^k_{0,t}}$	$\mathbf{1^{st}}$**Encoding**	$\mathbf{2^{nd}}$**Encoding**
$s^k_{0,1}$	$s^k_{1,1} = \frac{\alpha}{\sqrt{5}}(s^k_{0,1} + s^k_{0,3}\tau)$	$s^k_{2,1} = \frac{\alpha}{\sqrt{5}}(s^k_{1,1} + s^k_{1,3}\tau)$
$s^k_{0,2}$	$s^k_{1,2} = \frac{\hat{\alpha}}{\sqrt{5}}(s^k_{0,1} + s^k_{0,3}\mu)$	$s^k_{2,2} = \frac{\hat{\alpha}}{\sqrt{5}}(s^k_{1,1} + s^k_{1,3}\mu)$
$s^k_{0,3}$	$s^k_{1,3} = \frac{\alpha}{\sqrt{5}}(s^k_{0,2} + s^k_{0,4}\tau)$	$s^k_{2,3} = \frac{\alpha}{\sqrt{5}}(s^k_{1,2} + s^k_{1,4}\tau)$
$s^k_{0,4}$	$s^k_{1,4} = \frac{\hat{\alpha}}{\sqrt{5}}(s^k_{0,2} + s^k_{0,4}\mu)$	$s^k_{2,4} = \frac{\hat{\alpha}}{\sqrt{5}}(s^k_{1,2} + s^k_{1,4}\mu)$

Using (B2.1) and (B2.2), **Table B.1** illustrates the encoding for four-input symbol Golden code (4IS-GC). From **Table B.1**, it can be seen that the output codeword $s^k_{2,t}, t \in [1:4]$ is a combination of all input symbols $s^k_{0,t}, t \in [1:4]$. This paper, therefore, refers to $s^k_{l,t}, t \in [1:2^l]$ as MIS-GC codewords.

Each transmit-antenna in MIS-GC transmits 2^l MIS-GC codewords in 2^l time slots rendering the MIS-GC a full-rate STBC. In addition, since every input symbol in the MIS-GC encoder undergoes 2^l different fadings in 2^l time slots, the MIS-GC achieves a diversity order $2^l N_r$. This, in turn, improves the system's error performance in comparison to 2IS-GC. The MIS-GC codeword matrix may be written as [6]:

$$\begin{bmatrix} \boldsymbol{S}_1 & \cdots & \boldsymbol{S}_{2^l} \end{bmatrix} = \begin{bmatrix} s^1_{l,1} & \cdots & s^1_{l,2^l} \\ s^2_{l,1} & \cdots & s^2_{l,2^l} \end{bmatrix}, \tag{B.3}$$

where $\boldsymbol{S}_t = \begin{bmatrix} s^1_{l,t} & s^2_{l,t} \end{bmatrix}^T, t \in [1:2^l]$.

4 Generalised Differential Golden Code

In generalised differential Golden code modulation, every frame consists of B blocks. The first block acts as a reference to all the subsequent $(B-1)$ blocks and is typically referred to as a reference block. The other $(B-1)$ blocks are responsible for conveying information during each transmission and are referred to in this paper as data blocks. In order to enhance error performance, the reference block is transmitted with more power than that of the data blocks. Optimal allocation of power between the reference and the data blocks has been presented in open literature [14, 15]. Let the transmit power of the conventional differential modulation be denoted by ρ. Each frame, therefore, has a total transmit power of $B\rho$. For a constant transmit power, the optimal power ρ_0 allocated to the reference block

and the optimal power ρ_n allocated to each data block are respectively given by: [15]

$$\rho_0 = \frac{B}{1+\sqrt{(B-1)}}\rho, \tag{B4.1}$$

$$\rho_n = \frac{B}{(B-1)+\sqrt{(B-1)}}\rho, \tag{B4.2}$$

A key point to note is that in generalised differential Golden code modulation, the reference block transmission is used to estimate the channel at the receiver. In addition, we assume that the channels over which the B blocks are transmitted are quasi-static frequency-flat Rayleigh fading.This means that the channels do not change during the transmission of the first set of B blocks and only assume independent values during transmission of the next set of B blocks.

4.1 Two-Input Symbol Generalised Differential Golden Code (2IS-GD-GC)

Since the reference block transmission is used to estimate the channel, the received signal at the reference block of 2IS-GD-GC can be expressed as: [16]

$$\hat{\boldsymbol{h}}_{t,k} = \boldsymbol{h}_{t,k} + \boldsymbol{w}_{t,k}, \;\; t \in [1:2], k \in [1:2], \tag{B.5}$$

where $\hat{\boldsymbol{h}}_{t,k} \in \mathbb{C}^{(N_r \times 1)}$ represents the channel gain vector, while the vector $\boldsymbol{w}_{t,k} \in \mathbb{C}^{(N_r \times 1)}$ represents the additive white Gaussian noise (AWGN), $t \in [1:2], k \in [1:2]$. The entries $\boldsymbol{h}_{t,k}$ and $\boldsymbol{w}_{t,k}$ are independent and identically distributed (iid) complex Gaussian random variables (RVs) with the distribution $CN(0,1)$ and $CN(0,\sigma_0^2)$ respectively, with $\sigma_0^2 = \frac{1}{\rho_0}$. Like the entries of $\boldsymbol{h}_{t,k}$ and $\boldsymbol{w}_{t,k}$, the entries of $\hat{\boldsymbol{h}}_{t,k}$ are also iid RVs with the distribution $CN(0, 1+\sigma_0^2)$. It should be noted that $\hat{\boldsymbol{h}}_{t,k}$ in (B.5) is regarded as the estimation of $\boldsymbol{h}_{t,k}$. In 2IS-GD-GC, the four Golden codewords are transmitted in two time slots. The received information signal for the data blocks may be expressed as:

$$\boldsymbol{y}_1 = \boldsymbol{h}_{1,1}s_{1,1}^1 + \boldsymbol{h}_{1,2}s_{1,1}^2 + \boldsymbol{n}_1, \tag{B6.1}$$

$$\boldsymbol{y}_2 = \boldsymbol{h}_{2,1}s_{1,2}^1 + \boldsymbol{h}_{2,2}s_{1,2}^2 + \boldsymbol{n}_2, \tag{B6.2}$$

where $\boldsymbol{y}_t \in \mathbb{C}^{(N_r \times 1)}, t \in [1:2]$ represents the t^{th} received signal vector. The AWGN vector is given by $\boldsymbol{n}_t \in \mathbb{C}^{(N_r \times 1)}, t \in [1:2]$ The entries of $\boldsymbol{n}_t$ are iid complex Gaussian RVs with the distribution $CN(0,\sigma_n^2), \sigma_n^2 = \frac{2}{\rho_n}$. It is evident from (B6.1) and (B6.2) that 2IS-GD-GC is a full-rate code since each transmit-antenna transmits two input symbols in two time slots. It also achieves full-diversity order ($2N_r$) since each transmitted input symbol undergoes two different fadings during the two time slots.

4.2 Multiple-Input Symbol Generalised Differential Golden Code (MIS-GD-GC)

As mentioned in the previous section, the transmission in the reference block is used to estimate the channel at the receiver of MIS-GD-GC. Therefore, the received signal at the reference block of this system may be expressed as:

$$\hat{\boldsymbol{h}}_{t,k} = \boldsymbol{h}_{t,k} + \boldsymbol{w}_{t,k}, \quad t \in [1 : 2^l], k \in [1 : 2], \tag{B.7}$$

where $\hat{\boldsymbol{h}}_{t,k}$, $\boldsymbol{h}_{t,k}$ and $\boldsymbol{w}_{t,k}$ in (B.7) are similar to the discussions of $\hat{\boldsymbol{h}}_{t,k}$, $\boldsymbol{h}_{t,k}$ and $\boldsymbol{w}_{t,k}$ in (B.5). Also, as discussed in the previous section, the entries of $\hat{\boldsymbol{h}}_{t,k}$ are iid complex Gaussian RVs with the distribution $CN(0, 1 + \sigma_0^2)$. In MIS-GD-GC, the 2^l MIS-GC codewords are transmitted in 2^l time slots. The received signal for time slot $t, t \in [1 : 2^l]$ is expressed in general form as:

$$\boldsymbol{y}_t = \boldsymbol{H}_t \boldsymbol{S}_t + \boldsymbol{n}_t, \tag{B.8}$$

where $\boldsymbol{H}_t = \begin{bmatrix} \boldsymbol{h}_{t,1} & \boldsymbol{h}_{t,2} \end{bmatrix}$ and $\boldsymbol{S}_t$ is as defined in (B.3). The vectors $\boldsymbol{y}_t, \boldsymbol{h}_{t,k}, k \in [1 : 2]$, and $\boldsymbol{n}_t$ are similar to those discussed in (B6.1) and (B6.2). It should be noted that the received signal expression in (B.8) is with respect to the transmitted MIS-GC codewords. However, we can also obtain an expression of the received signal with respect to the transmitted MQAM input symbols $s_{0,t}^k, k \in [1 : 2], t \in [1 : 2^l]$. This is discussed further in section 5.2. It is evident from (B.7) and (B.8) that MIS-GD-GC is also a full rate code since each transmit-antenna transmits 2^l input symbols in 2^l time slots. It also achieves a diversity order of $2^l N_r$ since each transmitted input symbol undergoes 2^l different fadings during 2^l time slots. Note that both 2IS-GD-GC and MIS-GD-GC are designed with two transmit antennas in order to retain the full rate full diversity property of the conventional GC.

5 Detection of the Generalised Differential Golden Code Modulation

This section first presents the equivalent detection model for 2IS-GD-GC and MIS-GD-GC and then describes the sphere detection of the multiple-input symbol generalised differential Golden code. Lastly, we incorporate sorted detection subset in the sphere decoding of the MIS-GD-GC system.

5.1 Equivalent Detection Model for 2IS-GD-GC Modulation

In the 2IS-GD-GC scheme, $\boldsymbol{h}_{t,k}, t \in [1 : 2], k \in [1 : 2]$ in the received signals in (B6.1) and (B6.2) is unknown at the receiver. Therefore, we cannot directly apply coherent detection to (B6.1) and (B6.2). However, since the received signals at the reference block in (B.5) can be regarded as the channel estimations for $\boldsymbol{h}_{t,k}$, the received signals given in (B6.1) and (B6.2) can be converted into equivalent

received signals containing $\hat{\boldsymbol{h}}_{t,k}, t \in [1:2], k \in [1:2]$. Substituting $\boldsymbol{h}_{t,k}$ with $\hat{\boldsymbol{h}}_{t,k}$ in (B6.1) and (B6.2) and re-writing (B6.1) and (B6.2) yields:

$$\boldsymbol{y}_1 = \hat{\boldsymbol{h}}_{1,1}s^1_{1,1} + \hat{\boldsymbol{h}}_{1,2}s^2_{1,1} + \hat{\boldsymbol{n}}_1, \tag{B9.1}$$

$$\boldsymbol{y}_2 = \hat{\boldsymbol{h}}_{2,1}s^1_{1,2} + \hat{\boldsymbol{h}}_{2,2}s^2_{1,2} + \hat{\boldsymbol{n}}_2, \tag{B9.2}$$

where $\hat{\boldsymbol{n}}_1 = \boldsymbol{n}_1 - \boldsymbol{w}_{1,1}s^1_{1,1} - \boldsymbol{w}_{1,2}s^2_{1,1}$ and $\hat{\boldsymbol{n}}_2 = \boldsymbol{n}_2 - \boldsymbol{w}_{2,1}s^1_{1,2} - \boldsymbol{w}_{2,2}s^2_{1,2}$. The entries of $\hat{\boldsymbol{h}}_{t,k}, t \in [1:2], k \in [1:2]$ and those of $\hat{\boldsymbol{n}}_t, t \in [1:2]$ are iid complex Gaussian RVs with the distribution $CN(0, 1+\sigma_0^2)$ and $CN(0, \sigma_\epsilon^2)$ respectively where $\sigma_\epsilon^2 = \sigma_n^2 + 2\sigma_0^2 = \frac{2}{\rho_n} + \frac{2}{\rho_0}$.

5.2 Equivalent Detection Model for MIS-GD-GC Modulation

Similar to the case in section 5.1, the signals received at the reference block (B.7) of the MIS-GD-GC scheme are regarded as the estimations of the channel. Therefore, the receive signals (B.8) can be converted into equivalent received signals containing $\hat{\boldsymbol{H}}_t, t \in [1:2^l]$ Substituting $\boldsymbol{H}_t$ with $\hat{\boldsymbol{H}}_t$ in (B.8) and re-writing (B.8) yields:

$$\boldsymbol{y}_t = \hat{\boldsymbol{H}}_t\boldsymbol{S}_t + \hat{\boldsymbol{n}}_t, \;\; t \in [1:2^l], \tag{B.10}$$

where $\hat{\boldsymbol{H}}_t = \begin{bmatrix}\hat{\boldsymbol{h}}_{t,1} & \hat{\boldsymbol{h}}_{t,2}\end{bmatrix}, \boldsymbol{S}_t = \begin{bmatrix}s^1_{l,t} & s^2_{l,t}\end{bmatrix}^T$ and $\hat{\boldsymbol{n}}_t = \boldsymbol{n}_t - \boldsymbol{w}_{t,1}s^1_{l,t} - \boldsymbol{w}_{t,2}s^2_{l,t}, t \in [1:2^l]$. The entries of $\hat{\boldsymbol{H}}_t, \hat{\boldsymbol{H}}_t = \begin{bmatrix}\hat{\boldsymbol{h}}_{t,1} & \hat{\boldsymbol{h}}_{t,2}\end{bmatrix}$ and $\hat{\boldsymbol{n}}_t$ with their corresponding distributions are similar to the discussions in (B9.1) and (B9.2).It is important to note that (B.10) is based on the transmitted MIS-GC codewords. Therefore, in order to transform (B.10) to be based on transmitted MQAM symbols $s^k_{0,t}, s^k_{0,t} \in \boldsymbol{\Omega}_M$, let $\boldsymbol{S}_0 = \begin{bmatrix}\boldsymbol{S}_{0,1} & \boldsymbol{S}_{0,2}\end{bmatrix}^T$ and $\tilde{\boldsymbol{H}}_t = \begin{bmatrix}\tilde{\boldsymbol{H}}_{t,1} & \tilde{\boldsymbol{H}}_{t,2}\end{bmatrix}$ where $\boldsymbol{S}_{0,t} = \begin{bmatrix}s^t_{0,1} & \cdots & s^t_{0,2^l}\end{bmatrix}^T$ and $\tilde{\boldsymbol{H}}_{t,k} = \begin{bmatrix}\tilde{\boldsymbol{h}}^k_{t,1} & \cdots & \tilde{\boldsymbol{h}}^k_{t,2^l}\end{bmatrix}$. Consequently, we can express (B.10) as:

$$\boldsymbol{y}_t = \tilde{\boldsymbol{H}}_t\boldsymbol{S}_0 + \hat{\boldsymbol{n}}_t, \;\; t \in [1:2^l], \tag{B.11}$$

A more general expression is achieved by stacking (B.11) further. Let $\boldsymbol{Y} = \begin{bmatrix}\boldsymbol{y}_1 & \cdots & \boldsymbol{y}_{2^l}\end{bmatrix}^T$, $\boldsymbol{N} = \begin{bmatrix}\hat{\boldsymbol{n}}_1 & \cdots & \hat{\boldsymbol{n}}_{2^l}\end{bmatrix}^T$ and $\boldsymbol{H} = \begin{bmatrix}\tilde{\boldsymbol{H}}_1 & \cdots & \tilde{\boldsymbol{H}}_{2^l}\end{bmatrix}^T$ where $\boldsymbol{Y} \in \mathbb{C}^{(2^l N_r \times 1)}, \boldsymbol{N} \in \mathbb{C}^{(2^l N_r \times 1)}$, and $\boldsymbol{H} \in \mathbb{C}^{(2^l N_r \times 2^l N_t)}$. We may therefore re-write (B.11) as :

$$\boldsymbol{Y} = \boldsymbol{H}\boldsymbol{S}_0 + \boldsymbol{N}, \tag{B.12}$$

In this paper, the expresssion in (B.12) is used to illustrate the sphere detection of the MIS-GD-GC scheme.

6 Sphere Detection of MIS-GD-GC

Sphere detection has been widely discussed in [17]. Recently, sphere detection has also found detection application in Xu et al. [8, 18]. In this paper, we also apply sphere detection to decode

MIS-GD-GC. In order to decode MIS-GD-GC, we make use of the stacked equation in (B.12), which uses $\hat{\boldsymbol{h}}_{t,k}, t \in [1:2^l], k \in [1:2]$ to estimate the channel at the receiver. Firstly, we carry out QR factorisation of the channel matrix $\boldsymbol{H}$ in (B.12) to give:

$$\boldsymbol{H} = \boldsymbol{Q}\boldsymbol{R}, \tag{B.13}$$

From (B.13), the channel matrix $\boldsymbol{H}$ consists of an orthonormal (unitary) matrix $\boldsymbol{Q} \in \mathbb{C}^{(a\times a)}, a = 2^l N_r$ and an upper triangular matrix $\boldsymbol{R} \in \mathbb{C}^{(a\times b)}, b = 2^l N_t$. Secondly, we substitute (B.13) in (B.12) and multiply both sides of the equation by Q^H to give:

$$\hat{\boldsymbol{Y}} = \boldsymbol{R}\boldsymbol{S}_0 + \hat{\boldsymbol{N}}, \tag{B.14}$$

where $\hat{\boldsymbol{N}} = Q^H\boldsymbol{N}$ and $\hat{\boldsymbol{Y}} = \begin{bmatrix}\hat{\boldsymbol{Y}}_1 & \hat{\boldsymbol{Y}}_2\end{bmatrix}^T = Q^H\boldsymbol{Y}$. Note that $\hat{\boldsymbol{Y}}_1$ is a $b \times 1$ vector which can be expressed as $\hat{\boldsymbol{Y}}_1 = \begin{bmatrix}\hat{Y}_1(1) & \hat{Y}_1(2) & \cdots & \hat{Y}_1(b-1) & \hat{Y}_1(b)\end{bmatrix}^T$ and $\hat{\boldsymbol{Y}}_2$ is an $(a-b)\times 1$ vector. We may also partition $\boldsymbol{R}$ further into $\boldsymbol{R} = \begin{bmatrix}\boldsymbol{R}_1 & \boldsymbol{R}_2\end{bmatrix}^T$ with $\boldsymbol{R}_1$ being a $b \times b$ upper triangular matrix expressed as:

$$\boldsymbol{R}_1 = \begin{bmatrix} r_{1,1} & r_{1,2} & \cdots & r_{1,2^l} & \cdots & r_{1,b} \\ 0 & r_{2,2} & \cdots & r_{2,2^l} & \cdots & r_{2,b} \\ \vdots & \vdots & \vdots & \vdots & \ddots & \vdots \\ 0 & 0 & \cdots & \cdots & \cdots & r_{b,b} \end{bmatrix}, \tag{B.15}$$

$\boldsymbol{R}_2$ is a zero matrix of dimension $(a-b)\times b$. Finally, the sphere detection of (B.12) is formulated as:

$$\left\| \hat{\boldsymbol{Y}}_1 - \boldsymbol{R}_1\boldsymbol{S}_0 \right\|_F^2 \leq d^2, \tag{B.16}$$

where d is the search radius of the sphere detector whose value is typically based on Eq.(28) of [19]. For the benefit of this paper, we provide a simplified explanation of sphere detection as follows: Suppose $\boldsymbol{S}_0 = \begin{bmatrix}\boldsymbol{S}_{0,1} & \boldsymbol{S}_{0,2}\end{bmatrix}^T = \begin{bmatrix}s_1 & \cdots & s_b\end{bmatrix}^T$. The first step is to detect s_b. If we let $p_b(s_b) = \hat{Y}_1(b) - r_{b,b}s_b$, then we have:

$$|p_b(s_b)|^2 \leq d^2, \tag{B.17}$$

The sphere detector searches $s_b, s_b \in \boldsymbol{\Omega}_M$ to meet the condition in (B.17). Once s_b meets the requirement in (B.17), s_{b-1} is detected. Again, let $p_{b-1}\left(s|_{b-1}^b\right) = \hat{Y}_1(b-1) - r_{b-1,b-1}s_{b-1} - r_{b-1,b}s_b$. We then obtain:

$$\left|p_{b-1}\left(s|_{b-1}^b\right)\right|^2 \leq d^2 - |p_b(s_b)|^2, \tag{B.18}$$

Again, the sphere detector searches $s_{b-1}, s_{b-1} \in \boldsymbol{\Omega}_M$ to meet the condition in (B.18). In general, if $s|_m^k = \begin{bmatrix}s_m & \cdots & s_k\end{bmatrix}$, then in order to detect s_m we have: [6]

$$\left|p_m\left(s|_m^b\right)\right|^2 \leq d^2 - \sum_{k=m+1}^{b}\left|p_k\left(s|_k^b\right)\right|^2, \tag{B.19}$$

6.1 Sphere Detection of MIS-GD-GC with Sorted Detection Subset

It is evident from (B.17) - (B.19) that the detection complexity of a sphere decoder mainly depends upon the cardinality of the signal set and the search depth [17]. The smaller the size of the set of a given pair of symbols, the lower the detection complexity. A sphere decoding technique that uses a detection subset (SD-DS) has been proposed in recent literature [8, 18], where it is observed that the average cardinality of the GC signal set is reduced from 16^2 and 64^2 to 4^2 and 4.5^2 for 16QAM and 64QAM, respectively. If SD-DS is applied to MIS-GC, then the average cardinality of the signal set is reduced from 16^{2l-1} and 64^{2l-1} to 4^{2l-1} and 4.5^{2l-1} for 16QAM and 64QAM, respectively. However, as the number of multiple symbols in each MIS-GC codeword matrix increases, the average cardinality of the signal set in SD-DS increases exponentially. In addition, for a given cardinality of the signal set, SD-DS only exhibits low detection complexity at high SNR regions [18]. For these reasons therefore, this paper incorporates a modified detection subset method called sphere decoding with sorted detection subset (SD-SDS) [6] in order further reduce the detection complexity of the MIS-GD-GC scheme. In this method, the transmitted MQAM symbols $s_t, t \in [1:b]$ are estimated. Then all the MIS-GD-GC symbols within the signal set are sorted from those with the highest probability of transmission to those with the lowest probability of transmission. The most likely transmitted symbols form the set used for detection. The following steps summarise the process of sphere decoding with sorted detection subset:

Step 1: Carry out QR factorisation and use (B.14) to obtain $\hat{\mathbf{Y}}_1$.

Step 2: Obtain the transmitted MQAM symbols $s_t, t \in [1:b]$. From (B.14), we may write:

$$x_b = \frac{\hat{Y}_1(b)}{r_{b,b}}, \tag{B.20}$$

In order to obtain the estimations of s_b, we demodulate (B.20) as follows:

$$\tilde{s}_b = \mathfrak{D}(x_b), \tag{B.21}$$

Step 3: Using the signal set, sort all the symbols from those with the highest transmission probability to those with the lowest probability of transmission. This is done using the metric:

$$z_t(m) = |x_t - s_m|^2, \tag{B.22}$$

where $m \in [1:M]$ and $s_m \in \mathbf{\Omega}_M$. Suppose $\boldsymbol{z}_t = \{z_t(m), m \in [1:M]\}, t \in [1:b]$, in order to obtain the most probable estimation index of s_t, we evaluate:

$$\tilde{\boldsymbol{t}}_m = argsort(\boldsymbol{z}_t), \tag{B.23}$$

The $argsort(\cdot)$ operator sorts the M elements from the most likely transmitted to the least likely transmitted.

Step 4: Carry out sphere detection

Note that for any SNR, N symbols with the highest probability of transmission in each $\tilde{s}_t$ are selected. These symbols then form the set $\boldsymbol{\Omega}(\tilde{s}_t, N)$ which in turn is used to replace $\boldsymbol{\Omega}_M$ in performing sphere detection. Typically, small values of N are chosen at low SNRs and large values of N at high SNRs so as to increase the speed of detection while ensuring that the simulated BERs compare well with the theoretical ABEP. For the simulation of MIS-GD-GC with SD-SDS, the parameter N is specified for different SNR values as tabulated in **Table B.2**.

7 Error Performance Analysis of MIS-GD-GC

In the coherent MIS-GC system, it is assumed that only one MQAM symbol $s_{0,1}^1$ is detected with error while the rest of the input symbols $s_{0,t}^1, t \in [2 : 2^l]$ and $s_{0,t}^2, t \in [1 : 2^l]$ are correctly detected. In addition, the equivalent error performance model of MIS-GC may be regarded as the transmission of $s_{0,1}^1$ over 2^l non-identical fading channels with fading variances $|\beta_t|^2, t \in [1 : 2^l]$. It is also noted that the variance of each entry in $\boldsymbol{H}_t$ where $\boldsymbol{H}_t = \begin{bmatrix} \boldsymbol{h}_{t,1} & \boldsymbol{h}_{t,2} \end{bmatrix}$ and $\boldsymbol{n}_t$ of MIS-GC is 1 and $\frac{2}{\rho}$ respectively.

On the other hand, the error performance analysis of the MIS-GD-GC scheme is based on the equivalent received signal (B.11) where it is noted that the variance of each entry in $\tilde{\boldsymbol{H}}_t = \begin{bmatrix} \tilde{\boldsymbol{H}}_{t,1} & \tilde{\boldsymbol{H}}_{t,2} \end{bmatrix}$ where $\tilde{\boldsymbol{H}}_{t,k} = \begin{bmatrix} \tilde{\boldsymbol{h}}_{t,1}^k & \cdots & \tilde{\boldsymbol{h}}_{t,2^l}^k \end{bmatrix}, t \in [1 : 2^l], k \in [1 : 2]$ and $\hat{\boldsymbol{n}}_t$ is $(1 + \sigma_0^2)$ and $\sigma_\epsilon^2 = \frac{2}{\rho_n} + \frac{2}{\rho_0}$ respectively. Therefore the error performance analysis of the MIS-GD-GC scheme is done in a similar manner to that of the coherent MIS-GC, but with special attention given to the variance of the MIS-GD-GC.

Since the output of the reference block is known at the receiver, the ABEP of MIS-GD-GC is derived based on the classical expression of the exact symbol error probability of MQAM signals given in Eq. (8.10) of Simon et al. [20], together with the Gaussian Q-function which is tightly approximated using the trapezoidal rule of integration. Therefore, the ABEP of MIS-GD-GC for MQAM signals may be derived as:

$$P_e \approx \frac{a}{n \log_2 M} \Bigg[\frac{1}{2} \prod_{t=1}^{2^l} \left(\frac{2}{2 + |\beta_t|^2 b\hat{\gamma}} \right)^{N_r} - \left(\frac{a}{2} \right) \prod_{t=1}^{2^l} \left(\frac{1}{1 + |\beta_t|^2 b\hat{\gamma}} \right)^{N_r} + (1 - a) \sum_{k=1}^{n-1} \prod_{t=1}^{2^l} \left(\frac{u_k}{u_k + |\beta_t|^2 b\hat{\gamma}} \right)^{N_r} + \sum_{k=n}^{2n-1} \prod_{t=1}^{2^l} \left(\frac{u_k}{u_k + |\beta_t|^2 b\hat{\gamma}} \right)^{N_r} \Bigg], \quad \text{(B.24)}$$

where $n \geq 10$ is the total number of summations required to achieve convergence, $a = 1 - \frac{1}{\sqrt{M}}, b = \frac{3}{M-1}$, and $u_k = 2\sin^2\left(\frac{k\pi}{4n}\right)$. $\hat{\gamma}$ is the SNR of the MIS-GD-GC scheme and is given by:

$$\hat{\gamma} = \frac{(1+\sigma_0^2)}{\left(\frac{2}{\rho_n} + \frac{2}{\rho_0}\right)} = \frac{1}{2}\left(1+\sigma_0^2\right)\left(\frac{1}{\rho_n} + \frac{1}{\rho_0}\right)^{-1}, \tag{B.25}$$

Based on the MIS-GC encoding described in (B2.1) and (B2.2), it can be easily seen that the values of β_t are in terms of $\frac{1}{(\sqrt{5})^l}(\alpha + \hat{\alpha})^l$. [6] For instance, in 2IS-GD-GC (where $l = 1$), $\beta_1 = \frac{\alpha}{\sqrt{5}}$ and $\beta_2 = \frac{\hat{\alpha}}{\sqrt{5}}$. Similarly, in 4IS-GD-GC (where $l = 2$), $\beta_1 = \frac{\alpha^2}{5}, \beta_2 = \beta_3 = \frac{\alpha\hat{\alpha}}{5}$ and $\beta_4 = \frac{\hat{\alpha}^2}{5}$ and so on.

8 Computational Complexity Analysis of MIS-GD-GC

In MIMO systems, the conventional ML detector searches through M^{N_t} points to find an optimal solution. However, the complexity of tree search algorithms such as the SD is proportional to the number of visited nodes within a hypersphere to obtain a solution. [17] Various complexity investigations on SD algorithms have been done in literature; some are based on analytical evaluations [17, 21], while others use simulations. [6, 18, 22] For MIS-GD-GC with sphere decoding, the detection complexity consists of the pre-detection stage as well as the search stage.

8.1 Complexity of the Pre-Detection Stage

The pre-detection stage uses QR factorisation to calculate the upper triangular matrix $\boldsymbol{R}$ from the channel matrix $\boldsymbol{H}$. The orthonormal matrix $\boldsymbol{Q}$ is used to establish the minimum and maximum bounds for each closest lattice point. Typically, the computational complexity of the pre-detection stage is defined in terms of floating-point operations (flops), where each multiplication, division, addition, or subtraction is regarded as a single flop. [7, 8] Therefore, since $\boldsymbol{H}$ is a $2^l N_r \times 2^l N_t$ matrix, performing QR factorisation requires $8(2^l N_r) - \frac{16}{3}$ flops for each $t, t \in [1 : 2^l]$ using the Householder algorithm. [23] The computation of $\hat{\boldsymbol{Y}} = \boldsymbol{Q}^H \boldsymbol{Y}$ in (B.14) requires $(2^l N_r)^2$ multiplications and $2^l N_r(2^l N_r - 1)$ additions for each t. Therefore, the total number of flops for the pre-detection stage is given by: $\zeta_{QR} = 2^l\left[2(2^l N_r)^2 + 7(2^l N_r) - \frac{16}{3}\right]$.

8.2 Complexity of the Search Stage

The search stage involves the SD traversing the entire signal set to search for the transmitted symbols. In conventional sphere decoding for MIMO systems, the size of the search is M^{N_t}. However, SD-SDS reduces the constellation size; thus, the detection complexity is reduced. Noting that the detection complexity of QR factorisation is minimal compared to that of the search stage, [6, 18, 24] we ignore

the complexity of the pre-detection stage and only focus on the average detection complexity of the search stage in (B.17) to (B.19). Also, since the iterative search of the optimal point in the lattice of an SD algorithm is entirely random, [17] the average detection complexity of MIS-GD-GC with SD-SDS is analysed through simulations. Accordingly, this paper evaluates the complexity of SD-SDS for MIS-GD-GC by carrying out Monte Carlo simulations to obtain the average number of nodes visited, yielding results that are represented here as an average complexity. We only consider the 16QAM and 64QAM signal constellations with $N_r = 3$ and $N_r = 4$ at a frame length of $B = 400$. Additional constellations of different modulation order and receive antenna configurations may be analysed in a similar manner and are only omitted here for conciseness. The parameter N, used in the simulation of MIS-GD-GC, is tabulated in **Table B.2**. For comparison, the 2IS-GD-GC with conventional SD is also simulated for both 16QAM and 64QAM. The 4IS-GD-GC and 8IS-GD-GC with conventional SD can be simulated in the same manner and are only left out for brevity. The results are illustrated in **Figures B.1** and **B.2**. Note that the average detection complexities of **Figures B.1** and **B.2** are simulated based on the detection of four MQAM symbols.

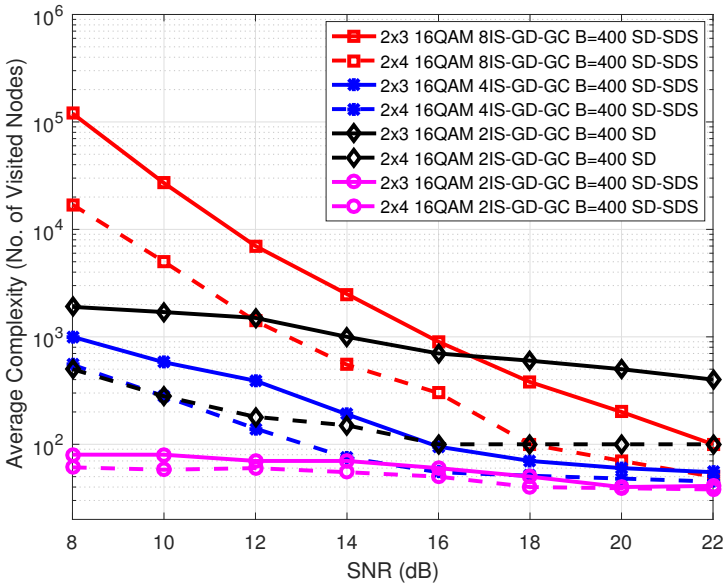

Figure B.1: Detection complexity of MIS-GD-GC for 16QAM with $N_r = 3$ and $N_r = 4$

The following observations are made from **Figures B.1** and **B.2**:

(i) As the SNR increases, the average detection complexity of MIS-GD-GC with SD-SDS decreases.

(ii) The proposed MIS-GD-GC scheme with $N_r = 4$ has a lower average detection complexity compared to MIS-GD-GC with $N_r = 3$. This is because, in SD-SDS, the reliability of the

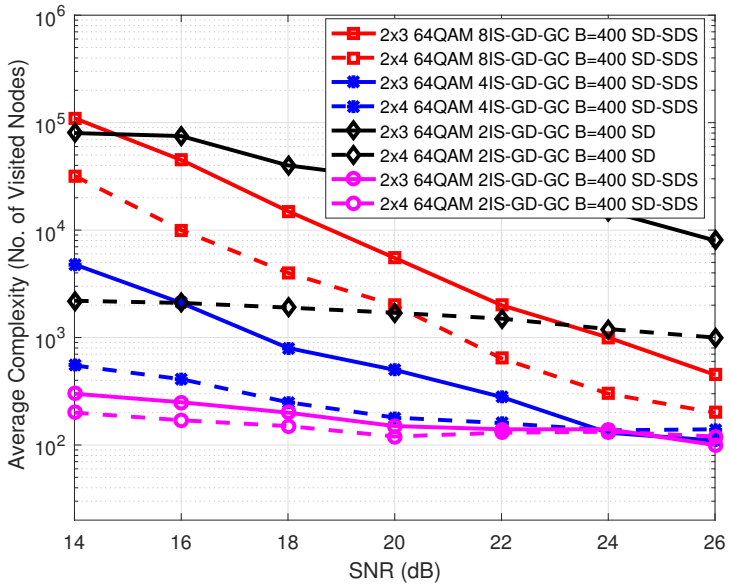

Figure B.2: Detection complexity of MIS-GD-GC for 64QAM with $N_r = 3$ and $N_r = 4$

symbols in the SDS increases as the number of receive antennas increases. Consequently, it only takes a few decoding iterations for each symbol to meet the constraint, thus reducing the average detection complexity.

(iii) As the number of input symbols increases, the average detection complexity also increases. For instance, the 8IS-GD-GC has a higher average complexity compared to 4IS-GD-GC and 2IS-GD-GC.

(iv) The average detection complexity of 2IS-GD-GC with SD-SDS is lower than that of 2IS-GD-GC with conventional SD.

9 Simulation Results

This section presents the simulation results for the MIS-GD-GC system in quasi-static frequency flat Rayleigh fading channel with AWGN. The parameter setting for MQAM, frame length, SNR and antenna configuration is tabulated in **Table B.2**. As mentioned in sections 3.1 and 3.2, the number of transmit antennas is assumed to be $N_t = 2$. It should also be noted from **Table B.2** that we have only considered the antenna configuration $N_r = 3$ and $N_r = 4$ just for purposes of comparison with the derived theoretical ABEP of section 7. However, MIS-GD-GC system is valid for $N_r \geq 2$. In addition, $K - IS$ in **Table B.2** represents the number of multiple input symbols in MIS-GD-GC.

In the simulations, we compare the error performance of MIS-GD-GC with the theoretical ABEP

Table B.2: Parameter settings for simulation

M	N_r	$K-IS$	B	SNR	N
16	3	2	100	[8:2:24]	[10 10 10 10 12 12 12 16 16]
			400		
	3	4	100	[8:2:22]	[10 10 10 10 10 12 14 16]
			400		
	3	8	100	[8:2:22]	[8 8 8 12 12 16 16 16]
			400		
	4	2	100	[6:2:22]	[10 10 10 12 12 12 16 16 16]
			400		
	4	4	100	[6:2:20]	[10 10 10 10 12 14 16 16]
			400		
	4	8	100	[6:2:20]	[8 8 8 8 16 16 16 16]
			400		
64	3	2	100	[14:2:30]	[20 20 20 30 30 30 60 60 60]
			400		
	3	4	100	[14:2:28]	[14 14 14 14 20 20 30 60]
			400		
	3	8	100	[14:2:28]	[14 14 14 14 20 30 30 60]
			400		
	4	2	100	[10:2:28]	[20 20 20 30 30 30 60 60 60 60]
			400		
	4	4	100	[10:2:26]	[14 14 14 14 14 20 20 30 60]
			400		
	4	8	100	[10:2:26]	[14 14 14 14 14 20 20 30 60]
			400		

derived in section 7. We also compare the BER of MIS-GD-GC systems to that of MIS-GC with coherent detection. All the simulation and theoretical results for both 16QAM and 64QAM MIS-GD-GC with $N_r = 3$ and $N_r = 4$ are shown in **Figure B.3** to **Figure B.8**. From the illustrations of **Figures B.3** to **B.8**, the following observations are made:

1. The simulated BER compares very well to the theoretical bound. In fact, as the number of receive antennas is increased, the simulated BER approaches the theoretical bound.

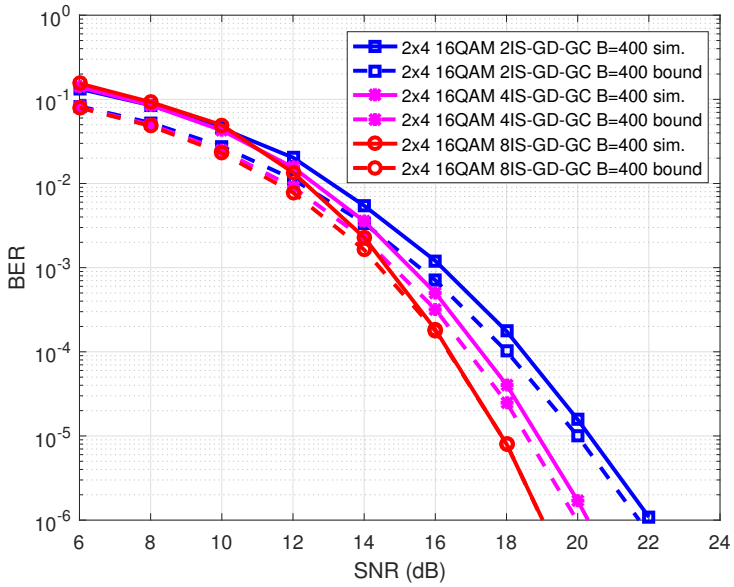

Figure B.3: BER Performance for 16QAM MIS-GD-GC with $N_r = 4$

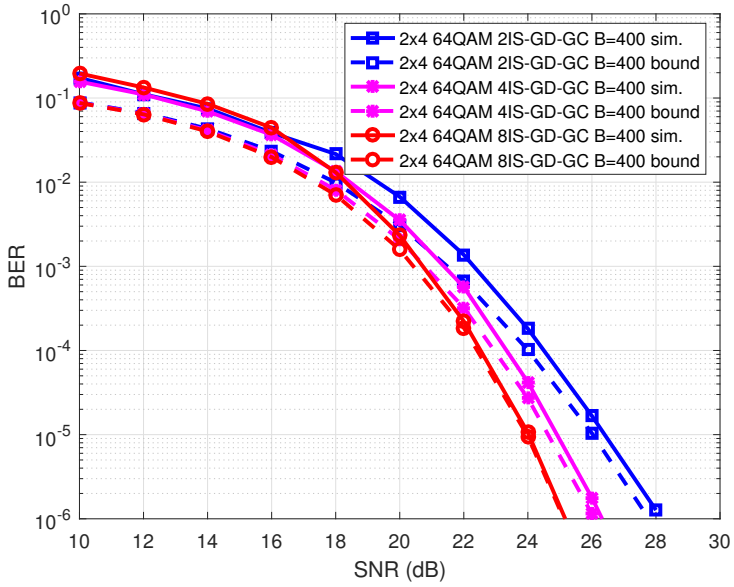

Figure B.4: BER Performance for 64QAM MIS-GD-GC with $N_r = 4$

2. It is further observed that the BER of MIS-GD-GC draws closer to that of MIS-GC with coherent detection as the frame length increases. For instance, when the frame length $B = 100$, the SNR gap is 0.8 dB while the SNR gap at a frame length of $B = 400$ is 0.4 dB. This is because at a longer frame length, more transmit power is allocated to the reference block, resulting in a more accurate estimation of the channel.

3. When $N_r = 3$, at a frame length $B = 400$ the 4IS-GD-GC achieves an SNR gain of approximately 2.1 dB compared to 2IS-GD-GC at a BER of 4×10^6, while the 8IS-GD-GC

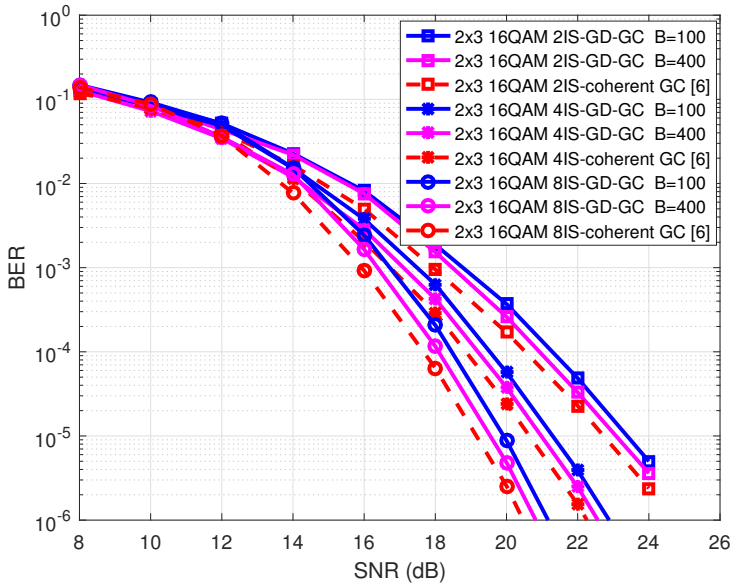

Figure B.5: BER Performance Comparison between 16QAM MIS-GD-GC and Coherent Detection with $N_r = 3$

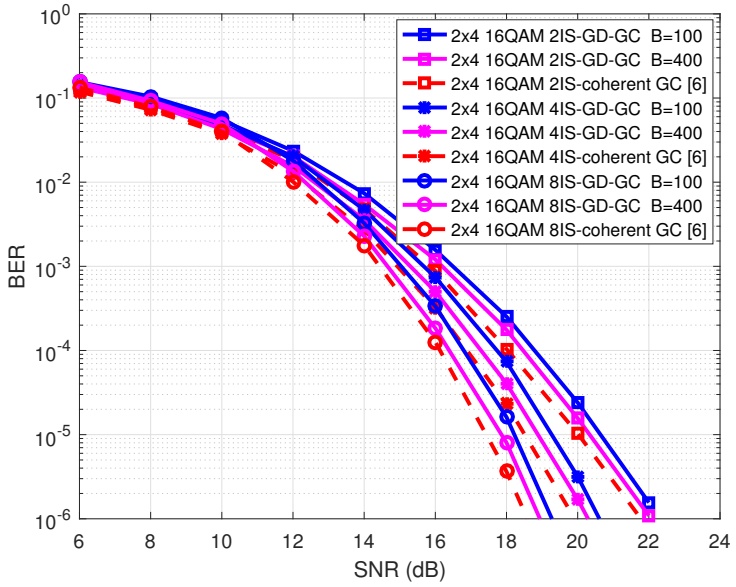

Figure B.6: BER Performance Comparison between 16QAM MIS-GD-GC and Coherent Detection with $N_r = 4$

achieves an SNR gain of approximately 1 dB compared to the 4IS-GD-GC.

4. When $N_r = 4$, at a frame length $B = 400$ the 4IS-GD-GC achieves an SNR gain of approximately 1.7 dB compared to 2IS-GD-GC at a BER of 4×10^6, while the 8IS-GD-GC achieves an SNR gain of approximately 0.8 dB compared to the 4IS-GD-GC.

5. The simulation and theoretical results demonstrate that the proposed MIS-GD-GC achieves full-rate as well as diversity order $2^l N_r$. In addition, the higher the value of the multiple input

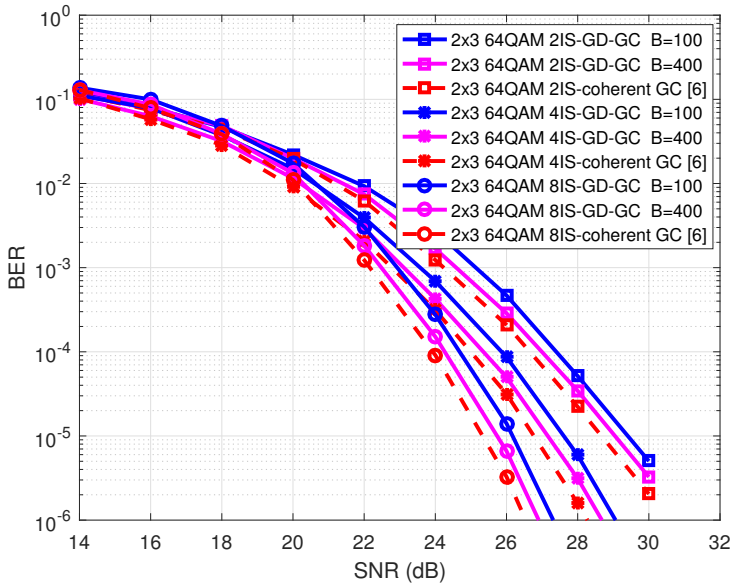

Figure B.7: BER Performance Comparison between 64QAM MIS-GD-GC and Coherent Detection with $N_r = 3$

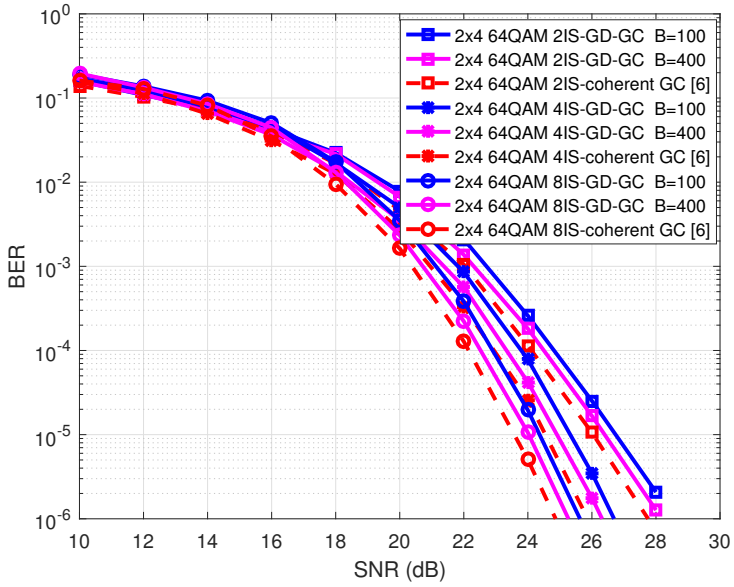

Figure B.8: BER Performance Comparison between 64QAM MIS-GD-GC and Coherent Detection with $N_r = 4$

symbols, the steeper the BER curve, which is in harmony with the error performance analysis of section 7.

10 Conclusion

A generalised differential Golden code modulation scheme based on MQAM and multiple input symbols was proposed in this paper. The proposed scheme detects the transmitted MQAM symbols without knowledge of CSI and achieves full-rate as well as multiple diversity order compared to the conventional Golden code. A sphere decoding technique that utilises a sorted detection subset was also incorporated to reduce the detection complexity of the MIS-GD-GC scheme. A theoretical bound was also derived which validated the simulation results. Both simulation and theoretical results showed that the error performance of MIS-GD-GC approached that of MIS-GC with coherent detection as the frame length increases. For example, when the frame length $B = 100$, the SNR gap is 0.8 dB while the SNR gap at a frame length of $B = 400$ is 0.4 dB. This was attributed to the optimal power allocation between the reference block and the normal blocks.

References

[1] L. Zheng and D. Tse, "Diversity and Multiplexing: A Fundamental Trade-off in Multiple-Antenna Channels," *IEEE Trans Inform Theory*, vol. 49, no. 5, pp. 1073–1096, 2003.

[2] S. Alamouti, "A simple transmit diversity technique for wireless communications," *IEEE Journ Sel Areas Commun*, vol. 16, no. 8, pp. 1451–1458, 1998.

[3] J.-C. Belfiore, G. Rekaya, and E. Viterbo, "The Golden Code: A 2x2 Full-Rate Space-Time Code with Nonvanishing Determinants," *IEEE Trans Inform Theory*, vol. 51, no. 4, pp. 1432–1436, 2005.

[4] M. Sinnokrot and J. Barry, "Fast Maximum-likelihood Decoding of the Golden Code," *IEEE Trans Wireless Commun*, vol. 9, no. 1, pp. 26–31, 2010.

[5] H. Xu and N. Pillay, "Golden Codeword based Modulation Schemes for Single-Input Multiple-Output Systems," *Inter Journ Commun Sys*, vol. 32, no. 1, pp. 1–12, 2019.

[6] H. Xuh and N. Pillay, "Multiple Complex Symbol Golden Code," *IEEE Access*, vol. 8, no. 1, pp. 103 576–103 584, 2020.

[7] S. Kahraman and M. Celebi, "Dimensionality Reduction for the Golden Code with Worst-Case Decoding Complexity of O($m^{1.5}$)," ser. Proc IEEE Wireless Communications and Networking Conference, USA, April, 2012.

[8] H. Xu and N. Pillay, "Reduced Complexity Detection Schemes for Golden Code Systems," *IEEE Access*, vol. 7, no. 1, pp. 139 140–139 149, 2019.

[9] L. Li, Z. Fang, Y. Zhu, and Z. Wang, "Generalized differential transmission for STBC systems," ser. Proc IEEE GLOBECOM Telecommunications Conference, New Orleans, USA, Dec 1–4, 2008.

[10] R. Manav, H. Are, and L. Song, "Differential coding for non-orthogonal space-time block codes with non-unitary constellations over arbitrarily correlated Rayleigh channels," *IEEE Trans Wireless Commun*, vol. 8, no. 8, pp. 1–11, 2009.

[11] C. Jorge, R. Sandra, C. Daniel, M. Yasser, H. Ramy, F. Jose, and Y. Halim, "Non-coherent open-loop MIMO communications over temporarily-correlated channels," *IEEE Access*, vol. 4, pp. 6161–6170, 2016.

[12] Z. Fang, L. Li, X. Bao, and Z. Wang, "Generalized differential modulation for amplify-and-forward wireless relay networks," *IEEE Trans Veh Tech*, vol. 58, no. 6, pp. 3058–3062, 2008.

[13] K. Kadathlal, H. Xu, and N. Pillay, "Generalised Differential Scheme for Spatial Modulation Systems," *IET Commun*, vol. 11, no. 13, pp. 2020–2026, 2017.

[14] K. Dwarika and H. Xu, "Differential full diversity spatial modulation using amplitude phase shift keying," *Radioengineering*, vol. 27, no. 1, pp. 151–158, 2018.

[15] K. Dwarikah and H. Xu, "Power Allocation and Low Complexity Detector for Differential Full Diversity Spatial Modulation Using Two Transmit Antennas," *Radioengineering*, vol. 26, no. 2, pp. 461–469, 2017.

[16] H. Xu, N. Pillay, and X. Jin, "Golden Codeword based Generalized Differential Alamouti Modulation," *IEEE Access*, vol. 8, no. 1, pp. 65 649–65 657, 2020.

[17] J. Jalden and B. Ottersen, "On the Complexity of Sphere Decoding in Digital Communications," *IEEE Trans Signal Proc*, vol. 53, no. 4, pp. 1474–1484, 2005.

[18] H. Xu and N. Pillay, "The Component-Interleaved Golden Code and its Low-Complexity Detection," *IEEE Access*, vol. 8, no. 1, pp. 59 550–59 558, 2020.

[19] B. Hochwald and S. Brink, "Achieving Near-Capacity on a Multiple Antenna Channel," *IEEE Trans On Commun*, vol. 51, no. 3, pp. 389–399, 2003.

[20] M. Simon and M.-S. Alouini, *Digital Communications over Fading Channels: A Unified Approach to Performance Analysis*. USA: A Wiley-Interscience Publication, 2000, iSBN 0-471-20069-7.

[21] B. Hassibi and H. Vikalo, "On Sphere Decoding Algorithm Part 1: The Expected Complexity," *IEEE Trans Signal Proc*, vol. 54, no. 5, pp. 2806–2818, 2005.

[22] S. Han and C. Tellambura, "A Complexity-Efficient Sphere Decoder for MIMO Systems," ser. Proc IEEE International Conference on Communications, Japan, June, 2011.

[23] G. Golub and C. Loan, *Matrix Computations, 4th Edition*. USA: The John Hopkins University Press, 2013, iSBN 1421408597, 9781421408590.

[24] G. Rekaya and J. Belfiore, "On the Complexity of ML Lattice Decoders for Decoding Linear Full Rate Space-Time Codes," ser. Proc IEEE International Symposium on Inf Theory, Japan, June, 2003.

Part IV

Paper C

Paper C

Enhanced Bandwidth Efficiency of the Generalised Differential Golden Code Modulation

Abstract

1 Abstract

Conventional differential modulation of the Golden code requires no knowledge of the receiver's channel state information (CSI). However, a performance loss of 3 dB is incurred compared to coherent modulation. Generalised differential modulation is used to improve this performance. This paper proposes an enhanced bandwidth-efficient generalised differential Golden code (EBE-GD-GC) based on quadrature amplitude modulation (QAM). We then derive the average bit error probability for the EBE-GD-GC scheme. Simulations on bit error rate (BER) are carried out to verify the derived theoretical framework, where it is shown that the BER results lie well within the derived bounds. In addition, compared to the conventional generalised differential Golden code, both 16QAM and 64QAM EBE-GD-GC result in < 1 dB performance loss from a BER of 1×10^{-5} at a frame length of $D = 400$.

2 Introduction

In the current era, extremely reliable wireless communication systems that provide ultra-high data rates are in great demand. For this reason, multiple-input multiple-output (MIMO) systems have been extensively deployed to increase data transmission rate and improve the reliability of these communication systems. However, MIMO systems are characterised by a trade-off between data transmission rate and communication reliability in regards to diversity order and multiplexing gain [1].

The Alamouti space-time block code (STBC) is a classic MIMO system that uses two transmit antennas. The encoder of the Alamouti STBC comprises an orthogonal codeword matrix containing two transmitted symbols that are easily decoupled [2]. The Alamouti scheme achieves full diversity but no multiplexing gain [2]. The Golden code (GC) STBC is another example of a MIMO system with two transmit antennas [3, 4]. Conventionally, it consists of two pairs of Golden codewords, where each codeword comprises two input symbols, and each pair of the Golden codewords is transmitted in different time slots. Unlike the Alamouti STBC, the GC STBC achieves both full-multiplexing gain and full diversity [3]. The Golden code STBC is so helpful that it is incorporated in the IEEE 802.16e WiMAX standard [4]. The only disadvantage of the GC is the very high detection complexity of its maximum likelihood (ML) detector at the receiver. This complexity of order $\mathcal{O}(M^4)$, where M is the modulation order, limits the GC applications due to the increased challenges in hardware implementation. Due to the Golden code's significance, numerous research undertakings have been carried out to reduce its detection complexity. A fast-ML detection scheme was proposed by [4] and shown to achieve a worst-case complexity of order $\mathcal{O}(M^{2.5})$. Another efficient technique that reduces the dimensions of the search tree in sphere decoding is proposed by [5] The only disadvantage of this technique is the 1 dB signal-to-noise ratio (SNR) loss it incurs in its error performance compared to the optimal detector.

Each of the techniques mentioned above, proposed in the literature, exhibit one or more limitations regarding their performance. Motivated by the works of [6], [7] and driven by the need to design a scheme that is capable of (a) improving the bandwidth efficiency of the differential Golden code without significantly degrading its error performance (b) exploiting the full-rate full-diversity property of the GC and (c) achieving a low computational complexity at the receiver, we propose a bandwidth-enhancement scheme hereinafter referred to as enhanced bandwidth-efficient generalised differential Golden code (EBE-GD-GC). The proposed scheme uses unitary matrix transformation [8] and generalised differential modulation of the Golden code [9]. We then derive the

theoretical average bit error probability (ABEP) of the EBE-GD-GC scheme. We also deploy low complexity sphere decoding with a sorted detection subset to decode the system. In summary, this paper makes the following contributions:

1. An enhanced bandwidth-efficient scheme for the generalised differential Golden code (EBE-GD-GC) is proposed.
2. The average bit error probability of the EBE-GD-GC scheme is also derived.

The remaining part of this paper is organised as follows: The system models for the conventional Golden code and the enhanced bandwidth-efficient generalised differential Golden code are presented in section 2. We then present the equivalent detection model of the proposed EBE-GD-GC scheme and incorporate sphere decoding with sorted detection subset in section 3. The error performance analysis of EBE-GD-GC is discussed in section 4, while its computational complexity is analysed in section 5. Section 6 presents the Monte Carlo simulation results, while Section 7 concludes the paper.

Notation: Bold letters are used to denote vectors and matrices. The transpose, Hermitian and Frobenius norm operations are denoted by $(\cdot)^T$, $(\cdot)^H$ and $\| \cdot \|_F$, respectively. The expected value of an argument is denoted by $E[\cdot]$. $\mathfrak{D}(\cdot)$ represents the demodulator function for the signal constellation. The inverse function is denoted by $(\cdot)^{-1}$, and j denotes a complex number.

3 System model

Firstly, this section analyses the system model of the Golden code. Secondly, generalised differential modulation of the GC is then briefly discussed. Lastly, the system model of the EBE-GD-GC scheme is presented.

3.1 The Golden Code

The Golden code is a space-time block code comprising of two transmit antennas $(N_t = 2)$ and two or more receive antennas. [3, 4] As mentioned previously, the GC is composed of two pairs of Golden codewords, and each pair contains two input symbols. The codeword matrix of the Golden code may be represented as [3]:

$$\boldsymbol{G} = \begin{bmatrix} g_1 & g_3 \\ g_2 & g_4 \end{bmatrix}, \tag{C.1}$$

where $g_1 = \frac{\alpha}{\sqrt{5}}(s_1 + s_2\tau), g_2 = \frac{\alpha}{\sqrt{5}}(s_3 + s_4\tau), g_3 = j\frac{\hat{\alpha}}{\sqrt{5}}(s_3 + s_4\mu)$, and $g_4 = \frac{\hat{\alpha}}{\sqrt{5}}(s_1 + s_2\mu)$. Also, $\tau = \frac{1+\sqrt{5}}{2}, \mu = 1 - \tau, \alpha = 1 + j\mu, \hat{\alpha} = 1 + j\tau$ and $j = \sqrt{-1}$. The input symbols are denoted by $s_i \in \boldsymbol{\Omega}_M, i \in [1:4]$, where $\boldsymbol{\Omega}_M$ is the M-ary quadrature amplitude modulation (MQAM) signal

set, and M is the modulation order. It is assumed that $E\left[|s_i|^2\right] = 1, i \in [1:4]$. The two pairs of the Golden codewords are $\left\{\frac{\alpha}{\sqrt{5}}(s_1 + s_2\tau), \frac{\hat{\alpha}}{\sqrt{5}}(s_1 + s_2\mu)\right\}$ and $\left\{\frac{\alpha}{\sqrt{5}}(s_3 + s_4\tau), j\frac{\hat{\alpha}}{\sqrt{5}}(s_3 + s_4\mu)\right\}$, respectively. However, only the first pair $\left\{\frac{\alpha}{\sqrt{5}}(s_1 + s_2\tau), \frac{\hat{\alpha}}{\sqrt{5}}(s_1 + s_2\mu)\right\}$ is used to establish the proposed EBE-GD-GC scheme.

3.2 Generalised Differential Modulation

Generalised differential modulation consists of D blocks in each frame. The first block forms the basis upon which all the other $(D-1)$ blocks are evaluated and is referred to as the reference block. The other $(D-1)$ blocks convey information in the course of transmission and are referred to as data blocks. Several research works have proposed optimal ways to apportion power between the reference and data blocks [10, 11]. The reference block is transmitted with more power than the data blocks to improve the error performance of generalised differential modulation. Suppose the transmit power of the conventional differential modulation is P, then each frame has a total transmit power given by DP. For a fixed transmit power, the optimal power P_r apportioned to the reference block, and the optimal power P_d apportioned to each data block is, respectively, given by [11]:

$$P_r = \frac{D}{1 + \sqrt{D-1}}P, \tag{C2.1}$$

$$P_d = \frac{D}{(D-1) + \sqrt{D-1}}P, \tag{C2.2}$$

A fundamental principle in generalised differential modulation is that the receiver estimates the channel using the transmission of the reference block. Additionally, we assume that D blocks are transmitted over quasi-static frequency-flat Rayleigh fading channels. This means that the channels remain unchanged during the transmission of the first D blocks and only take on independent values when transmitting the next set of D blocks.

3.3 Generalised Differential Modulation of the Golden Code

As mentioned in the previous section, the reference block transmission is used at the receiver to estimate the channel of the generalised differential Golden code (GD-GC) scheme. Therefore, the received signal at the reference block may be expressed as:

$$\hat{\boldsymbol{h}}_{ik} = \boldsymbol{h}_{ik} + \boldsymbol{w}_{ik}, \;\; i \in [1:2], k \in [1:2], \tag{C.3}$$

where $\hat{\boldsymbol{h}}_{ik} \in \mathbb{C}^{(N_r \times 1)}$ is a vector representing the channel gain, while $\boldsymbol{w}_{ik} \in \mathbb{C}^{(N_r \times 1)}$ represents the additive white Gaussian noise (AWGN) vector. The elements of $\boldsymbol{h}_{ik}$ and $\boldsymbol{w}_{ik}$ are considered independent and identically distributed (iid) complex Gaussian random variables (RVs) with

distributions $CN(0,1)$ and $CN(0,\sigma_r^2), \sigma_r^2 = \frac{1}{P_r}$, respectively. Similarly, the elements of $\hat{\boldsymbol{h}}_{ik}$ are also regarded as iid RVs with the distribution $CN(0, 1+\sigma_r^2)$. Note that $\hat{\boldsymbol{h}}_{ik}$ in (C.3) is considered as the estimate of $\boldsymbol{h}_{ik}$.

In GD-GC, the two pairs of Golden codewords are transmitted in two different time slots. Therefore, the information signal for the data blocks at the receiver may be expressed as:

$$\boldsymbol{y}_1 = \boldsymbol{h}_{11} g_1 + \boldsymbol{h}_{12} g_2 + \boldsymbol{n}_1, \tag{C4.1}$$

$$\boldsymbol{y}_2 = \boldsymbol{h}_{21} g_3 + \boldsymbol{h}_{22} g_4 + \boldsymbol{n}_2, \tag{C4.2}$$

where $\boldsymbol{y}_i \in \mathbb{C}^{(N_r \times 1)}, i \in [1:2]$ is the i^{th} received signal vector. The AWGN vector is represented by $\boldsymbol{n}_i \in \mathbb{C}^{(N_r \times 1)}, i \in [1:2]$. The terms of $\boldsymbol{n}_i$ are iid complex Gaussian RVs with the distribution $CN(0, \sigma_d^2), \sigma_d^2 = \frac{2}{P_d}$. From (C4.1) and (C4.2), it is apparent that GD-GC is a full rate code since two input symbols are transmitted in two time slots by each of the two transmit antennas. GD-GC also attains full diversity of order $2N_r$ as each input symbol transmitted undergoes two distinct fadings during two time slots.

3.4 Enhanced Bandwidth Efficient Generalised Differential Golden Code

Consider a MIMO STBC system with $N_t = 2$ transmit antennas and $N_r \geq N_t$ receive antennas. The information bits at the input are divided into two bit-streams $\boldsymbol{b}_i = [b_{i1} b_{i2} \cdots b_{ik}], i \in [1:2], k = \log_2 M$. Therefore, each bit-stream has a corresponding decimal equivalent represented by $d_i = 1 + \sum_{n=1}^{2k} 2^{2k-n} b_{in}, i \in [1:2]$. As a result, $d_i \in [1:M^2]$. Bit-stream $\boldsymbol{b}_i$ is fed onto Mapper 1 ($\boldsymbol{\Omega}_1$), and Mapper 2 ($\boldsymbol{\Omega}_2$), which project the $2k$ input bits onto constellation points from the signal set $\left\{\frac{\alpha}{\sqrt{5}}(s_1 + s_2\tau)\right\}$ and $\left\{\frac{\hat{\alpha}}{\sqrt{5}}(s_1 + s_2\mu)\right\}$ in the Argand plane, giving rise to the symbols: $s_{d_1}^1 = \boldsymbol{\Omega}_1(d_1) = \frac{\alpha}{\sqrt{5}}(s_1 + s_2\tau), s_{d_1}^2 = \boldsymbol{\Omega}_2(d_1) = \frac{\hat{\alpha}}{\sqrt{5}}(s_1 + s_2\mu), s_{d_2}^1 = \boldsymbol{\Omega}_1(d_2) = \frac{\alpha}{\sqrt{5}}(s_3 + s_4\tau)$ and $s_{d_2}^2 = \boldsymbol{\Omega}_2(d_2) = \frac{\hat{\alpha}}{\sqrt{5}}(s_3 + s_4\mu)$. Mappers 1 and 2 are obtained from the constellation point $s_i, i \in [1:4]$ of MQAM, $s_i \in \boldsymbol{\Omega}_M$, where $\boldsymbol{\Omega}_M$ is the set of MQAM signals. Suppose $E\left[|s_i|^2\right] = 1$; four symbols are transmitted over two time slots. In each time slot, the corresponding received signals may be expressed as:

$$\boldsymbol{y}_1 = \boldsymbol{h}_{11} s_{d_1}^1 + \boldsymbol{h}_{12} e^{j\theta} s_{d_2}^1 + \boldsymbol{n}_1, \tag{C5.1}$$

$$\boldsymbol{y}_2 = \boldsymbol{h}_{21} e^{j\theta} s_{d_1}^2 + \boldsymbol{h}_{22} s_{d_2}^2 + \boldsymbol{n}_2, \tag{C5.2}$$

where $\boldsymbol{y}_i$ and $\boldsymbol{n}_i, i \in [1:2]$ in (C5.1) and (C5.2) have similar properties as $\boldsymbol{y}_i$ and $\boldsymbol{n}_i, i \in [1:2]$ discussed in (C4.1) and (C4.2). The channel vector $\boldsymbol{h}_{ik}, i \in [1:2], k \in [1:2]$ is estimated as discussed in (C.3). In addition, $\theta = \frac{2\pi z}{2^r}, z = [0 : 2^r - 1]$, with r bit(s) being responsible for improving the bandwidth efficiency of the EBE-GD-GC scheme.

4 Detection of the EBE-GD-GC Scheme

The optimal technique for decoding the EBE-GD-GC scheme is ML detection. However, the Golden code's computational complexity is exceptionally high due to the four complex-valued symbols in its codeword matrix. The most effective way of reducing the complexity of EBE-GD-GC without compromising the error performance is by using sphere detection. Therefore, this section firstly presents the equivalent detection model for EBE-GD-GC. Secondly, we describe the sphere detection method in detail. Finally, sorted detection subset (SDS) is incorporated in the sphere detection of EBE-GD-GC to reduce its computational complexity further.

4.1 Equivalent Detection Model for the EBE-GD-GC Scheme

In the EBE-GD-GC scheme, $\boldsymbol{h}_{ik}, i \in [1:2], k \in [1:2]$ in the received signals of (C5.1) and (C5.2) is unknown at the receiver. Consequently, coherent detection cannot be applied directly to (C5.1) and (C5.2). However, since the received signals at the reference block in (C.3) may be regarded as the channel estimations for $\boldsymbol{h}_{ik}$, the received signals of (C5.1) and (C5.2) can be converted into equivalent received signals containing $\hat{\boldsymbol{h}}_{ik}, i \in [1:2], k \in [1:2]$. Substituting $\boldsymbol{h}_{ik}$ with $\hat{\boldsymbol{h}}_{ik}$ in (C5.1) and (C5.2) and re-writing (C5.1) and (C5.2) yields:

$$\boldsymbol{y}_1 = \hat{\boldsymbol{h}}_{11} s_{d_1}^1 + \hat{\boldsymbol{h}}_{12} e^{j\theta} s_{d_2}^1 + \hat{\boldsymbol{n}}_1, \tag{C6.1}$$

$$\boldsymbol{y}_2 = \hat{\boldsymbol{h}}_{21} e^{j\theta} s_{d_1}^2 + \hat{\boldsymbol{h}}_{22} s_{d_2}^2 + \hat{\boldsymbol{n}}_2, \tag{C6.2}$$

where $\hat{\boldsymbol{n}}_1 = \boldsymbol{n}_1 - \boldsymbol{w}_{11} s_{d_1}^1 - \boldsymbol{w}_{12} e^{j\theta} s_{d_2}^1$ and $\hat{\boldsymbol{n}}_2 = \boldsymbol{n}_2 - \boldsymbol{w}_{21} e^{j\theta} s_{d_1}^2 - \boldsymbol{w}_{22} s_{d_2}^2$. The entries of $\hat{\boldsymbol{h}}_{ik}, i \in [1:2], k \in [1:2]$ and those of $\hat{\boldsymbol{n}}_i, i \in [1:2]$ are iid complex Gaussian RVs with the distribution $CN(0, 1+\sigma_r^2)$ and $CN(0, \sigma_\epsilon^2)$, respectively. The term $\sigma_\epsilon^2 = \sigma_d^2 + 2\sigma_r^2 = \frac{2}{P_d} + \frac{2}{P_r}$.

The EBE-GD-GC symbol matrix may therefore be written as:

$$\boldsymbol{S} = \begin{bmatrix} \boldsymbol{S_1} & \boldsymbol{S_2} \end{bmatrix} = \begin{bmatrix} s_{d_1}^1 & e^{j\theta} s_{d_1}^2 \\ e^{j\theta} s_{d_2}^1 & s_{d_2}^2 \end{bmatrix}, \tag{C.7}$$

where $\boldsymbol{S_1} = \begin{bmatrix} s_{d_1}^1 & e^{j\theta} s_{d_2}^1 \end{bmatrix}^T$ and $\boldsymbol{S_2} = \begin{bmatrix} e^{j\theta} s_{d_1}^2 & s_{d_2}^2 \end{bmatrix}^T$. Therefore, the received signals of (C6.1) and (C6.2) can be re-written in a more compact form as:

$$\boldsymbol{y}_i = \hat{\boldsymbol{H}}_i \boldsymbol{S}_i + \hat{\boldsymbol{n}}_i, \;\; i \in [1:2], \tag{C.8}$$

where $\boldsymbol{y}_i \in \mathbb{C}^{(N_r \times 1)}$ is the i^{th} received signal vector and $\hat{\boldsymbol{H}}_i = \begin{bmatrix} \hat{\boldsymbol{h}}_{i1} & \hat{\boldsymbol{h}}_{i2} \end{bmatrix}$. Again, $\hat{\boldsymbol{h}}_{ik}, k \in [1:2]$ and $\boldsymbol{n}_i$ are the same as the discussion in (C6.1) and (C6.2). Suppose $\boldsymbol{S_Q}_i = \begin{bmatrix} \boldsymbol{S_Q}_{i1} & \boldsymbol{S_Q}_{i2} \end{bmatrix}^T, i \in [1:2]$, where $\boldsymbol{S_Q}_{11} = \begin{bmatrix} s_1 & s_2 \end{bmatrix}^T$, $\boldsymbol{S_Q}_{12} = e^{j\theta} \begin{bmatrix} s_3 & s_4 \end{bmatrix}^T$, $\boldsymbol{S_Q}_{21} = e^{j\theta} \begin{bmatrix} s_1 & s_2 \end{bmatrix}^T$, $\boldsymbol{S_Q}_{22} = \begin{bmatrix} s_3 & s_4 \end{bmatrix}^T$ and $\tilde{\boldsymbol{H}}_i = \begin{bmatrix} \tilde{\boldsymbol{H}}_{i1} & \tilde{\boldsymbol{H}}_{i2} \end{bmatrix}$, where $\tilde{\boldsymbol{H}}_{ik} = \begin{bmatrix} \tilde{\boldsymbol{h}}_{i1}^k & \tilde{\boldsymbol{h}}_{i2}^k \end{bmatrix}$, we can write (C.7) as:

$$\boldsymbol{y}_i = \tilde{\boldsymbol{H}}_i \boldsymbol{S_Q}_i + \hat{\boldsymbol{n}}_i, \;\; i \in [1:2], \tag{C.9}$$

The received signal of (C.8) is due to the EBE-GD-GC transmitted symbols, while the receive signal of (C.9) is due to the transmitted MQAM symbols $s_i \in \boldsymbol{\Omega}_M, i \in [1:4]$. Again, suppose $\boldsymbol{Y} = \begin{bmatrix} \boldsymbol{y}_1 & \boldsymbol{y}_2 \end{bmatrix}^T, \boldsymbol{N} = \begin{bmatrix} \hat{\boldsymbol{n}}_1 & \hat{\boldsymbol{n}}_2 \end{bmatrix}^T$ and $\boldsymbol{H} = \begin{bmatrix} \tilde{\boldsymbol{H}}_1 & \tilde{\boldsymbol{H}}_2 \end{bmatrix}^T$, where $\boldsymbol{Y} \in \mathbb{C}^{(2N_r \times 1)}, \boldsymbol{N} \in \mathbb{C}^{(2N_r \times 1)}$, and $\boldsymbol{H} \in \mathbb{C}^{(2N_r \times 2N_t)}$, then (C.9) may be stacked as follows:

$$\boldsymbol{Y} = \boldsymbol{H}\boldsymbol{S_Q} + \boldsymbol{N}, \tag{C.10}$$

Note that this paper uses the expression in (C.10) to illustrate sphere detection of the EBE-GD-GC scheme.

4.2 Sphere Detection of EBE-GD-GC Scheme

The error performance of sphere decoding closely matches ML detection while achieving low detection complexity compared to the naïve ML decoder. This has led to the wide application of sphere decoding [12–14] to decode available MIMO systems. This paper employs sphere decoding to perform EBE-GD-GC detection. We use the stacked equation in (C.8), which utilises $\hat{\boldsymbol{h}}_{ik}, i \in [1:2], k \in [1:2]$ to estimate the channel at the receiver.

Firstly, QR factorisation of $\boldsymbol{H}$ in (C.8) is performed. This may be written as:

$$\boldsymbol{H} = \boldsymbol{Q}\boldsymbol{R}, \tag{C.11}$$

where the matrix $\boldsymbol{Q} \in \mathbb{C}^{(a \times a)}, a = 2N_r$ is unitary. $\boldsymbol{R} \in \mathbb{C}^{(a \times b)}, b = 2N_t$ is an upper triangular matrix. Secondly, substituting (C.11) into (C.10) and multiplying both sides of the equation by $\boldsymbol{Q}^H$ gives:

$$\hat{\boldsymbol{Y}} = \boldsymbol{R}\boldsymbol{S_Q} + \hat{\boldsymbol{N}}, \tag{C.12}$$

where $\hat{\boldsymbol{N}} = \boldsymbol{Q}^H\boldsymbol{N}$ and $\hat{\boldsymbol{Y}} = \begin{bmatrix} \hat{\boldsymbol{Y}}_1 & \hat{\boldsymbol{Y}}_2 \end{bmatrix}^T = \boldsymbol{Q}^H\boldsymbol{Y}$. It should be noted that $\hat{\boldsymbol{Y}}_1$ is a $b \times 1$ vector expressed as $\hat{\boldsymbol{Y}}_1 = \begin{bmatrix} \hat{Y}_1(1) & \hat{Y}_1(2) & \cdots & \hat{Y}_1(b-1) & \hat{Y}_1(b) \end{bmatrix}^T$, and $\hat{\boldsymbol{Y}}_2$ is a vector of dimension $(a-b) \times 1$. $\boldsymbol{R}$ can also be partitioned as $\boldsymbol{R} = \begin{bmatrix} \boldsymbol{R}_1 & \boldsymbol{R}_2 \end{bmatrix}^T$ with $\boldsymbol{R}_1$ being a $b \times b$ upper triangular

matrix expressed as:

$$\boldsymbol{R}_1 = \begin{bmatrix} r_{11} & r_{12} & \cdots & r_{1b} \\ 0 & r_{22} & \cdots & r_{2b} \\ \vdots & \vdots & \ddots & \vdots \\ 0 & 0 & \cdots & r_{bb} \end{bmatrix}, \tag{C.13}$$

The dimension of the matrix $\boldsymbol{R}_2$ is $(a-b) \times b$. Finally, sphere detection of (C.10) may be formulated as:

$$\left\| \hat{\boldsymbol{Y}}_1 - \boldsymbol{R}_1 \boldsymbol{S}_{\boldsymbol{Q}} \right\|_F^2 \leq d^2, \tag{C.14}$$

with the search radius of the sphere decoder denoted as d. The error performance of the SD algorithm highly depends upon the choice of the initial search radius, d. For example, if the chosen value of d is too small, the algorithm could fail to find any point inside the hyper-sphere. On the other hand, choosing a significantly large value of d slows the decoder down because it searches through many candidates before finding the best solution, thus resulting in high complexity. Typically, the choice of d is based on Eq. (28) of [15]. A simplified explanation of sphere decoding is provided as follows: Suppose $\boldsymbol{S}_{\boldsymbol{Q}} = \begin{bmatrix} \boldsymbol{S}_{\boldsymbol{Q}_1} & \boldsymbol{S}_{\boldsymbol{Q}_2} \end{bmatrix}^T = \begin{bmatrix} s_1 & \cdots & s_b \end{bmatrix}^T$. The first step is to detect s_b. Therefore, if we let $p_b(s_b) = \hat{Y}_1(b) - r_{bb}s_b$, then we may write:

$$|p_b(s_b)|^2 \leq d^2, \tag{C.15}$$

The sphere detector searches $s_b, s_b \in \boldsymbol{\Omega}_M$ to meet the condition in (C.15). Once the requirement in (C.15) is met, s_{b-1} is then detected. Similarly, if we let $p_{b-1}\left(s|_{b-1}^{b}\right) = \hat{Y}_1(b-1) - r_{b-1b-1}s_{b-1} - r_{b-1b}s_b$. then we have:

$$\left| p_{b-1}\left(s|_{b-1}^{b}\right) \right|^2 \leq d^2 - |p_b(s_b)|^2, \tag{C.16}$$

The sphere decoder then searches $s_{b-1}, s_{b-1} \in \boldsymbol{\Omega}_M$ to satisfy the condition in (C.16). Generally, if $s|_m^k = \begin{bmatrix} s_m & \cdots & s_k \end{bmatrix}$, then s_m is detected using the condition: [13]

$$\left| p_m\left(s|_m^b\right) \right|^2 \leq d^2 - \sum_{k=m+1}^{b} \left| p_k\left(s|_k^b\right) \right|^2, \tag{C.17}$$

4.3 Sphere Detection of EBE-GD-GC with Sorted Detection Subset

The detection complexity of a sphere decoder generally depends upon the cardinality of its signal set as well as the search depth. [16] If the size of the set of a given pair of symbols is reduced, then the detection complexity is reduced.A sphere decoding technique that uses a detection subset (SD-DS) has recently been proposed [12, 16], where it is observed that the average cardinality of the Golden code signal set reduces from 16^2 and 64^2 to 4^2 and 4.5^2 for 16QAM and 64QAM, respectively. However,

in most cases, SD-DS only exhibit low detection complexity at high SNR regions. Therefore, this paper adopts a modified technique referred to as sphere decoding with sorted detection subset [9, 13] to reduce the detection complexity of EBE-GD-GC further. In this technique, the transmitted MQAM symbols $s_i, i \in [1:b]$ are first estimated, then all the EBE-GD-GC symbols within the signal set are sorted from those with the highest probability of transmission to those with the lowest probability of transmission. Those symbols with the highest probability of transmission form the detection set. In summary, the process of SD-SDS is highlighted in the following steps:

Step 1: Perform QR factorisation and obtain $\hat{\mathbf{Y}}_1$ using (C.12).

Step 2: Find the transmitted MQAM symbols, $s_i, i \in [1:b]$. From (C.12), we may write:

$$x_b = \frac{\hat{Y}_1(b)}{r_{bb}}, \tag{C.18}$$

The estimations of s_b are obtained by demodulating (C.18) as follows:

$$\tilde{s}_b = \mathfrak{D}(x_b), \tag{C.19}$$

Step 3: Sort all the symbols in the signal set from those with the highest transmission probability to those with the lowest transmission probability. We use the metric:

$$z_i(m) = |x_i - s_m|^2, \tag{C.20}$$

where $m \in [1:M]$ and $s_m \in \mathbf{\Omega}_M$. Suppose $\boldsymbol{z}_i = \{z_i(m), m \in [1:M]\}, i \in [1:b]$, the most probable estimation index of s_i is evaluated as:

$$\tilde{\boldsymbol{i}}_m = argsort(\boldsymbol{z}_i), \tag{C.21}$$

where the $argsort(\cdot)$ operator is responsible for sorting M elements from the most likely transmitted to the least likely transmitted.

Step 4: Perform sphere detection

It is important to note that for any SNR, a total of N symbols with the highest likelihood of transmission in each $\tilde{s}_i$ are selected. These symbols then form the setn $\mathbf{\Omega}(\tilde{s}_i, N)$ that is used to replace $\mathbf{\Omega}_M$ in performing sphere detection. Generally, small values of N are chosen at low SNRs. In contrast, large values of N are chosen at high SNRs to increase the rate of detection while ensuring that the simulated BERs compare very well with the theoretical ABEP. For EBE-GD-GC simulation with SD-SDS, the parameter N is specified for different SNR values as tabulated in **Table C.1**.

5 Error Performance Analysis of the EBE-GD-GC Scheme

In coherent Golden code, the assumption is that only one MQAM symbol, s_1, is detected with error while all the other input symbols $s_i, i \in [2:4]$ are correctly detected. Moreover, the equivalent error performance model of the Golden code is regarded as the transmission of the symbol s_1 over two non-identical fading channels with fading variances $|\beta_i|^2, i \in [1:2]$ [12]. Also, the variance of each entry $\boldsymbol{H}_i$, where $\boldsymbol{H}_i = \begin{bmatrix} \boldsymbol{h}_{i1} & \boldsymbol{h}_{i2} \end{bmatrix}$ and $\boldsymbol{n}_i$ of the Golden code is given by 1 and $\frac{2}{P}$, respectively. In this paper, however, the error performance analysis of the EBE-GD-GC scheme is based on the equivalent received signal (C.9), where the variance of each entry in $\tilde{\boldsymbol{H}}_i = \begin{bmatrix} \tilde{\boldsymbol{H}}_{i1} & \tilde{\boldsymbol{H}}_{i2} \end{bmatrix}$, where $\tilde{\boldsymbol{H}}_{ik} = \begin{bmatrix} \tilde{\boldsymbol{h}}_{i1}^k & \tilde{\boldsymbol{h}}_{i2}^k \end{bmatrix}, i \in [1:2], k \in [1:2]$ and $\hat{\boldsymbol{n}}_i$ is $(1+\sigma_r^2)$ and $\sigma_\epsilon^2 = \frac{2}{P_d} + \frac{2}{P_r}$, respectively. It is noted that the error performance analysis of the EBE-GD-GC scheme is done in a similar manner to that of the coherent GC, except that particular focus is given to the variance of EBE-GD-GC. The received signals of (C6.1) and (C6.2) may be re-written as:

$$\boldsymbol{y}_1 = \frac{\alpha}{\sqrt{5}} \left[\hat{\boldsymbol{h}}_{11}(s_1 + s_2\tau) + \hat{\boldsymbol{h}}_{12} e^{j\theta}(s_3 + s_4\tau) \right] + \hat{\boldsymbol{n}}_1, \tag{C22.1}$$

$$\boldsymbol{y}_2 = \frac{\hat{\alpha}}{\sqrt{5}} \left[\hat{\boldsymbol{h}}_{21} e^{j\theta}(s_1 + s_2\mu) + \hat{\boldsymbol{h}}_{22}(s_3 + s_4\mu) \right] + \hat{\boldsymbol{n}}_2, \tag{C22.2}$$

Since s_1 is assumed to be detected with error, while the other input symbols $s_i, i \in [2:4]$ are correctly detected, then (C22.1) and (C22.2) may be simplified as:

$$\boldsymbol{y}_1 = \beta_1 \hat{\boldsymbol{h}}_{11} s_1 + \hat{\boldsymbol{n}}_1, \tag{C23.1}$$

$$\boldsymbol{y}_2 = \beta_2 \hat{\boldsymbol{h}}_{21} s_1 + \hat{\boldsymbol{n}}_2, \tag{C23.2}$$

where $\beta_1 = \frac{\alpha}{\sqrt{5}}$ and $\beta_2 = \frac{\hat{\alpha}}{\sqrt{5}} e^{j\theta}$. Since the output of the reference block is known at the receiver, we derive the ABEP of EBE-GD-GC using the classical expression of the exact symbol error probability of MQAM signals provided in Eq. (8.10) of [17]. The expression is simplified using the Gaussian Q-function approximation and the trapezoidal rule of integration. As a result, the ABEP of EBE-GD-GC for MQAM signals may be derived as:

$$\begin{aligned} P_e \approx \frac{a}{n \log_2 M} \Bigg[& \frac{1}{2} \prod_{i=1}^{2} \left(\frac{2}{2 + |\beta_i|^2 b\hat{\gamma}} \right)^{N_r} - \left(\frac{a}{2} \right) \prod_{i=1}^{2} \left(\frac{1}{1 + |\beta_i|^2 b\hat{\gamma}} \right)^{N_r} \\ & + (1-a) \sum_{k=1}^{n-1} \prod_{i=1}^{2} \left(\frac{u_k}{u_k + |\beta_i|^2 b\hat{\gamma}} \right)^{N_r} + \sum_{k=n}^{2n-1} \prod_{i=1}^{2} \left(\frac{u_k}{u_k + |\beta_i|^2 b\hat{\gamma}} \right)^{N_r} \Bigg], \end{aligned} \tag{C.24}$$

where $n \geq 10$ is the number of summations required for convergence, $a = 1 - \frac{1}{\sqrt{M}}, b = \frac{3}{M-1}$, and $u_k = 2\sin^2\left(\frac{k\pi}{4n}\right)$. The SNR of the EBE-GD-GC scheme is denoted by $\hat{\gamma}$ and is given by:

$$\hat{\gamma} = \frac{(1+\sigma_r^2)}{\left(\frac{2}{P_d} + \frac{2}{P_r}\right)} = \frac{1}{2}\left(1+\sigma_r^2\right)\left(\frac{1}{P_d} + \frac{1}{P_r}\right)^{-1}, \tag{C.25}$$

6 Computational Complexity Analysis of the EBE-GD-GC Scheme

In MIMO systems, the conventional maximum likelihood decoder searches through M^{N_t} points to find an optimal solution. However, tree search algorithms such as the sphere decoder have their complexities proportional to the number of nodes traversed within a hypersphere before an optimal solution is obtained. [14] Numerous investigations have been carried out on the complexity of the SD algorithms. Some of these investigations are based on analytical evaluations [14, 18], while others utilise simulations. [13, 16, 19] For EBE-GD-GC with sphere decoding, the detection complexity comprises a pre-detection stage and a search stage.

6.1 The Complexity of the Pre-Detection Stage

QR factorisation is done in the pre-detection stage to obtain the upper triangular matrix $\boldsymbol{R}$ from the channel matrix $\boldsymbol{H}$. The unitary matrix $\boldsymbol{Q}$ establishes the minimum and the maximum bounds for each closest lattice point. The computational complexity of the pre-detection stage is generally defined in terms of floating-point operations (flops), where each multiplication, division, addition and subtraction is considered a single flop [5, 12]. Therefore, since $\boldsymbol{H}$ is a $2N_r \times 2N_t$ matrix, QR factorisation takes up $8(2N_r) - \frac{16}{3}$ flops for each $i \in [1:2]$ using the Householder algorithm. [20]. Computing $\hat{\boldsymbol{Y}} = \boldsymbol{Q}^H \boldsymbol{Y}$ in (C.12) requires $(2N_r)^2$ multiplications and $2N_r(2N_r - 1)$ additions for each i. Therefore, the total number of flops in the pre-detection stage is given by: $\zeta_{QR} = 2\left[(2N_r)^2 + 7(2N_r) - \frac{16}{3}\right]$.

6.2 The Complexity of the Search Stage

In the search stage, the sphere decoder traverses the whole signal set to decode the transmitted symbols. As mentioned in the previous section, the conventional SD for MIMO systems searches through M^{N_t} points. However, the EBE-GD-GC scheme uses SD-SDS, which reduces the constellation size, and in turn, the detection complexity is reduced. In EBE-GD-GC complexity analysis, we focus on the complexity of the search stage only and ignore the pre-detection stage complexity because the complexity of QR factorisation is negligible compared to that of the search stage [13, 16, 21]. Moreover, the iterative search of the optimal point in an SD algorithm's lattice is entirely rand [14]. Therefore, the average detection complexity of EBE-GD-GC with SD-SDS is done via simulations.

As such, this paper performs Monte Carlo simulations on SD-SDS of the EBE-GD-GC scheme to obtain the average number of nodes traversed and the results represented here as an average complexity. Only 16QAM and 64QAM signal constellations with $N_r = 3$ and $N_r = 4$ at a frame

length of $D = 400$ are considered. In addition, **Table C.1** provides the values chosen for parameter N in each simulated SNR. For comparison purposes, we also simulate EBE-GD-GC with conventional SD for both 16QAM and 64QAM configurations.

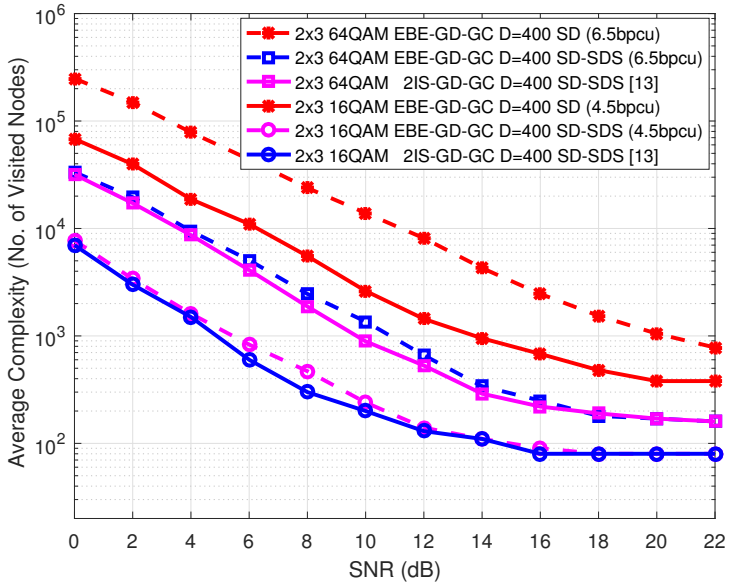

Figure C.1: Detection complexity of 16QAM and 64QAM EBE-GD-GC with SD-SDS when $N_r = 3$

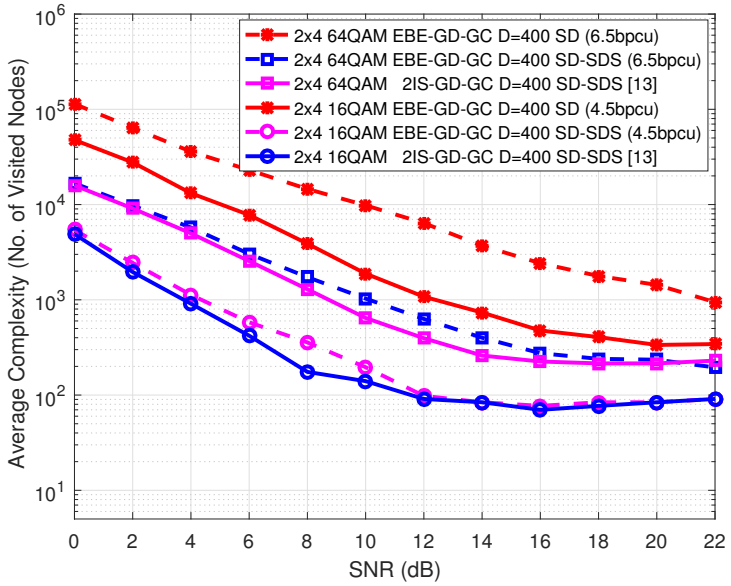

Figure C.2: Detection complexity of 16QAM and 64QAM EBE-GD-GC with SD-SDS when $N_r = 4$

The simulation results obtained are illustrated in **Figures C.1** and **C.2**. The average detection complexities of **Figures C.1** and **C.2** are simulated based upon the detection of four MQAM symbols. From the illustrations of **Figures C.1** and **C.2**, the following observations are deduced for both the 16QAM and 64QAM configurations:

(i) The average detection complexity of EBE-GD-GC with SD-SDS decreases as the SNR increases.

(ii) At a bandwidth efficiency of 4.5 bits per channel use, the average detection complexity of EBE-GD-GC with SD-SDS is slightly higher than that of GD-GC with SD-SDS.

(iii) The average detection complexity of EBE-GD-GC with SD-SDS is much lower than that of EBE-GD-GC with conventional SD.

7 Simulation Results

This section presents the Monte Carlo simulation results for the EBE-GD-GC scheme. The following assumptions and parameters govern the simulations carried out:

(a) We assume two transmit antennas $N_t = 2$ for all the cases investigated.

(b) We also assume a quasi-static Rayleigh frequency flat fading channel with AWGN.

(c) The simulations are carried out for:

(i) $M = 16$ and $M = 64$

(ii) $N_r = 3$ and $N_r = 4$

(iii) $r = 1$ and $r = 2$, where the achievable bandwidth efficiency investigated in this paper is defined as $\frac{r}{4} + \log_2 M$ bits per channel use.

(iv) The frame length used for all simulations is $D = 400$

(d) The values of the parameter N chosen for detection of EBE-GD-GC with SD-SDS are tabulated in **Table C.1**

Table C.1: Parameter settings for simulation

$\boldsymbol{M}$	$\boldsymbol{N_r}$	$\boldsymbol{SNR}$	$\boldsymbol{N}$
16	3	[0:2:26]	[8 8 8 8 10 10 10 10 12 12 12 12 16 16]
	4	[0:2:22]	[8 8 8 10 10 10 12 12 12 16 16 16]
64	3	[0:2:32]	[10 10 10 10 14 14 14 20 20 20 20 30 30 30 60 60 60]
	4	[0:2:28]	[14 14 14 14 20 20 20 20 30 30 30 30 60 60 60]

The following observations are made from **Figure C.3** to **Figure C.6**:

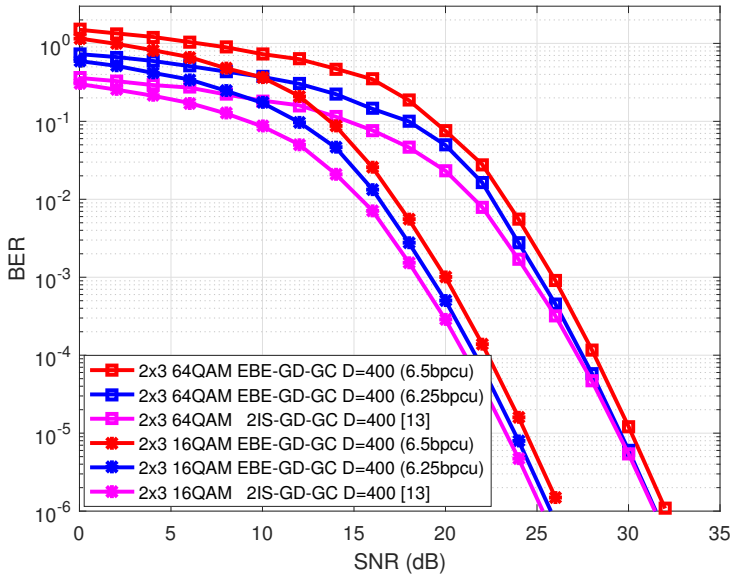

Figure C.3: BER performance for 16QAM and 64QAM EBE-GD-GC with $N_r = 3$

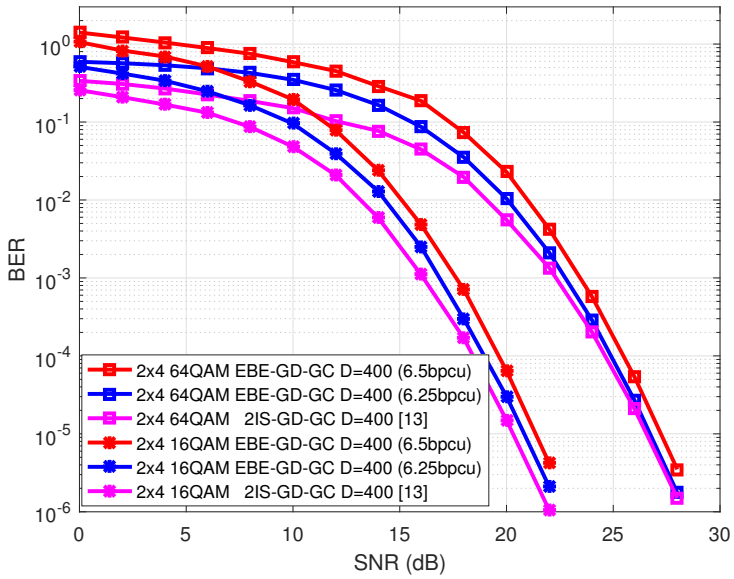

Figure C.4: BER performance for 16QAM and 64QAM EBE-GD-GC with $N_r = 4$

1. The simulated BER curves compare very well to their corresponding theoretical bounds derived in (C.24). In fact, for both $N_r = 3$ and $N_r = 4$ antenna configurations, the simulated BERs draw closer to their corresponding theoretical bounds as SNR increases.

2. It is further observed that, for all simulated bandwidths, the BER of EBE-GD-GC approaches that of the conventional generalised differential Golden code at higher SNR regions. For instance, the BER performance gap between 2×3 16QAM EBE-GD-GC with 4.25 bpcu $(r = 1)$ and the corresponding conventional GD-GC at 1×10^{-5} is approximately 0.6 dB.

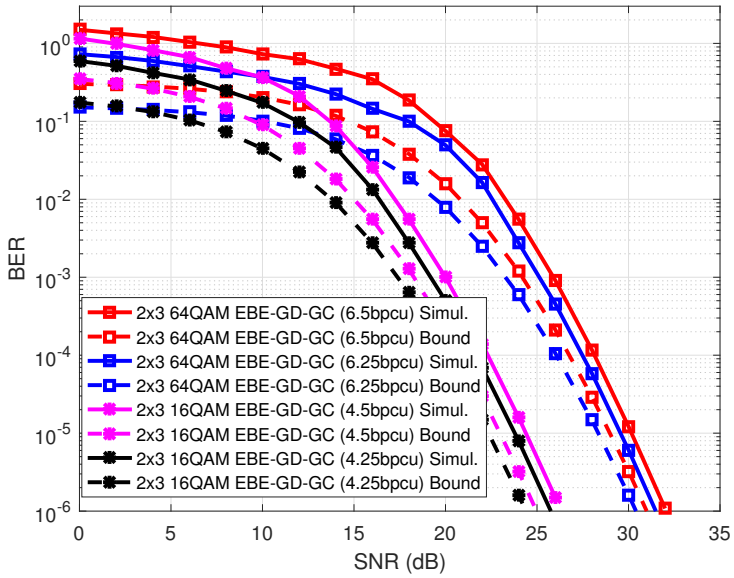

Figure C.5: Error performance comparison for 16QAM and 64QAM EBE-GD-GC with theoretical bounds when $N_r = 3$

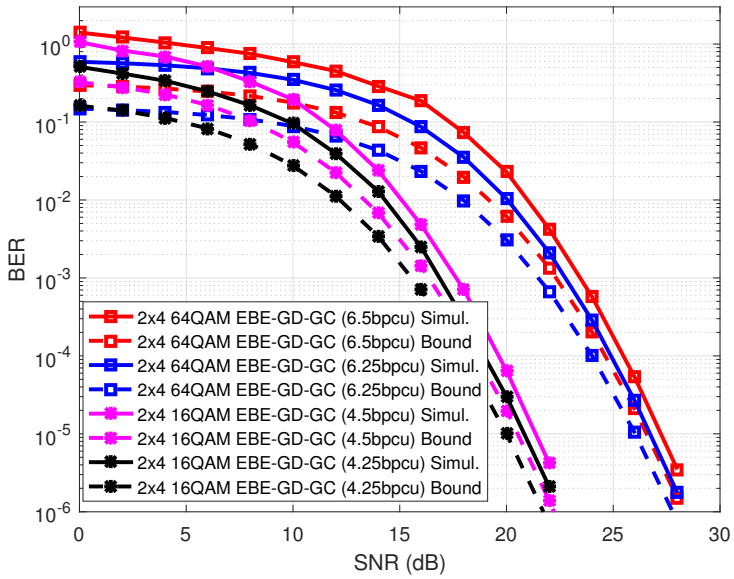

Figure C.6: Error performance comparison for 16QAM and 64QAM EBE-GD-GC with theoretical bounds when $N_r = 4$

Moreover, the BER of 2×3 64QAM EBE-GD-GC with 6.25 bpcu $(r = 1)$ converges with the conventional GD-GC at a BER of 1×10^{-4}. Similarly, the BER performance gap between 2×4 16QAM EBE-GD-GC with 4.25 bpcu $(r = 1)$ and the corresponding conventional GD-GC at 1×10^{-5} is approximately 0.5 dB. In comparison, the BER of 2×4 64QAM EBE-GD-GC with 6.25 bpcu $(r = 1)$ converges with the conventional GD-GC at a BER of 2×10^{-5}.

3. As the value of r increases (higher values of bpcu), the BER performance slightly degrades

compared to the conventional GD-GC. For instance, the BER performance of both 2×4 16QAM and 2×4 64QAM EBE-GD-GC with 4.5 bpcu and 6.5 bpcu $(r = 2)$, respectively, results in < 1 dB performance loss compared to their corresponding conventional GD-GC from a BER of 1×10^{-5}. A similar pattern is observed for both 2×3 16QAM and 2×3 64QAM EBE-GD-GC with 4.5 bpcu and 6.5 bpcu $(r = 2)$, respectively. Consequently, this validates the trade-off that exists between error performance and bandwidth efficiency.

4. The simulated BER draws closer to the theoretical bound as the number of receive antennas increase.

8 Conclusion

An enhanced bandwidth-efficient generalised differential Golden code scheme is proposed in this paper. The scheme accommodates extra bit(s) for more data transmission and performs very well compared to the conventional generalised differential Golden code. A sphere decoding technique that utilises a sorted detection subset is also incorporated to reduce the average detection complexity of the EBE-GD-GC scheme. A theoretical bound that validates the simulation results is also derived. Both the simulation and theoretical results show that the error performance of the EBE-GD-GC scheme approaches that of the conventional GD-GC. For instance, the BER performance gap between 2×4 16QAM EBE-GD-GC with 4.25 bpcu $(r = 1)$ and the corresponding conventional GD-GC at 1×10^{-5} is approximately 0.5 dB, while the BER of 2×4 64QAM EBE-GD-GC with 6.25 bpcu $(r = 1)$ converges with the conventional GD-GC at a BER of 2×10^{-5}. In addition, it is shown that at higher bpcu values, the BER performance of EBE-GD-GC degrades slightly compared to the conventional GD-GC. The simulations conclusively show that the bandwidth-efficient EBE-GD-GC allows for the transmission of more data to help meet the ever-rising demands of modern wireless communication systems.

References

[1] L. Zheng and D. Tse, "Diversity and Multiplexing: A Fundamental Trade-off in Multiple-Antenna Channels," *IEEE Trans Inform Theory*, vol. 49, no. 5, pp. 1073–1096, 2003.

[2] S. Alamouti, "A simple transmit diversity technique for wireless communications," *IEEE Journ Sel Areas Commun*, vol. 16, no. 8, pp. 1451–1458, 1998.

[3] J.-C. Belfiore, G. Rekaya, and E. Viterbo, "The Golden Code: A 2x2 Full-Rate Space-Time Code with Nonvanishing Determinants," *IEEE Trans Inform Theory*, vol. 51, no. 4, pp. 1432–1436, 2005.

[4] M. Sinnokrot and J. Barry, "Fast Maximum-likelihood Decoding of the Golden Code," *IEEE Trans Wireless Commun*, vol. 9, no. 1, pp. 26–31, 2010.

[5] S. Kahraman and M. Celebi, "Dimensionality Reduction for the Golden Code with Worst-Case Decoding Complexity of O$(m^{1.5})$," ser. Proc IEEE Wireless Communications and Networking Conference, USA, April, 2012.

[6] H. Xu, N. Pillay, and X. Jin, "Golden Codeword based Generalized Differential Alamouti Modulation," *IEEE Access*, vol. 8, no. 1, pp. 65 649–65 657, 2020.

[7] B. Dlodlo, H. Xu, and N. Pillay, "Bandwidth efficiency improvement for differential alamouti space-time block codes," ser. Proc. SAIEEE, South Africa, Dec, 2018, pp. 217–223.

[8] S. Das, N. Al-Dhahir, and R. Calderbank, "Novel full-diversity high rate stbc for 2 and 4 transmit antennas," *IEEE Commun. Lett.*, vol. 10, no. 3, pp. 171–173, Jun. 2006.

[9] G. Omondi, H. Xu, P. Akuon, and N. Pillay, "Multiple input symbol generalised differential golden code modulation," *International Journal of Communication Systems*, vol. 35, no. 4, pp. 1–16, 2022.

[10] K. Dwarika and H. Xu, "Differential full diversity spatial modulation using amplitude phase shift keying," *Radioengineering*, vol. 27, no. 1, pp. 151–158, 2018.

[11] K. Dwarikah and H. Xu, "Power Allocation and Low Complexity Detector for Differential Full Diversity Spatial Modulation Using Two Transmit Antennas," *Radioengineering*, vol. 26, no. 2, pp. 461–469, 2017.

[12] H. Xu and N. Pillay, "Reduced Complexity Detection Schemes for Golden Code Systems," *IEEE Access*, vol. 7, no. 1, pp. 139 140–139 149, 2019.

[13] H. Xuh and N. Pillay, "Multiple Complex Symbol Golden Code," *IEEE Access*, vol. 8, no. 1, pp. 103 576–103 584, 2020.

[14] J. Jalden and B. Ottersen, "On the Complexity of Sphere Decoding in Digital Communications," *IEEE Trans Signal Proc*, vol. 53, no. 4, pp. 1474–1484, 2005.

[15] B. Hochwald and S. Brink, "Achieving Near-Capacity on a Multiple Antenna Channel," *IEEE Trans On Commun*, vol. 51, no. 3, pp. 389–399, 2003.

[16] H. Xu and N. Pillay, "The Component-Interleaved Golden Code and its Low-Complexity Detection," *IEEE Access*, vol. 8, no. 1, pp. 59 550–59 558, 2020.

[17] M. Simon and M.-S. Alouini, *Digital Communications over Fading Channels: A Unified Approach to Performance Analysis*. USA: A Wiley-Interscience Publication, 2000, iSBN 0-471-20069-7.

[18] B. Hassibi and H. Vikalo, "On Sphere Decoding Algorithm Part 1: The Expected Complexity," *IEEE Trans Signal Proc*, vol. 54, no. 5, pp. 2806–2818, 2005.

[19] S. Han and C. Tellambura, "A Complexity-Efficient Sphere Decoder for MIMO Systems," ser. Proc IEEE International Conference on Communications, Japan, June, 2011.

[20] G. Golub and C. Loan, *Matrix Computations, 4th Edition*. USA: The John Hopkins University Press, 2013, iSBN 1421408597, 9781421408590.

[21] G. Rekaya and J. Belfiore, "On the Complexity of ML Lattice Decoders for Decoding Linear Full Rate Space-Time Codes," ser. Proc IEEE International Symposium on Inf Theory, Japan, June, 2003.

[22] H. Xu, K. Govindasamy, and N. Pillay, "Uncoded space-time labeling diversity," *IEEE Communication Letters*, vol. 20, no. 8, pp. 111–114, 2016.

[23] Z. A. Baloch, M. U. Baloch, and N. Hussain, "Efficiency improvement of space-time block codes," *Inter. Journ. Commun., Network and Sys. Sciences*, vol. 3, no. 6, pp. 507–510, Jun. 2010.

[24] Q. Ling and T. Li, "Efficiency improvement for alamouti codes," ser. Proc IEEE 40th Annual Conference on Information Sciences and Systems, Princeton, USA, Mar, 2006.

[25] L. Li, Z. Fang, Y. Zhu, and Z. Wang, "Generalized differential transmission for STBC systems," ser. Proc IEEE GLOBECOM Telecommunications Conference, New Orleans, USA, Dec 1–4, 2008.

Part V

Conclusion

1 Conclusion

This research study leads to the following key outcomes:

Paper A shows how Golden code symbols are differentially encoded and detected without knowledge of the channel state information at the receiver. This is significant because it helps to reduce the detection complexity. The error performance of the proposed GDM-GC scheme is also enhanced using a novel power allocation technique that apportions more transmit power to the reference block than the data blocks. The theoretical analysis and simulations also verify that the error performance improves when the frame length is increased. Compared to the coherent Golden code with ML detection, both 16QAM and 64QAM GDM-GC result in approximately 0.4 dB performance loss for a frame length of $L = 400$. However, the GDM-GC scheme exhibits a significant reduction in computational complexity compared to the coherent ML detector. This performance, coupled with the substantial reduction in computational complexity, provides a trade-off between the error probability in non-coherent systems and the complexity of coherent optimal ML detectors.

Paper B extends the generalised differential modulation scheme to multiple input symbol Golden code and proposes an MIS-GD-GC scheme based on MQAM. This scheme improves the error performance compared to the conventional differential multiple input symbol Golden code (MIS-GC). It also attains a diversity order of $2^l N_r$ in comparison to the conventional Golden code, $l \geq 1$ being an integer. A sphere decoder with a sorted detection subset is used at the receiver of MIS-GD-GC to reduce the average detection complexity of the scheme. Derived theoretical bounds also compare very well to the simulation results. The error performance of MIS-GD-GC is also improved when the frame length is increased. For instance, the SNR gap is 0.8 dB at a frame length of $B = 100$, while the SNR gap reduces to 0.4 dB at $B = 400$.

Paper C proposes an enhanced bandwidth efficiency scheme based on MQAM referred to as EBE-GD-GC. The scheme can transmit extra bit(s) of information while performing very well compared to the conventional generalised differential Golden code. Both the theoretical analysis and simulation results show that the error performance of the EBE-GD-GC scheme approaches that of the conventional generalised differential Golden code. For instance, the BER performance gap between 2×4 16QAM EBE-GD-GC with 4.25 bpcu and the corresponding conventional GD-GC at 1×10^{-5} is approximately 0.5 dB, while the BER of 2×4 64QAM EBE-GD-GC with 6.25 bpcu converges with the conventional GD-GC at a BER of 2×10^{-5}. The bandwidth-efficient EBE-GD-GC scheme is suitable for STBC systems that require higher data transmission to meet the demands of modern wireless communication systems.

2 Further Research Work

Further investigations into the generalised differential Golden code scheme presented in this study are critical in extending the Golden code's applications to more areas of wireless communication systems. The following areas of interest have been identified for future study. Firstly, the proposed schemes presented in this thesis are designed with only two transmit antennas. In future, the focus should be on designing a general procedure for GC codewords to operate with any arbitrary number of transmit antennas without significantly compromising the full-rate full-diversity gain property.

Secondly, this research study incorporates sphere decoding with a sorted detection subset to significantly reduce the detection complexity of the proposed schemes. However, at higher modulation order ($M \geq 64$), the detection complexity of these schemes remain high. Consequently, there is a need to investigate more efficient low-complexity detection algorithms for the generalised differential GC schemes to ensure their practicability in hardware implementation. In addition, more research needs to be done on the BER performance of the proposed generalised differential GC scheme at low SNR regions compared to the derived theoretical bounds.

Multiple antenna arrays are incorporated in MIMO systems to provide transmit and receive diversities. A hybrid scheme that increases the capacity of MIMO systems while maintaining an impressive BER performance is necessary. In this regard, a combination between V-BLAST and generalised Golden code STBC may be explored to achieve both spatial and diversity gains simultaneously.

Finally, since the GC is a full rank, full-rate STBC that achieves the best possible trade-off between diversity gain and multiplexing gain, generalised differential Golden code can be fused with orthogonal frequency division multiplexing (OFDM). This is suitable for broadband applications, where multiple antenna systems must transmit information at high data rates.